Quantum Rotational Effects in Nanomagnetic Systems

by

Michael F. O'Keeffe

A dissertation submitted to the Graduate Faculty in Physics in partial fulfillment of the requirements for the degree of Doctor of Philosophy, The City University of New York

2013

This manuscript has been read and accepted for the Graduate Faculty in Physics in satisfaction of the dissertation requirement for the degree of Doctor of Philosophy.

Date	Dist. Prof. Eugene Chudnovsky Chair of Examining Committee
Date	Prof. Steven Greenbaum Executive Officer
Prof. Dmitry Garanin	
Prof. Andrew Kent	
Prof. Vadim Oganesyan	
Dist. Prof. Myriam Sarachik	

Supervisory Committee

THE CITY UNIVERSITY OF NEW YORK

Abstract

Quantum Rotational Effects in Nanomagnetic Systems

by

Michael F. O'Keeffe

Advisor: Eugene Chudnovsky, Distinguished Professor of Physics

Quantum tunneling of the magnetic moment in a nanomagnet must conserve the total angular momentum. For a nanomagnet embedded in a rigid body, reversal of the magnetic moment will cause the body to rotate as a whole. When embedded in an elastic environment, tunneling of the magnetic moment will cause local elastic twists of the crystal structure. In this thesis, I will present a theoretical study of the interplay between magnetization and rotations in a variety of nanomagnetic systems which have some degree of rotational freedom.

We investigate the effect of rotational freedom on the tunnel splitting of a nanomagnet which is free to rotate about its easy axis. Calculating the exact instanton of the coupled equations of motion shows that mechanical freedom of the particle renormalizes the easy axis anisotropy, increasing the tunnel splitting.

To understand magnetization dynamics in free particles, we study a quantum mechanical model of a tunneling spin embedded in a rigid rotor. The exact energy levels for a symmetric rotor exhibit first and second order quantum phase transitions between states with different values the magnetic moment. A quantum phase diagram is obtained in which the magnetic moment depends strongly on the moments of inertia.

An intrinsic contribution to decoherence of current oscillations of a flux qubit must come from the angular momentum it transfers to the surrounding body. Within exactly solvable models of a

qubit embedded in a rigid body and an elastic medium, we show that slow decoherence is permitted if the solid is macroscopically large.

The spin-boson model is one of the simplest representations of a two-level system interacting with a quantum harmonic oscillator, yet has eluded a closed-form solution. I investigate some possible approaches to understanding its spectrum.

The Landau-Zener dynamics of a tunneling spin coupled to a torsional resonator show that for certain parameter ranges the system exhibits multiple Landau-Zener transitions. These transitions coincide in time with changes in the oscillator dynamics. A large number of spins on a single oscillator coupled only through the in-phase oscillations behaves as a single large spin, greatly enhancing the spin-phonon coupling.

To my family.

Acknowledgements

An African proverb on one of the office doors across from mine says, “If you want to go fast, go alone. If you want to go far, go with others.” While I have not gone very far or fast, I certainly could not have gotten here on my own. Many thanks to the people who have helped me along the way.

My advisor, Dist. Prof. Eugene Chudnovsky, has been a patient source of encouragement and guidance as he has mentored me through the beginning of my research career. He has been generous with his time and resources, inviting me to join him at memorable conferences and workshops. As a physicist, Eugene has a knack for starting with a simple physical picture when understanding complex physical phenomena. On a personal level, his support of my decision to become an officer in the United States Marine Corps Reserve, a rare step for a doctoral student in physics, has meant as much to me as his mentorship in physics. Prof. Dmitry Garanin, my unofficial advisor, has acted as a unique counterpart to Eugene, always asking deep questions about what we have found and what we could pursue next. I hope I will be able to emulate his ability to separate hand-waving from fundamentally sound arguments, and the humor with which he does this.

I appreciate the members of my second and final exam committees, both for the time they have dedicated and their influence on my development as a physicist. Prof. Andy Kent, Dist. Prof. Myriam Sarachik, and Prof. Javier Tejada have laid the experimental foundation for the field of quantum tunneling in single molecule magnets. Their work has shaped how I think about these fascinating materials. Prof. Vadim Oganesyan has introduced me to the wider world of modern condensed matter physics through an independent study on the critical phenomena, invitations to summer schools, and many enlightening conversations.

Prof. Timothy Boyer guided me through my first days of graduate studies as a masters student

at City College and assisted me during the transition to the Ph.D. program. Prof. Steve Greenbaum and Mr. Daniel Moy have supported me at every step during my doctoral studies at the Graduate Center. Steve has particularly helped me plan my military and research careers over the next few years, while Daniel has taken care of every administrative detail.

The faculty and students at Lehman College have provided a welcoming environment for research and teaching. To my fellow graduate students - Reem Jaafar, Liufei Cai, Debajyoti Sarkar, and Tom Proctor - for sharing blackboard discussions on physics and conversations ranging from cricket to dragon boats, thanks for teaching me new things and making me laugh.

Mr. Whelan, my high school physics teacher, introduced me to physics. When he offered me the opportunity to come back, I declined in order to finish my doctoral work. For both the offer and his affirmation of path I took, I am truly grateful.

My Mom, Dad, and sister Katherine, have each in their own way given me the love and encouragement to pursue my doctorate in physics. I cannot thank you enough for your patience, especially at times when mine has worn thin. Through the ups and downs, we know my brother Jimmy is here with us in spirit, and we are fortunate for the happiness he has brought to our lives. I know the rest of my family and friends have been pulling for me from places near and far, and I do appreciate it.

The joy my wife Maura brings to our life together has made the trials of doctoral work bearable, especially over the past few months which have been particularly challenging. On top of everything you have done to help me along the way, you make it all worthwhile.

Contents

Abstract **iv**

Acknowledgements **vii**

1 Introduction **1**

1.1 Background 3

2 Renormalization of the tunnel splitting in a rotating nanomagnet **12**

2.1 Magnetization Dynamics 13

2.2 Instanton Solution 17

2.3 Discussion and Conclusions 19

3 Quantum Tunneling of the Magnetic Moment in a Free Nanoparticle **20**

3.1 Quantization of rigid body rotations 21

3.2 Tunneling of a large spin 22

3.3 Coupling of Spin and Rotational Angular Momentum 24

3.4 Ground state 31

3.5 Ground-state magnetic moment 35

3.6 Conclusions 37

4 Conservation of Angular Momentum in a Flux Qubit **39**

4.1 Rigid Body 40

4.1.1 Rotational states of a flux qubit 40

4.1.2 Decoherence from rotations 44

4.2 Elastic Body . . . 48
4.2.1 Flux qubit in the elastic environment . . . 48
4.2.2 Decoherence from internal torques . . . 53
4.2.3 Renormalization of the tunnel splitting by the elastic environment . . . 56
4.3 Discussion and Conclusions . . . 57

5 Spin-Boson Model **62**
5.1 Background . . . 62
5.2 Parity Chains and Diagonalization . . . 64
5.3 Displaced Oscillator Basis . . . 66

6 Landau-Zener dynamics of a nanoresonator containing a tunneling spin **69**
6.1 Model . . . 71
6.1.1 Landau-Zener Transitions in a Two-State System . . . 71
6.1.2 Landau-Zener Transitions in a Spin-Oscillator System . . . 73
6.2 Landau-Zener Spin-Oscillator Dynamics . . . 76
6.2.1 Adiabatic energy levels . . . 76
6.2.2 Strong coupling . . . 77
6.2.3 Weak coupling . . . 81
6.3 Oscillator dynamics . . . 81
6.4 Collective dynamics of spins coupled to a mechanical resonator . . . 83
6.5 Discussion and conclusions . . . 88

7 Conclusion **91**

Bibliography **93**

Publications **103**

List of Figures

1.1 (a) Normalized saturation magnetization of a Mn_{12}-ac crystal as a function of longitudinal magnetic field for different temperatures below the blocking temperature and a sweep rate of 10 mT / s. (b) Derivative of the magnetization in (a) as a function of the magnetic field. Reprinted from Ref. [1] 6

1.2 Double well potential and energy levels of a large spin with strong magnetic anisotropy. The left figure shows all $2S+1$ energy levels and the right shows the lowest tunneling doublet. 7

2.1 Spin and angular momentum tunneling in a rotating magnetic nanoparticle. 13

2.2 Geometry of particle and laboratory frames. 14

2.3 Dependence of ϕ on τ for clockwise and counterclockwise underbarrier rotations of $\mathbf{M}$. 18

3.1 Coordinate frames of rigid body rotations. 25

3.2 (a) Dependence of energy on J at $K = J$ and $I_z/I_x = 0$ for different values of α. The plot shows second-order quantum phase transition on α. (b) Dependence of energy on J at $K = J$ and $I_z/I_x = 2$ for different values of α. The plot shows first-order quantum phase transition on α. 32

3.3 Dependence of the ground-state energy on α for a spherical particle. Inset shows the discontinuity of the derivative of the ground state energy on α. 33

3.4 Ground state magnetic moment for a needle of vanishing diameter ($\lambda = 0$), finite-diameter needle ($\lambda = 0.1$), sphere ($\lambda = 1$), and a disk of vanishing thickness ($\lambda = 2$). 35

3.5 Quantum phase diagram for the ground-state magnetic moment and the total angular momentum. 36

5.1 Energy spectrum as a function of coupling (both in units of ω) for $\Delta = 0.8\omega$. Comparison of first order approximation (Eq. (5.25), dotted line), second order correction (Eq. (5.28), thick dashed line) and numerical diagonalization (solid line). 68

6.1 Possible experimental geometries described by the models studied here. In both cases the easy axis of the macrospin coincides with the rotation axis of the oscillator. (a) Single molecule magnet grafted on a carbon nanotube. (b) Ensemble of single molecule magnets on a nanocantilever. 70

6.2 (a) Adiabatic $E_{\pm}(t)$ and diabatic $E_{\uparrow\downarrow}(t)$ energy levels of the LZ Hamiltonian as a function of time. (b) Probability $P(t)$ of staying in the initial $|\downarrow\rangle$ state as a function of time, and asymptotic staying probability P_{LZ}. 72

6.3 Energy (in units of Δ) as a function of time for $r = 20$, $\lambda = 1$, $\epsilon = 1.35$. Solid lines are adiabatic energy levels $E_{n\pm}$, and diabatic energies $E_{n\downarrow\uparrow}$ are dashed lines in the insets. Crossings occur at t_k. 76

6.4 Time dependence of the probability that the spin stays in the initial spin-down state for initial state $\Psi(-\infty) = |0\rangle|\downarrow\rangle$ with $\epsilon = 1.35$. Vertical lines at t_k denote avoided crossing of adiabatic energy levels. Horizontal lines are exact results P_N for independent transitions. 79

6.5 Time dependence of the probability that the spin stays in the initial spin-down state for an initial coherent oscillator state $\Psi(-\infty) = |\beta\rangle|\downarrow\rangle$ with $\epsilon = 1.35$. Vertical lines at t_k denote avoided crossing of adiabatic energy levels. Horizontal lines are exact results P_N for independent transitions when starting in the $|0\rangle|\downarrow\rangle$ state. 80

6.6 Time dependence of the rotation angle expectation value for initial state $\Psi(-\infty) = |0\rangle|\downarrow\rangle$ with $\epsilon = 1.35$. Vertical lines at t_k denote avoided crossing of adiabatic energy levels. 82

6.7 Time dependence of the rotation angle expectation value for initial coherent state $\Psi(-\infty) = |\beta\rangle|\downarrow\rangle$ with $\epsilon = 1.35$. Vertical lines at t_k denote avoided crossing of adiabatic energy levels. 83

6.8 Time dependence of the effective probability $P(t) = (1-\langle\sigma_z\rangle)/2$ for the z-component of a large spin in the semiclassical model, with various initial conditions and $\epsilon = 1.35$. 86

6.9 Time dependence of the rotation angle in the semiclassical model, with various initial conditions and $\epsilon = 1.35$. 87

1

Introduction

Quantum tunneling allows a particle to go through a potential energy barrier that it does not have enough energy to surmount classically [2]. Quantum tunneling was originally used to describe microscopic phenomena such as molecular structure [3, 4], ionization [5], and radioactive alpha decay [6, 7, 8, 9, 10]. In the textbook example [11] of an ammonia molecule, NH_3, three hydrogen atoms in a triangle with a nitrogen atom on one side or the other of that plane form a tetrahedron. These two states, say with the nitrogen to the left $|L\rangle$ or right $|R\rangle$ of the hydrogen plane, are equal in energy yet separated by a potential barrier due to Coulomb repulsion between the nitrogen nucleus and the hydrogen protons. Tunneling between these two states creates quantum superpositions of $|L\rangle$ and $|R\rangle$, with the lowest energy doublet given by $|L\rangle \pm |R\rangle$. If the molecule is initially in the $|L\rangle$ state, the expectation value of the position of the nitrogen atom will oscillate harmonically between left and right with frequency $\omega = \Delta/\hbar$, where Δ is the tunnel splitting of the doublet.

Macroscopic quantum tunneling addresses the question of whether macroscopic systems can be in quantum states which are linear superpositions of states with different macroscopic properties [12]. Macroscopic quantum tunneling of the magnetic moment in a single domain magnetic particles and single molecule magnets [13] describes the reversal of a macroscopically large magnetic moment, by under-barrier processes allowed only by quantum mechanics. A similar situation occurs in a flux qubit [14], a superconducting ring with one or more Josephson junctions, which can support a superposition of clockwise and counterclockwise currents of a few micro-Amperes.

The simplest picture of quantum tunneling between metastable states involves a double well potential with quantized energy levels in each well. In the case of NH_3 we can think of this as a

potential barrier for the N atom to go from one side of the H_3 triangle to the other, or vice versa. A more complete consideration shows that the nitrogen atom and hydrogen triangle must co-tunnel in order to conserve the linear momentum of the molecule's center of mass. A tunneling process such as gamma ray emission results in nuclear recoil, which means the final energy of the gamma ray is less than the nuclear transition that created it. The Mössbauer effect describes gamma ray emission in which the entire solid absorbs the recoil, allowing resonance absorption [15, 16].

Similarly, quantum tunneling of the magnetic moment must conserve the total angular momentum $\mathbf{J} = \mathbf{L} + \mathbf{M}/\gamma$, where $\mathbf{L}$ is the angular momentum due to mechanical rotations, $\mathbf{M}$ is the magnetic moment, and γ is the gyromagnetic ratio. The necessity to conserve angular momentum in quantum tunneling of the magnetization was first pointed out by Chudnovsky [17] and later worked out with precision in Refs. [18, 19, 20]. In a rigid body, reversal of the magnetic moment $\mathbf{M} \longrightarrow -\mathbf{M}$ must be accompanied by a change in the angular momentum $2\mathbf{M}/\gamma$, with corresponding rotational kinetic energy $\mathbf{L}^2/2I$, with I being the moment of inertia. For a tunneling magnetic moment embedded in a large solid matrix this energy gain is negligible due to a large moment of inertia, thus there is no observable effect on spin dynamics. However, for a nanometer-sized particle this energy is non-negligible and must be considered in conjunction with quantum tunneling of the magnetic moment. Without coupling to a large solid matrix, tunneling should be suppressed. Real solids are not absolutely rigid and tunneling of a spin involves elastic twists that absorb the change of angular momentum. The change propagates away from the spin in the form of sound waves.

Motivated by fundamental questions of angular momentum conservation in macroscopic quantum tunneling of the magnetization and recent experiments on nanoscale magnetic systems with rotational degrees of freedom, we study quantum rotational effects in nanomagnetic systems. Following recent theoretical work [21], we study renormalization of the tunnel splitting by calculating the exact instanton of a nanomagnet that is free to rotate about its anisotropy axis. We solve the problem of a tunneling spin in a free symmetric particle, finding that the ground state energy exhibits first and second order quantum phase transitions, and present the phase diagram of the magnetic moment. In our study of flux qubit, we find that coupling to a macroscopically large rigid body or elastic environment is consistent with low decoherence. Considering the recent theoretical [22, 23, 24] and experimental [25, 26, 27, 28] interest in nanomagnet-oscillator systems, we study the Landau-Zener dynamics in such a system, finding multi-stage transitions in certain parameter

ranges which should be experimentally observable.

This thesis is organized as follows. The remainder of Chapter 1 will give a brief history of nanomagnetism, discuss the interplay between magnetization and rotations, and outline developments leading up to the work described here. In Chapter 2 we study renormalization of the tunnel splitting due to rotational freedom of a nanomagnet using the instanton method. Chapter 3 gives the exact solution of a quantum model of a tunneling spin embedded in a symmetrical rigid rotor. We present a study of decoherence of a flux qubit due to transfer of angular momentum to the surrounding body in Chapter 4. In this chapter we also consider a magnetic molecule embedded in helium crystal where effects of angular momentum conservation can be quite significant. Chapter 5 is devoted to the mathematics of the spin-boson model. In Chapter 6 we study the Landau-Zener dynamics of a nanomagnet-oscillator system. Chapter 7 offers concluding remarks and possible directions for future work.

1.1 Background

A nanomagnet is a particle whose magnetization can be described as a single magnetic moment or large spin of fixed length. In the absence of an external magnetic field, neighboring spins in a bulk ferromagnet such as iron will tend to align due to strong exchange interaction, with energy ϵ_{ex}. The ferromagnet will generally break up into magnetic domains in which all the spins point in the same direction within a single domain, but different domains will point in different directions in order to reduce the magnetostatic energy due to dipole interactions ϵ_d. Domains are separated by domain walls in which the magnetization changes direction from one domain to the next over a small distance. The typical size $\delta \simeq a\sqrt{\epsilon_{ex}/\epsilon_{an}}$ of a domain wall in a ferromagnet is generally a few hundred lattice spacings a, and is determined by the balance of the exchange energy and anisotropy energy ϵ_{an}. Strong exchange interaction makes nonuniform rotation of magnetization on scales less than δ unlikely. Dipolar interactions depend on the shape of the particle and effectively contribute to the magnetic anisotropy. A sufficient, but not necessary, condition for a single domain particle is that the size of the particle be smaller than the domain wall width. For weak crystal field anisotropy ($\epsilon_{an} \ll \epsilon_d$) the maximum size of the particle is [13] $R_0 = \delta\sqrt{\epsilon_{an}/\epsilon_d}$ whereas for strong crystal field anisotropy ($\epsilon_{an} \gg \epsilon_d$), $R_0 = \delta\epsilon_{an}/\epsilon_d$. For weak anisotropy, e.g. iron, the domain wall size $\delta \simeq 50$

nm gives the maximum single domain particle size $R_0 \simeq 15$ nm, whereas for strong anisotropy, e.g. MnBi, $\delta \simeq 10$ nm and $R_0 \simeq 500$ nm [13]. For strong anisotropy, even particles large compared to the domain wall size will have a single magnetic domain of fixed magnitude. Alternatively, for smaller particles with stronger anisotropy the anisotropy will be determined by the strong crystal field which dominates dipolar effects due to shape of the particle.

With strong anisotropy, the magnetic moment of a single domain particle will point in either direction along the anisotropy axis, say up and down. These degenerate energy minima are separated by a potential barrier U. At thermal equilibrium the temperature dependence of the flipping time t_f between up and down follows an Arrhenius law [29] $t_f = t_0 e^{-U/k_B T}$, where the prefactor t_0 is of the order of the ferromagnetic resonance frequency. As the temperature is lowered, spin flips are effectively blocked beneath a blocking temperature $T_B = U/\ln(t/t_0)$, where t is the typical measurement time in the experiment. Since parameters of nanoparticles appear in the exponent, the differences in relaxation times between single domain ferromagnetic particles and single molecule magnets can be astronomical. Thermal transitions between different orientations of the magnetic moment, separated by energy barriers, freeze out below the blocking temperature.

The possibility of quantum tunneling of the magnetic moment in small particles was first suggested by Bean and Livingston [30]. They proposed this to explain experiments [31] which showed that transitions between different orientations of the magnetic moment persisted even as the temperature was reduced towards absolute zero. Two explanations were suggested. The first [32] involved nucleation of a domain wall in relatively large particles, although the tunneling probability of this transition is very small due to the finite mass of the wall and the fact that the height of the energy barrier scales with the volume of the particle [33]. The second mechanism, uniform subbarrier rotation of the magnetic moment in particles smaller than the domain wall width, was suggested by Chudnovsky [34] within a path integral method. Later, Chudnovsky and Gunther used the instanton method developed in Ref. [34] to compute tunneling probability for various symmetries of magnetic anisotropy [35], see also Refs. [36, 37]. The macroscopic dynamics of a fixed-length magnetic moment, $\mathbf{M}$, of a single-domain ferromagnetic particle is described by the Landau-Lifshitz equation [38, 29]. When dissipation (which is usually weak) is neglected this equation reads

$$\frac{\partial \mathbf{M}}{\partial t} = \gamma \mathbf{M} \times \mathbf{B}_{eff}, \;\; \mathbf{B}_{eff} = -\frac{\delta \mathcal{E}}{\delta \mathbf{M}}\,, \tag{1.1}$$

where $\mathcal{E}$ is the classical magnetic energy of the particle that depends on the orientation of $\mathbf{M}$. Besides real-time solutions, Eq. (2.1) also possesses imaginary-time solutions, instantons, that describe macroscopic quantum tunneling of $\mathbf{M}$ between classically degenerate energy minima [35, 13].

Measurements of individual nanometer-sized single domain particles [39] soon gave way to the discovery of crossover between thermally-assisted magnetization reversal and quantum tunneling in small ferromagnetic particles [40, 41, 42]. Around this same time, the discovery large spin [43] and magnetic bistability [44] of the single molecule magnet Mn_{12}, originally synthesized in 1980 [45]. The observation of nonmonotonic dependence of relaxation time on external magnetic field [46], also included the first suggestion of the coincidence of energy level schemes in two sides of the potential well.

The first unambiguous evidence of macroscopic quantum tunneling of the magnetic moment in crystals of Mn_{12} was obtained by Friedman et al. [47] in 1996, and confirmed shortly thereafter by other researchers [48, 49]. This discovery is recognized as one of the major breakthroughs in spin physics [50]. Friedman et al. [47] were the first to discover steps in the hysteresis curve of a crystal of Mn_{12}-ac. An example of the stepwise hysteresis curve is shown in Fig. 1.1. The steps occur only as specific values of the magnetic field, in this case regular multiples of about 0.5 T. A single molecule magnet with uniaxial anisotropy in a magnetic field applied along the easy axis is described by the Hamiltonian

$$\hat{H} = -DS_z^2 - g\mu_B B_z S_z + \hat{H}_\perp, \tag{1.2}$$

where g is the Landé g-factor, μ_B is the Bohr magneton, and B_z is the magnetic field. $\hat{H}_\perp$ contains terms that do not commute with S_z and breaks the degeneracy between eigenstates of S_z at zero field. Although $\hat{H}_\perp$ is small compared to the first term, without it there would be no quantum tunneling between states on opposite sides of the potential barrier. $\hat{H}_\perp$ can arise from transverse anisotropy, an external transverse field, or lattice imperfections.

Major results on single molecule magnets since their discovery include understanding the crossover between thermally assisted and quantum tunneling [51], and explanation of hysteresis curve steps by distribution of local easy axis orientation [52]. Berry phase interference [53] was proposed in quantum tunneling of the magnetization [54, 55, 56] even before its unambiguous discovery, and realized not long after in Fe_8 [57] and Mn_{12} [58]. Variants of Mn_{12} have motivated the prediction [59]

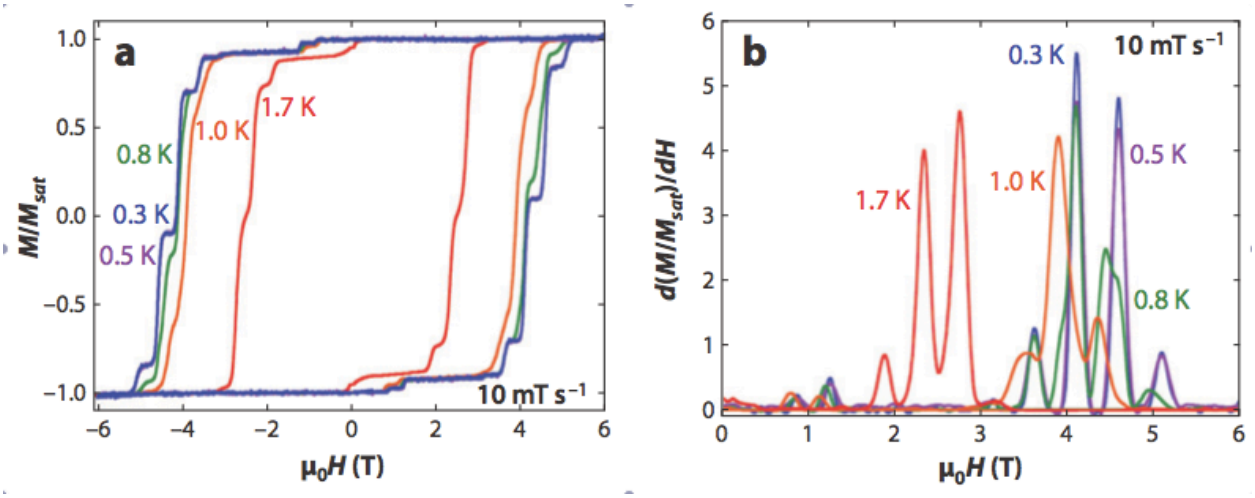

Figure 1.1: (a) Normalized saturation magnetization of a Mn_{12}-ac crystal as a function of longitudinal magnetic field for different temperatures below the blocking temperature and a sweep rate of 10 mT / s. (b) Derivative of the magnetization in (a) as a function of the magnetic field. Reprinted from Ref. [1]

and realization [60] of the random-field Ising model.

In early experiments on spin tunneling, single-domain magnetic particles were always frozen in a solid matrix so that their physical position and orientation were fixed and only rotation of the magnetic moment was allowed. Later, beams of small magnetic clusters were investigated [61, 62, 63, 64, 65, 66, 67, 68, 69]. More recently, free magnetic nanoparticles confined within solid nanocavities have been studied [70]. Experimentalists have also worked with molecular nanomagnets deposited on surfaces [71, 72, 73, 74], grafted onto carbon nanotubes [75, 76, 77], and bridged between metallic electrodes [78, 79, 80, 81, 82]. In such experiments the magnetic particles retain some mechanical freedom.

Magneto-mechanical effects were discovered almost a century ago. The Einstein-de Haas effect [83, 84] and Barnett effect [85] describe rotation by magnetization and magnetization by rotation, respectively. Experiments focusing on the relationship between magnetic and mechanical dynamics on the microscale include measurement of the magneto-mechanical ratio of a thin ferromagnetic film on a microcantilever [25], and demonstration of precision torque magnetometers in nanomechanical detection of itinerant electron spin-flip at a ferromagnet-normal metal junction [86] and phase transitions of small magnetic disks in and out of the vortex state [26]. Theoretical interest in classical magnetization dynamics combined with oscillatory motion [87, 88, 89, 90] provided

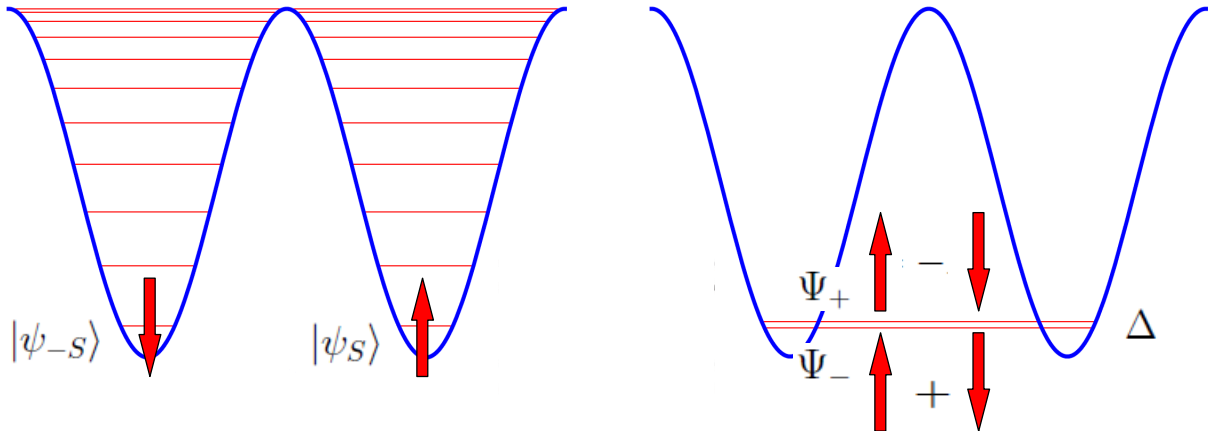

Figure 1.2: Double well potential and energy levels of a large spin with strong magnetic anisotropy. The left figure shows all $2S+1$ energy levels and the right shows the lowest tunneling doublet.

possible explanations of recent observations and suggestions for new directions in experimental and applied research. Realizing a quantum magneto-mechanical system with strong spin-phonon coupling has been an experimental challenge.

The first attempt to understand how mechanical freedom of a small magnetic particle affects tunneling of the magnetic moment was made in Ref. [17], where it was noticed that tunneling of a macrospin in a free particle must be entangled with mechanical rotations in order to conserve the total angular momentum. Subsequent work focusing on conservation of momentum in tunneling processes [18, 19, 20] provided lower bounds on coherence lifetimes in spin tunneling systems.

A recent experiment [28] has shown the first evidence of strong spin-phonon coupling in a single molecule magnet grafted onto a carbon nanotube. Semiclassical models of Landau-Zener dynamics have been developed to describe magnetic molecules coupled to mechanical resonators and bridged between conducting leads [22, 91]. A full quantum treatment of the interaction between a single spin and a torsional oscillator predicts interference and entanglement effects [24, 23]. We investigate the Landau-Zener dynamics in a fully quantum model [92] in Chapter 6.

Theoretical work describing spin tunneling in free magnetic partices has been scarce. Recently, it was demonstrated [21] that the problem of a rigid rotor with a spin can be solved exactly in the laboratory frame when mechanical rotation is allowed only about a fixed axis and the spin states are reduced to spin-up and spin-down due to strong magnetic anisotropy. The latter is typical for

magnetic molecules and small ferromagnetic clusters. The reduction to two spin states in a system rotating about a fixed axis also allows one to obtain simple solution of the problems of a magnetic molecule embedded in a microcantilever [90], magnetic molecule vibrating between conducting leads [22], and of a macrospin tunneling inside a torsional resonator [24, 23]. As demonstrated in Ref. [21], the exact eigenstates and exact energy levels can be obtained analytically for a nanomagnet that, due to a large magnetic anisotropy, can be described as a two-state spin system and is free to rotate about its magnetic anisotropy axis. Such a system at rest is described by the Hamiltonian

$$\hat{\mathcal{H}}_\sigma = -(\Delta/2)\sigma_x, \tag{1.3}$$

where σ_x is a Pauli matrix and Δ is the tunnel splitting of spin-up and spin-down states, with z being the anisotropy axis. It arises from the terms in the full Hamiltonian that do not commute with the z-component of the total spin $\mathbf{S}$. Rotation of the particle by the angle φ about the Z-axis transforms the two-state Hamiltonian into [21]

$$\hat{\mathcal{H}}'_\sigma = -\frac{\Delta}{2}\left[\cos(2S\varphi)\sigma_x + \sin(2S\varphi)\sigma_y\right] \tag{1.4}$$

(S is dimensionless). Exact eigenvalues of the full Hamiltonian of a nanomagnet rotating about its anisotropy axis,

$$\hat{\mathcal{H}} = (\hbar L_z)^2/(2I) + \hat{\mathcal{H}}'_\sigma \tag{1.5}$$

(where L_z is the z-component of the dimensionless mechanical angular momentum and I is the moment of inertia), were obtained in Ref. [21], where it was shown that parameter

$$\alpha = \frac{2(\hbar S)^2}{I\Delta} \tag{1.6}$$

determines low energy states of the particle. At $\alpha < \alpha_1 \equiv \left[1 - 1/(2S)^2\right]^{-1}$ the ground state and the first excited state are respectively symmetric and antisymmetric superpositions of $\mathbf{J} = \mathbf{L} + \mathbf{S} = 0$ with energies $\pm\Delta$ (up to an unessential constant). The general problem of a tunneling spin in a free particle is solved exactly in Chapter 3 for a symmetric rotor [93]. We note here that in this and other models, the tunnel splitting Δ is treated as a fixed parameter. In Chapter 2 we show that the

tunnel splitting is renormalized by mechanical freedom [94].

Flux qubits are formed by quantum superposition of current states in a superconducting loop interrupted by one or more Josephson junctions [95, 96]. The same necessity of angular momentum conservation occurs for tunneling of a superconducting current between clockwise and counterclockwise directions in a SQUID [14, 97, 96, 98, 99]. Quantum mechanics of such a qubit is also described by a double-well potential similar to the ammonia molecule, see above. In the simplest formulation of the flux qubit problem the role of left and right is played by clockwise and counterclockwise directions of the current. Typical values of the angular momentum associated with the current range from a few hundred $\hbar$ for a submicron SQUID loop [97], to $10^5\hbar$ for a micron-size loop [100], to $10^{10}\hbar$ for larger SQUIDs [14]. To conserve the angular momentum the tunneling of the current between clockwise and counterclockwise directions must be accompanied by quantum transitions between mechanical clockwise and counterclockwise rotations of the body containing the flux qubit. This creates a controversy [101]. Indeed, the co-tunneling of the superconducting current and mechanical rotation needed to conserve the angular momentum requires entanglement of quantum states of the flux qubit with quantum states of a macroscopic body. In any reasonable experiment the phase of the wave function of the equipment containing the flux qubit must be destroyed instantaneously. Then how can the flux qubit preserve coherence on a measurable time scale? Our work, described in Chapter 4, is devoted to the detailed analysis of the entanglement of current states with mechanical rotations and its implications for superconducting qubits [102]. Zero point oscillations of a crystal lattice will also renormalize the tunnel splitting of a nanomagnet. We derive an exact expression for this effect in Chapter 4 and propose an experiment in which a magnetic nanoparticle is embedded in a helium crystal.

The model of a flux qubit in an elastic environment is a variant of the spin-boson model [103] used to describe a two-level system interacting with a bath of quantum harmonic oscillators. Similarly, a tunneling macrospin coupled to a torsional oscillator is related to the single-mode spin-boson model, also known as the quantum Rabi model. The Rabi model has found widespread usage especially in describing atom-field interactions in cavity quantum electrodynamics, and has been applied to describe a variety of two-level systems interacting with a single bosonic mode. The (semiclassical) Rabi model [104, 105] was originally proposed to describe the dynamics of a spin in a rotating classical magnetic field. Applying the rotating wave approximation to the quantum Rabi model gives

the Jaynes-Cummings model [106], which is exactly solvable and has become one of the most widely studied models in quantum optics [107], valid for small detuning and weak coupling. While there was some early theoretical work on the Rabi model without the rotating wave equation [108, 109], the success of the Jaynes-Cummings model in describing atom-field interactions left it relatively untouched. Recent experimental progress in circuit quantum electrodynamics [110, 111] has shown that the Jaynes-Cummings model fails to describe the strongly coupled dynamics. This has renewed theoretical interest in the strong coupling regime [112, 113, 114]. In particular, Braak has found an analytical solution of the quantum Rabi model [115] and states that quantum integrability requires characterization of quantum numbers corresponding to every degree of freedom which characterized each eigenstate, but not necessarily the existence of additional conserved quantities. This has ignited intense interest both in this particular model and in the definition of quantum integrability [116, 117, 118]. In Chapter 5 we study some mathematical aspects of this problem.

One other problem we study is the Landau-Zener dynamics of a mechanical resonator containing a tunneling spin. The Landau-Zener model [119, 120, 121, 122] describes a two-state system in which the bias between diagonal states varies linearly with time as they are swept through an avoided crossing. It is one of the few practically important time-dependent Hamiltonians for which the Scrhödinger equation is exactly solvable. The Landau-Zener method has recently found a natural application in the experimental characterization of single molecule magnets [57]. Theoretical studies of Landau-Zener transitions in nanomagnets have included many-body effects [123] and superradiance [124, 125]. Some important theorems have been proven about generalizations of the Landau-Zener problem [126, 127], and certain multilevel cases have been exactly solved [128]. It has been used as a model for the dynamics of quantum phase transitions [129], and topological defect formation [130]. A natural extension of the two-level quantum physics is the two-level system coupled to one or several quantized modes of a harmonic oscillator. Studies of Landau-Zener oscillator dynamics have probed coherent [131, 132], dissipative [133, 134], and temperature-dependent [135] effects. Landau-Zener interferometry has provided a quantitative measure of coupled dynamics [136] and has been experimentally verified in the nanomechanical measurement of a superconducting qubit [98].

The Landau-Zener effect in spin systems should be considered in conjunction with the transfer of angular momentum manifested in the Einstein - de Haas effect. We propose multiple schemes to

realize strongly coupled dynamics of a tunneling macrospin with torsional oscillations of a nanoresonator in a Landau-Zener experiment. We investigate the Landau-Zener dynamics of a tunneling spin coupled to a torsional oscillator, using a fully quantum mechanical model. The oscillator could be a torsional paddle resonator, a microcantilever, a carbon nanotube, or a single magnetic molecule between two point contacts. The tunneling spin could be a single molecule magnet, an ensemble of single molecule magnets, or a single-domain ferromagnetic particle with strong uniaxial anisotropy. For a collection of single molecule magnets placed on a torsional resonator or cantilever far apart from each other that they are not directly coupled through dipole interactions, we develop a semiclassical model of magnetization dynamics. We predict superradiant enhancement [125] of the spin-phonon coupling for this ensemble system. Comparison of these two models shows their correspondence.

As has been already pointed out, the coupling between spin and mechanical angular momentum is mandated by the conservation of total angular momentum. Similar effects arise in systems that undergo torsional oscillations [22, 23, 24]. Examples are a single molecule magnet bridged between conducting leads, a nanomagnet attached to a carbon nanotube bridge, or a nanomagnet coupled to a resonator such as a torsional paddle oscillator or microcantilever. The mechanical resonance occurs at a frequency $\omega_r = \sqrt{k/I_z}$, where k is the effective stiffness against the linear restoring torque and I_z is the moment of inertia of the nanomagnet-resonator combination. A convenient measure of the effect of oscillations is the dimensionless parameter $r = \hbar\omega_r/\Delta$, the ratio between the oscillator energy to tunnel splitting. As we will see in Sec. 6.1, the coupling between magnetization and oscillator dynamics is given by the factor $\lambda = \sqrt{\alpha/r} = \sqrt{2\hbar S^2/I_z\omega_r}$. The most interesting effects occur for strong coupling $\lambda \sim 1$ and oscillator frequency much larger than tunnel splitting $r \gg 1$. A large spin, small moment of inertia, and weak torsional spring constant are required for strong coupling.

2

Renormalization of the tunnel splitting in a rotating nanomagnet

In this chapter we study quantum tunneling of the magnetic moment in a magnetic nanoparticle with biaxial anisotropy that is free to rotate about its anisotropy axis. The exact instanton of the coupled equations of motion is found that connects degenerate classical energy minima. We show that mechanical freedom of the particle renormalizes magnetic anisotropy and increases the tunnel splitting.

The exact eigenstates and energy levels for a nanomagnet with spin S that can rotate about its anisotropy axis [21], discussed in Sec. 1.1, were found to depend on the parameter

$$\alpha = \frac{2\hbar^2 S^2}{I\Delta},$$

where I is the moment of inertia about the axis of rotation, and Δ is the tunnel splitting due to a large magnetic anisotropy. α determines the low energy states of the particle. At $\alpha < \alpha_1 \equiv \left[1 - 1/(2S)^2\right]^{-1}$ the ground state and the first excited state are respectively symmetric and anti-symmetric superpositions of $\mathbf{J} = \mathbf{L} + \mathbf{S} = 0$ states shown in Fig. 2.1, with energies $E_\pm = \frac{\hbar^2 S^2}{2I} \pm \frac{\Delta}{2}$.

The derivation of these results was based upon the assumption that the parameter Δ is the same for a stationary magnetic particle and for a particle that is free to rotate. The instanton method allows one to test this assumption. Below we find the exact instanton solution of the equations of motion describing the dynamics of the magnetic moment and the rotation of the particle. It shows

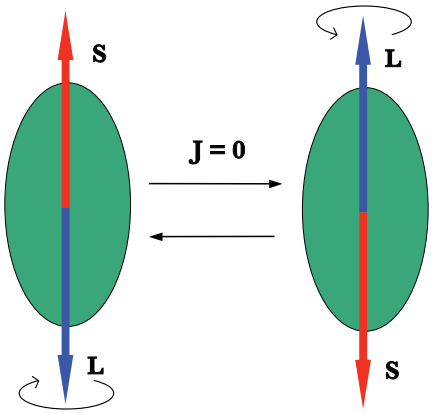

Figure 2.1: Spin and angular momentum tunneling in a rotating magnetic nanoparticle.

that mechanical freedom does renormalize the tunnel splitting Δ. However, this renormalization is small unless Δ is very large and α is close to α_1.

2.1 Magnetization Dynamics

The Landau-Lifshitz equation

$$\frac{\partial \mathbf{M}}{\partial t} = \gamma \mathbf{M} \times \mathbf{B}_{eff}, \quad \mathbf{B}_{eff} = -\frac{\delta \mathcal{E}}{\delta \mathbf{M}}, \tag{2.1}$$

describes the dynamics of a fixed-length magnetic moment $\mathbf{M}$ [38, 29]. Instanton solutions of this equation, found by switching to imaginary time, describe tunneling of the magnetic moment between classically degenerate energy minima [34, 35, 13].

Consider a high-spin magnetic particle with biaxial anisotropy that is free to rotate about its easy axis. The initial state of the particle is such that its total angular momentum is zero, $\mathbf{J} = \mathbf{S} + \mathbf{L} = 0$. In other words, the total spin (magnetization) vector points along the easy axis and the particle rotates about this axis such that these angular momenta are equal in magnitude and opposite in direction, see Fig. 2.1. The exchange interaction between individual spins is strong, so the magnitude of the total spin of the particle is a constant. The magnetic energy will be expressed below in terms of $\mathbf{M}$ which is proportional to the spin, $\hbar \mathbf{S} = \mathbf{M}/\gamma$. Here $\gamma = -e/2mc < 0$ is

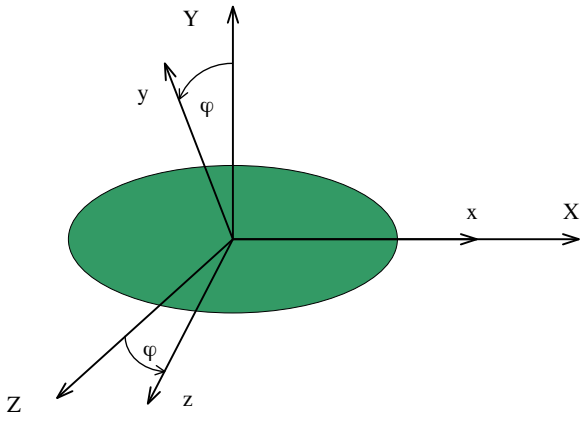

Figure 2.2: Geometry of particle and laboratory frames.

the electron gyromagnetic ratio. The orbital angular momentum is associated with the rotational motion of the particle itself, $\hbar\mathbf{L} = I\dot{\boldsymbol{\varphi}}$, where I is the particle's moment of inertia and $\dot{\boldsymbol{\varphi}}$ is its angular velocity.

We define coordinate systems of the lab frame (x, y, z) and particle frame (X, Y, Z) as shown in Fig. 2.2. In the particle frame the x-axis is along the easy axis in the xy easy plane, and the z-axis is the hard axis. The lab frame is centered at the same origin such that the X-axis of the lab frame coincides with the x-axis of the particle frame. The particle is free to rotate about this axis. At some initial time $t = 0$ we choose the two coordinate frames to coincide. The angle of rotation of the x- and z-axes with respect to the X- and Z-axes is $\varphi(t)$. Notice the change of the easy axis as compared to the choice of Ref. [21], which is dictated by the mathematics of the problem.

The anisotropy energy is naturally defined in the particle frame: $\mathcal{E}_A = k_\perp M_z^2 - k_\parallel M_x^2$. It can be written in terms of spherical polar coordinates (θ, ϕ) which are defined with respect to the particle-frame axes,

$$\mathcal{E}_A(\theta, \phi) = \frac{1}{2}\mu_0 M_0^2 V[(K_\perp + K_\parallel \cos^2\phi)\cos^2\theta + K_\parallel \sin^2\phi]\,. \tag{2.2}$$

Here μ_0 is the magnetic permeability of vacuum, V is the volume of the particle and $M_0 = M/V$

represents the magnetization which is a constant of the ferromagnetic material. Anisotropy constants $K_\perp > 0$ and $K_\parallel > 0$ have been redefined to show the explicit proportionality of the anisotropy energy to the volume. They are dimensionless numbers, typically of order unity.

The rotational kinetic energy of the particle is $\mathcal{E}_R = \frac{1}{2} I \dot{\boldsymbol{\varphi}}^2$. The Lagrangian of our system consists of the trivial kinetic Lagrangian for the variable $\boldsymbol{\varphi}$,

$$\mathcal{L}_L = \hbar \mathbf{L} \cdot \dot{\boldsymbol{\varphi}} - \mathcal{E}_R = \frac{1}{2} I \dot{\boldsymbol{\varphi}}^2 \,, \tag{2.3}$$

and the magnetic Lagrangian,

$$\mathcal{L}_S = \left(\frac{M_0 V}{\gamma} \right) \dot{\phi} \cos\theta - \mathcal{E}'_A(\theta, \phi) \,, \tag{2.4}$$

for the variables θ and ϕ. The first term in Eq. (2.4) follows from the fact that $\hbar S_z = \hbar S \cos\theta$ is the generalized momentum for the coordinate ϕ. The second term is the effective magnetic energy in the rotating frame,

$$\mathcal{E}'_A = \mathcal{E}_A(\theta, \phi) - \hbar \mathbf{S} \cdot \dot{\boldsymbol{\varphi}} \,. \tag{2.5}$$

The last term in this equation is related to the fact that in the particle frame the rotation is equivalent to the magnetic field $\mathbf{B} = \dot{\boldsymbol{\varphi}}/\gamma$.

The total Lagrangian of the particle is a sum of $\mathcal{L}_L$ and $\mathcal{L}_S$:

$$\mathcal{L} = \hbar(\mathbf{L} + \mathbf{S}) \cdot \dot{\boldsymbol{\varphi}} + \left(\frac{M_0 V}{\gamma} \right) \dot{\phi} \cos\theta - \left[\frac{1}{2} I \dot{\boldsymbol{\varphi}}^2 + \mathcal{E}_A(\phi, \theta) \right] . \tag{2.6}$$

The first term reflects the fact that in the presence of a spin the generator of rotations is $\mathbf{J} = \mathbf{L} + \mathbf{S}$. The explicit form of the total Lagrangian in terms of the generalized coordinates θ, ϕ, and φ is

$$\begin{aligned} \mathcal{L} = {} & \frac{1}{2} I \dot{\boldsymbol{\varphi}}^2 + \left(\frac{M_0 V}{\gamma} \right) \dot{\phi} \cos\theta + \left(\frac{M_0 V}{\gamma} \right) \dot{\varphi} \sin\theta \cos\phi \\ & - \frac{1}{2} \mu_0 M_0^2 V [(K_\perp + K_\parallel \cos^2\phi) \cos^2\theta + K_\parallel \sin^2\phi] \,. \end{aligned} \tag{2.7}$$

The equations of motion are Euler-Lagrange equations for θ, ϕ, and φ:

$$\frac{d\phi}{d\tilde{t}} = (K_\perp + K_\parallel \cos^2\phi)\cos\theta + \dot{\tilde{\varphi}}\,\frac{\cos\theta\cos\phi}{\sin\theta} \tag{2.8}$$

$$\frac{d(\cos\theta)}{d\tilde{t}} = -K_\parallel \cos\phi\sin\phi\sin^2\theta - \dot{\tilde{\varphi}}\sin\theta\sin\phi \tag{2.9}$$

$$\frac{d}{d\tilde{t}}\left[I\dot{\tilde{\varphi}} + \frac{V}{\mu_0\gamma^2}\cos\phi\sin\theta\right] = 0\,, \tag{2.10}$$

where we have introduced dimensionless time $\tilde{t} = \gamma\mu_0 M_0 t$ and $\dot{\tilde{\varphi}} = d\varphi/d\tilde{t}$.

Note that the equations of motion for ϕ and θ can also be obtained from the Landau-Lifshitz equation with $\mathcal{E} = \mathcal{E}'_A$. Indeed, the equations for ϕ and θ that follow from Eq. (2.1) (see, e.g., Ref. [29]),

$$\frac{\partial\phi}{\partial t} = -\frac{\gamma}{M\sin\theta}\left(\frac{\partial\mathcal{E}'_A}{\partial\theta}\right), \qquad \frac{\partial\theta}{\partial t} = \frac{\gamma}{M\sin\theta}\left(\frac{\partial\mathcal{E}'_A}{\partial\phi}\right), \tag{2.11}$$

are identical to the equations (2.8) and (2.9). The third equation of motion, Eq. (2.10), is the conservation of the total angular momentum:

$$\frac{d}{dt}[L_X + S_X] = \frac{d}{dt}J_X = 0\,. \tag{2.12}$$

At $J_X = 0$ it is equivalent to the constraint:

$$I\dot{\varphi} = -\frac{M_0 V}{\gamma}\sin\theta\cos\phi\,. \tag{2.13}$$

With account of this constraint the equations of motion for ϕ and θ become

$$\frac{d\phi}{d\tilde{t}} = (K_\perp + K'_\parallel \cos^2\phi)\cos\theta \tag{2.14}$$

$$\frac{d(\cos\theta)}{d\tilde{t}} = -K'_\parallel \cos\phi\sin\phi\sin^2\theta\,, \tag{2.15}$$

where

$$K'_\parallel = K_\parallel - K_R, \qquad K_R = \frac{V}{\mu_0\gamma^2 I}\,. \tag{2.16}$$

We see that for $\mathbf{J} = 0$ the effect of rotations reduces to the renormalization of the easy axis anisotropy $K_\parallel$. This is easy to understand from the following consideration. In a state with $J_x = 0$,

equilibrium vectors **S** and **L** look in the opposite directions along the x-axis. If **S** deviates from the x-axis, S_x decreases and so should L_x to preserve the condition $J_x = 0$. The decrease of L_x corresponds to the decrease of the rotational energy, $(\hbar L_x)^2/(2I)$, mandated by $J_x = 0$. Thus, effectively, the magnetic anisotropy energy associated with the deviation of **S** from the easy axis becomes smaller when mechanical rotation is allowed.

We should now look for solutions of equations (4.40) and (2.15). We first notice that

$$\mathcal{E} = \frac{1}{2}\mu_0 M_0^2 V[(K_\perp + K'_\parallel \cos^2\phi)\cos^2\theta + K'_\parallel \sin^2\phi] \tag{2.17}$$

is the integral of motion. This is easy to see by differentiating this equation on time and substituting in the resulting equation the time derivatives ϕ and θ from equations (4.40) and (2.15). Not surprisingly, up to a constant, Eq. (2.17) equals the total energy of the particle in the laboratory frame, $\mathcal{E} = \mathcal{E}_A + \frac{1}{2}I\dot{\boldsymbol{\varphi}}^2$, with account of the constraint (2.13). Eq. (4.40) gives

$$\cos\theta = \frac{d\phi/d\tilde{t}}{K_\perp + K'_\parallel \cos^2\phi}\,. \tag{2.18}$$

This allows one to express $\mathcal{E}$ in terms of the angle ϕ and its time derivative:

$$\mathcal{E} = \frac{1}{2}M_0^2 V\left[\frac{(d\phi/d\tilde{t})^2}{K_\perp + K'_\parallel \cos^2\phi} + K'_\parallel \sin^2\phi\right]. \tag{2.19}$$

Since this expression is positively defined, the classical energy minima occur at $\mathcal{E} = 0$. They correspond to the stationary magnetization pointing in either direction along the easy axis, i.e., $\phi = 0, \pi$ with $\cos\theta = 0$ in accordance with Eq. (2.18).

2.2 Instanton Solution

Equation $\mathcal{E} = 0$ has no real-time solutions for ϕ that connect the two degenerate classical energy minima. However, in imaginary time, $\tilde{\tau} = i\tilde{t}$, equation $\mathcal{E} = 0$ is equivalent to

$$\left(\frac{d\phi}{d\tilde{\tau}}\right)^2 = K'_\parallel \sin^2\phi\,(K_\perp + K'_\parallel \cos^2\phi)\,. \tag{2.20}$$

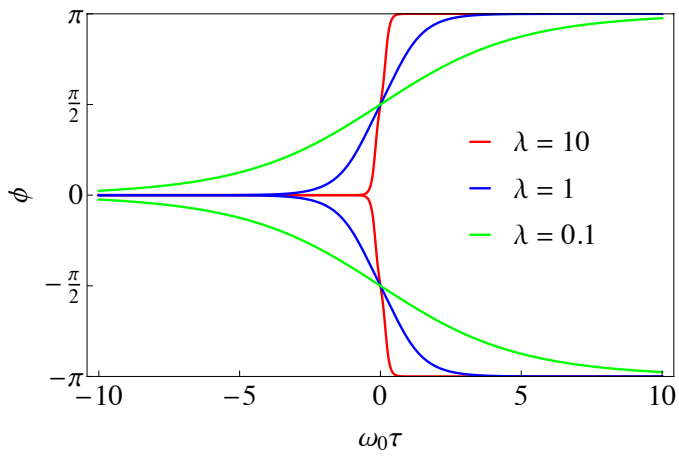

Figure 2.3: Dependence of ϕ on τ for clockwise and counterclockwise underbarrier rotations of $\mathbf{M}$.

Such equation has instanton solutions that connect the classical energy minima:

$$\phi(\tau) = \pm \arccos\left\{ -\frac{\sinh(\omega_0 \tau)}{\sqrt{\lambda + \cosh^2(\omega_0 \tau)}} \right\} . \tag{2.21}$$

The τ-dependence of θ is given by Eq. (2.18), and the τ-dependence of φ is given by Eq. (2.13). Here

$$\lambda = K'_{\parallel}/K_{\perp}, \qquad \omega_0 = |\gamma|\mu_0 M_0 \sqrt{K'_{\parallel}(K'_{\parallel} + K_{\perp})} \, . \tag{2.22}$$

The positive and negative signs correspond to the two possible trajectories, which are counterclockwise and clockwise rotations of the magnetization from $\phi = 0$ at $\tau = -\infty$ to $\phi = \pm\pi$ at $\tau = +\infty$, respectively, see Fig. 2.3.

The tunnel splitting has the form $\Delta = Ae^B$, where A is of the order of quantized oscillations near the minimum of the potential well and

$$B = \frac{i}{\hbar} \int_{-\infty}^{+\infty} dt \mathcal{L} \tag{2.23}$$

is the WKB exponent. Substituting here $\mathcal{L}$ of Eq. (2.6) at $\mathbf{J} = 0$, one obtains for the instanton

trajectory

$$B = -S \ln \left(\frac{\sqrt{1+\lambda} + \sqrt{\lambda}}{\sqrt{1+\lambda} - \sqrt{\lambda}} \right) . \tag{2.24}$$

2.3 Discussion and Conclusions

To see the effect of the mechanical freedom of the particle on spin tunneling we define a dimensionless parameter $\alpha' = K_R/K_\parallel$. In a microscopic theory the easy-axis crystal field is presented as $-DS_z^2$. The connection between D and the parameter $K_\parallel$ of the macroscopic theory is [29]

$$K_\parallel = \left(2 - \frac{1}{s}\right) \frac{DV_0}{\mu_0(\hbar\gamma)^2} , \tag{2.25}$$

where s is spin per unit cell of the crystal and V_0 is the volume of the unit cell. (Singularity at $s = 1/2$ reflects the fact that single-ion magnetic anisotropy does not exist for spin 1/2). The total spin of a ferromagnetic particle can be presented as $S = s(V/V_0)$. Consequently,

$$\alpha' = \frac{S\hbar^2}{(2s-1)ID} = \frac{\Delta}{(2s-1)2SD}\,\alpha , \tag{2.26}$$

where we have used Eqs. (1.6) and (2.16). Renormalization of the easy-axis anisotropy by rotations can be presented in the form $K'_\parallel = K_\parallel(1-\epsilon)$, where

$$\epsilon = \left(\frac{\alpha}{2s}\right) \left(\frac{1 - \frac{1}{2S}}{1 - \frac{1}{2s}} \right) \frac{\Delta}{E_1} \tag{2.27}$$

and $E_1 = (2S-1)D$ is the energy of the first excited spin state at $\Delta = 0$. The low energy limit that we are studying corresponds to $\Delta \ll E_1$ and $\alpha < \alpha_1 \equiv \left[1 - 1/(2S)^2\right]^{-1}$, see Ref. [21]. In this limit ϵ is small. Consider, e.g., the case of large S and large λ (small tunneling rate). According to Eq. (2.24) in this case $B = -S\ln(4\lambda)$ so that $\Delta \propto \exp\left[-S\ln(4\lambda)\right]$. It is easy to see from this expression that mechanical rotation renormalizes Δ by a factor $\exp(\epsilon S)$. Normally it would not be large compared to one. However, since small ϵ in the exponent is multiplied by a large S, it is not out of question that at sufficiently large Δ a slight increase of the tunnel splitting would be observable in spin clusters that are free to rotate.

3

Quantum Tunneling of the Magnetic Moment in a Free Nanoparticle

We study spin tunneling in a particle that has full rotational freedom. We show that the problem of a two-state macrospin inside a symmetric rigid rotor has a rigorous solution for arbitrary rotations in the coordinate frame that is rigidly coupled to the rotor. We calculate the exact energy levels and eigenstates. Mechanical freedom of the rotor manifests itself in a strong dependence of the ground-state magnetic moment on the moments of inertia of the rotor. The energy exhibits quantum phase transitions between states with different values of the magnetic moment, and we obtain the quantum phase diagram.

Recent experimental studies of free magnetic particles in molecular beams [66, 67, 68, 69] and inside solid nanocavities [70] pose the problem of a rigid quantum rotor with a spin. Recently, it was demonstrated [21] that the problem of a rigid rotor with a spin can be solved exactly in the laboratory frame when mechanical rotation is allowed only about a fixed axis and the spin states are reduced to spin-up and spin-down due to strong magnetic anisotropy. Without a spin this problem is tractable by analytical methods only for a symmetric rotor [137]. Complications resulting from spin degrees of freedom make even symmetric cases significantly more difficult [138]. The reduction to two spin states in a system rotating about a fixed axis also allows one to obtain a simple solution of the problems of a magnetic molecule embedded in a microcantilever [90], magnetic molecule vibrating between conducting leads [22], and of a macrospin tunneling inside a torsional resonator

[24, 23]. We solve the problem of arbitrary rotations of a two-state spin system in a symmetric rotor, which is relevant to free magnetic nanoparticles.

The magnetic moment of an electrically neutral rotor is entirely due to its spin, and depends on the relative contribution of the up and down spin states. When a nanoparticle is embedded in a solid, tunneling of the spin results in a zero ground-state magnetic moment. This situation changes for a free particle due to a complex interplay between spin and mechanical angular momentum that conserves the total angular momentum. We show that the energy of the particle exhibits first- or second-order quantum phase transitions between states with different values of the total angular momentum. The order of the transition depends on the shape of the particle. The ground-state magnetic moment of a free particle with a total spin S can be anything between zero and $g\mu_B S$, depending on the principal moments of inertia (with μ_B being the Bohr magneton and g being the gyromagnetic factor associated with the spin).

The structure of this chapter is as follows. Quantum theory of a rigid rotator is briefly reviewed in Sec. 3.1. Theory of a tunneling macrospin is reviewed in Sec. 3.2. Quantum states of a rigid rotator containing a tunneling macrospin are constructed in Sec. 3.3. The ground state of a symmetric rotor with a spin is analyzed in Sec. 3.4. The ground-state magnetic moment is studied in Sec. 3.5. Our conclusions are presented in Section 3.6.

3.1 Quantization of rigid body rotations

Consider first the problem of rigid body rotations without a spin. We choose the coordinate frame that is rigidly coupled with the rotating body and direct the axes of that frame x, y, and z along the principle axes of the tensor of moments of inertia of the body. In this coordinate frame the Hamiltonian of mechanical rotations is given by [137]

$$\hat{H}_R = \frac{\hbar^2}{2}\left(\frac{L_x^2}{I_x} + \frac{L_y^2}{I_y} + \frac{L_z^2}{I_z}\right). \tag{3.1}$$

Here I_x, I_y, I_z are the principal moments of inertia and L_x, L_y, L_z are projections of the operator of the mechanical angular momentum, defined in the rotating (body) frame, onto the body axes x, y, z. Such a choice of coordinates and operators results in the anomalous commutation relations

[139], $[L_i, L_j] = -i\epsilon_{ijk}L_k$ (notice the minus sign in the right-hand side), but does not affect the relations $\mathbf{L}^2 = L(L+1)$, $[\mathbf{L}^2, L_z] = 0$.

For a symmetric rotor two of the moments of inertia are the same, $I_x = I_y$, and the Hamiltonian can be written as

$$\hat{H}_R = \frac{\hbar^2 \mathbf{L}^2}{2I_x} + \frac{\hbar^2 L_z^2}{2}\left(\frac{1}{I_z} - \frac{1}{I_x}\right). \tag{3.2}$$

The corresponding eigenstates are characterized by three quantum numbers L, K, and M,

$$\begin{aligned}
&\mathbf{L}^2|LKM\rangle = L(L+1)|LKM\rangle,\ L = 0, 1, 2, \ldots \\
&L_z|LKM\rangle = K|LKM\rangle,\ K = -L, -L+1, \ldots, L-1, L \\
&L_Z|JKM\rangle = M|LKM\rangle,\ M = -L, -L+1 \ldots, L-1, L\,,
\end{aligned} \tag{3.3}$$

where L_Z is the angular momentum operator defined with respect to the laboratory coordinate frame (X, Y, Z). The eigenvalues of (3.2) are degenerate on M:

$$E_{LK} = \frac{\hbar^2 L(L+1)}{2I_x} + \frac{\hbar^2 K^2}{2}\left(\frac{1}{I_z} - \frac{1}{I_x}\right). \tag{3.4}$$

The general form for the energy levels of a rotating asymmetric rigid body, $I_x \neq I_y \neq I_z$, does not exist, although it is possible to calculate matrix elements of the Hamiltonian for a given L.

3.2 Tunneling of a large spin

Let $\mathbf{S}$ be a fixed-length spin embedded in a stationary body. Naturally, the magnetic anisotropy is defined with respect to the body axes. The general form of the crystal field Hamiltonian is

$$\hat{H}_S = \hat{H}_\parallel + \hat{H}_\perp\,, \tag{3.5}$$

where $\hat{H}_\parallel$ commutes with S_z and $\hat{H}_\perp$ is a perturbation that does not commute with S_z. The states $|\pm S\rangle$ are degenerate ground states of $\hat{H}_\parallel$, where S is the total spin of the nanomagnet. $\hat{H}_\perp$ slightly perturbs these states, adding to them small contributions from other $|m_S\rangle$ states. We will call these degenerate perturbed states $|\psi_{\pm S}\rangle$. Physically they describe the magnetic moment aligned in

one of the two directions along the anisotropy axis. Full perturbation theory with account of the degeneracy of $\hat{H}_S$ provides quantum tunneling between the $|\psi_{\pm S}\rangle$ states for integer S. The ground state and first excited state are symmetric and antisymmetric combinations of $|\psi_{\pm S}\rangle$, respectively [13],

$$\begin{aligned}\Psi_+ &= \frac{1}{\sqrt{2}}(|\psi_S\rangle + |\psi_{-S}\rangle) \\ \Psi_- &= \frac{1}{\sqrt{2}}(|\psi_S\rangle - |\psi_{-S}\rangle)\,,\end{aligned} \tag{3.6}$$

which satisfy

$$\hat{H}_S\Psi_\pm = E_\mp\Psi_\pm\,, \tag{3.7}$$

where

$$E_+ - E_- \equiv \Delta. \tag{3.8}$$

The tunnel splitting Δ is generally many orders of magnitude smaller than the distance to other spin energy levels, which makes the two-state approximation very accurate at low energies. For example,

$$\hat{H}_S = -DS_z^2 + dS_y^2 \tag{3.9}$$

with $d \ll D$ describes the biaxial anisotropy of spin-10 molecular nanomagnet Fe-8, where the tunnel splitting in the limit of large S is given by[140]

$$\Delta = \frac{8S^{3/2}}{\pi^{1/2}}\left(\frac{d}{4D}\right)^S D. \tag{3.10}$$

The distance to the next excited spin level is $(2S-1)D$, which is large compared to Δ.

It is convenient to describe these lowest energy spin states $\Psi_\pm$ with a pseudospin-1/2. Components of the corresponding Pauli operator $\boldsymbol{\sigma}$ are

$$\begin{aligned}\sigma_x &= |\psi_{-S}\rangle\langle\psi_S| + |\psi_S\rangle\langle\psi_{-S}| \\ \sigma_y &= i|\psi_{-S}\rangle\langle\psi_S| - i|\psi_S\rangle\langle\psi_{-S}| \\ \sigma_z &= |\psi_S\rangle\langle\psi_S| - |\psi_{-S}\rangle\langle\psi_{-S}|\,.\end{aligned} \tag{3.11}$$

The projection of $\hat{H}_S$ onto $|\psi_{\pm S}\rangle$ states is

$$\hat{H}_\sigma = \sum_{m,n=\psi_{\pm S}} \langle m|\hat{H}_S|n\rangle \; |m\rangle\langle n|. \tag{3.12}$$

Expressing $|\psi_{\pm S}\rangle$ in terms of $\Psi_\pm$ one obtains

$$\langle\psi_{\pm S}|\hat{H}_S|\psi_{\pm S}\rangle = 0, \qquad \langle\psi_{\pm S}|\hat{H}_S|\psi_{\mp S}\rangle = -\frac{\Delta}{2}\,, \tag{3.13}$$

which gives the two-state Hamiltonian

$$\hat{H}_\sigma = -\frac{\Delta}{2}\sigma_x \tag{3.14}$$

having eigenvalues $\pm\Delta/2$.

In the absence of tunneling a classical magnetic moment is localized in the up or down state. It is clear that delocalization of the magnetic moment due to spin tunneling reduces the energy by $\Delta/2$. In a free particle, however, tunneling of the spin must be accompanied by mechanical rotations in order to conserve the total angular momentum. Such rotations cost energy, so it is not a priori clear whether the tunneling will survive in a free particle and what the ground state is going to be. This problem is addressed in Section 3.4.

3.3 Coupling of Spin and Rotational Angular Momentum

In this section, we derive the so-called anomalous commutation relations of angular momentum in a rotating frame. This treatment applies to the general case of mechanical rotations of a quantum system with internal angular momentum degrees of freedom [138]. Starting with the usual commutation relations for the components of spin $\mathbf{S}$, angular momentum of mechanical rotations (analogous to orbital angular momentum) $\mathbf{L}$, and total angular momentum $\mathbf{J} = \mathbf{S} + \mathbf{L}$ in the fixed frame, we derive commutation relations in the rotating frame. We show that in the body frame all components of $\mathbf{J}$ and $\mathbf{S}$ commute, and therefore the corresponding quantum numbers are good quantum numbers.

The nanomagnet is a rigid rotator around its center of mass, which we define as the common

origin O of two right-handed coordinate systems, shown in Fig. 3.1. The X, Y, Z axes make up the lab frame that is fixed in space. The x, y, z axes define the coordinate system that is rigidly coupled to the body, and are directed along the principle moments of inertia of the rotator with z chosen along the symmetry axis of the rotator. Initially, these two frames coincide. At any other instant the orientation of the rotating xyz frame relative to the fixed XYZ frame is specified by the Euler angles ϕ, θ, ψ, which are defined using the zyz-convention (see, e.g., Ref. [141]). The spherical polar angles represent the orientation of the symmetry axis z of the moving frame relative to the fixed frame. θ is a tipping away from the Z axis and ϕ is a rotation around the the Z-axis. ψ is the angle of rotation about the z axis.

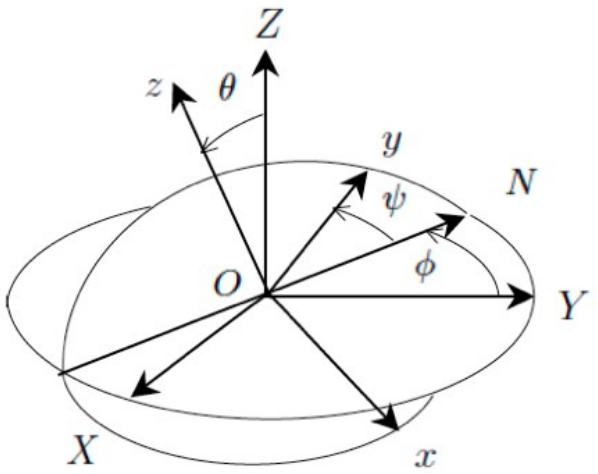

Figure 3.1: Coordinate frames of rigid body rotations.

A vector $\mathbf{R}$ with components R_A (we use uppercase Roman letters to indicate fixed frame components) as measured in the fixed XYZ frame can be projected onto the rotating xyz coordinate frame. In the rotating frame, this vector is described by $\mathbf{r}$ and has components r_α (lowercase Greek indices denote components in the rotating frame). The transformation between these two frames is

given by the rotation matrix $\mathbf{C}$,

$$\mathbf{C} = \begin{pmatrix} \lambda_{xX} & \lambda_{xY} & \lambda_{xZ} \\ \lambda_{yX} & \lambda_{yY} & \lambda_{yZ} \\ \lambda_{zX} & \lambda_{zY} & \lambda_{zZ} \end{pmatrix}$$
$$= \begin{pmatrix} \cos\psi\cos\theta\cos\phi - \sin\psi\sin\phi & \cos\psi\cos\theta\sin\phi - \sin\psi\cos\phi & -\cos\psi\sin\theta \\ -\sin\psi\cos\theta\cos\phi - \cos\psi\sin\phi & -\sin\psi\cos\theta\sin\phi + \cos\psi\cos\phi & \sin\psi\sin\theta \\ \sin\theta\cos\phi & \sin\theta\sin\phi & \cos\theta \end{pmatrix} \tag{3.15}$$

where the $\lambda_{\alpha A}$ are direction cosines between fixed frame and rotating frame axes.

The total angular momentum $\mathbf{J}$ obeys the usual commutation relations in the fixed XYZ frame,

$$[J_A, J_B] = i\epsilon_{ABC}J_C, \tag{3.16}$$

where ϵ_{ABC} is the fully antisymmetric Levi-Civita tensor (summation over repeated indices is implicit throughout this Appendix). In the rotating xyz frame, the total angular momentum has components

$$J_\alpha = \lambda_{\alpha A}J_A \tag{3.17}$$

and the sign of i in the commutation relation is reversed,

$$[J_\alpha, J_\beta] = -i\epsilon_{\alpha\beta\gamma}J_\gamma. \tag{3.18}$$

The components of the mechanical angular momentum can be resolved in either frame, or in terms of the Euler angles ϕ, θ, ψ which describe precession of the symmetry axis z about the fixed Z axis, rotation about the axis of symmetry z, nutation of the z axis with respect to the Z axis, and precession of the body about its axis of symmetry, respectively. The operator forms of the corresponding angular momenta are

$$p_\phi = -i\hbar\frac{\partial}{\partial\phi}, \qquad p_\theta = -i\hbar\frac{\partial}{\partial\theta}, \qquad p_\psi = -i\hbar\frac{\partial}{\partial\psi} \tag{3.19}$$

which mutually commute. The rotational angular momentum operators can be projected onto the

laboratory frame coordinate system,

$$\begin{aligned} L_X &= -\cot\theta\cos\phi\, p_\phi - \sin\phi\, p_\theta + \csc\theta\cos\phi\, p_\psi \\ L_Y &= -\cot\theta\sin\phi\, p_\phi + \cos\phi\, p_\theta + \csc\theta\sin\phi\, p_\psi \\ L_Z &= p_\phi, \end{aligned} \tag{3.20}$$

or the body frame coordinate system,

$$\begin{aligned} L_x &= -\csc\theta\cos\psi\, p_\phi + \sin\psi\, p_\theta + \cot\theta\cos\psi\, p_\psi \\ L_y &= \csc\theta\sin\psi\, p_\phi + \cos\psi\, p_\theta - \cot\theta\sin\psi\, p_\psi \\ L_z &= p_\psi. \end{aligned} \tag{3.21}$$

The commutation relations can be obtained by direct calculation, with the fixed frame components satisfying

$$[L_A, L_B] = i\epsilon_{ABC} L_C, \tag{3.22}$$

while the rotating frame components obey

$$[L_\alpha, L_\beta] = -i\epsilon_{\alpha\beta\gamma} L_\gamma. \tag{3.23}$$

The spin obeys the same regular commutation relations in either frame. To show this, we define the spin components in the laboratory frame where

$$[S_A, S_B] = i\epsilon_{ABC} S_C. \tag{3.24}$$

Using the fact that $[S_A, L_B] = 0$, it is easy to see that the components of $\mathbf{J} = \mathbf{L} + \mathbf{S}$ in the fixed frame satisfy the commutation relation given by Eq. (3.16). Projecting this spin onto the rotating axes, $S_\alpha = \lambda_{\alpha A} S_A$, and noticing $[S_A, \lambda_{\beta B}] = 0$, we obtain

$$[S_\alpha, S_\beta] = \lambda_{\alpha A}\lambda_{\beta B}[S_A, S_B] = i\epsilon_{ABC}\lambda_{\alpha A}\lambda_{\beta B} S_C = i\epsilon_{\alpha\beta\gamma}\lambda_{\gamma C} S_C = i\epsilon_{\alpha\beta\gamma} S_\gamma. \tag{3.25}$$

The rotation matrix is orthogonal and has unit determinant. It follows that any element is equal to its cofactor, which implies

$$\epsilon_{ABC}\lambda_{\alpha A}\lambda_{\beta B} = \epsilon_{\alpha\beta\gamma}\lambda_{\gamma C} \tag{3.26}$$

In order to obtain the same sign for all angular momenta in the rotating frame, we define reversed spin $\mathbf{S} \to \tilde{\mathbf{S}} = -\mathbf{S}$, giving

$$[\tilde{S}_\alpha, \tilde{S}_\beta] = -i\epsilon_{\alpha\beta\gamma}\tilde{S}_\gamma. \tag{3.27}$$

Now we may write $\mathbf{J} = \mathbf{L} - \tilde{\mathbf{S}}$, and the components of $\mathbf{J}$ satisfy the anomalous commutation relations, Eq. (3.18). Alternatively, the commutation relation for the total angular momentum in the lab frame can be calculated directly. Using the fact that the direction cosines transform according to

$$[\lambda_{\alpha A}, J_B] = [\lambda_{\alpha A}, L_B] = -L_B\lambda_{\alpha A} = i\epsilon_{ABC}\lambda_{\alpha C}, \tag{3.28}$$

and that the spin and rotational angular momentum do not commute in the rotating frame

$$[\tilde{S}_\alpha, L_\beta] = -[\lambda_{\alpha A}S_A, \lambda_{\beta B}L_B] = -\lambda_{\beta B}[\lambda_{\alpha A}, L_B]S_A = -i\epsilon_{\alpha\beta\gamma}\tilde{S}_\gamma \tag{3.29}$$

gives

$$\begin{aligned}[J_\alpha, J_\beta] = [L_\alpha - \tilde{S}_\alpha, L_\beta - \tilde{S}_\beta] &= [L_\alpha, L_\beta] - [L_\alpha, \tilde{S}_\beta] - [\tilde{S}_\alpha, L_\beta] + [\tilde{S}_\alpha, \tilde{S}_\beta] \\ &= -i\epsilon_{\alpha\beta\gamma}(L_\gamma + \tilde{S}_\gamma) = -i\epsilon_{\alpha\beta\gamma}J_\gamma.\end{aligned} \tag{3.30}$$

Similarly, we can show that $[J_\alpha, \tilde{S}_\beta] = 0$, allowing us to choose quantum numbers corresponding to $\mathbf{J}$ and $\mathbf{S}$.

The full Hamiltonian is given by the sum of the rotational energy and magnetic anisotropy energy

$$\hat{H} = \frac{\hbar^2 L_x^2}{2I_x} + \frac{\hbar^2 L_y^2}{2I_y} + \frac{\hbar^2 L_z^2}{2I_z} + \hat{H}_S\,. \tag{3.31}$$

Note that the mechanical part and the spin part of this Hamiltonian are not independent because in the body frame the operators $\mathbf{L}$ and $\mathbf{S}$ do not commute, $[L_i, S_j] = -i\epsilon_{ijk}S_k$. It, therefore, makes sense to express the above Hamiltonian in terms of the commuting body-frame operators of the

total angular momentum **J** and spin **S**:

$$\hat{H} = \frac{\hbar^2}{2}\left(\frac{J_x^2}{I_x} + \frac{J_y^2}{I_y} + \frac{J_z^2}{I_z}\right) + \frac{\hbar^2}{2}\left(\frac{S_x^2}{I_x} + \frac{S_y^2}{I_y} + \frac{S_z^2}{I_z}\right) - \hbar^2\left(\frac{J_x S_x}{I_x} + \frac{J_y S_y}{I_y} + \frac{J_z S_z}{I_z}\right) + \hat{H}_S\,. \tag{3.32}$$

For a symmetric rigid rotor with $I_x = I_y$ this Hamiltonian reduces to

$$\begin{aligned}\hat{H} &= \frac{\hbar^2 \mathbf{J}^2}{2I_x} + \frac{\hbar^2 J_z^2}{2}\left(\frac{1}{I_z} - \frac{1}{I_x}\right) \\ &- \hbar^2\left(\frac{J_x S_x + J_y S_y}{I_x} + \frac{J_z S_z}{I_z}\right) + \hat{H}'_S\,,\end{aligned} \tag{3.33}$$

where

$$\hat{H}'_S = \hat{H}_S + \frac{\hbar^2}{2}\left(\frac{1}{I_z} - \frac{1}{I_x}\right) S_z^2 + \frac{\hbar^2 \mathbf{S}^2}{2I_x}\,. \tag{3.34}$$

The last term in $\hat{H}'_S$ is an unessential constant, $\hbar^2 S(S+1)/(2I_x)^2$. The second term provides renormalization of the crystal field in a freely rotating particle. For, e.g., the biaxial spin Hamiltonian given by Eq. (3.9) it leads to

$$D \to D - \frac{\hbar^2}{2}\left(\frac{1}{I_z} - \frac{1}{I_x}\right)\,. \tag{3.35}$$

This, in turn, renormalizes the tunnel splitting given by Eq. (3.10). For a particle that is allowed to rotate about the Z-axis only (that is, in the limit of $I_x \to \infty$) these results coincide with the results obtained by the instanton method in Ref. [94], where it was shown that, in practice, the renormalization of the magnetic anisotropy and spin tunnel splitting by mechanical rotations is small. Eq. (3.35) provides generalization of this effect for arbitrary rotations of a symmetric rotator with a spin. According to this equation and Eq. (3.9), when rotations are allowed the effective easy-axis magnetic anisotropy and the tunnel splitting can decrease or increase, depending on the ratio I_x/I_z.

Projection of Eq. (3.33) on the two spin states along the lines of the previous Section gives

$$\hat{H} = \frac{\hbar^2 \mathbf{J}^2}{2I_x} + \frac{\hbar^2 J_z^2}{2}\left(\frac{1}{I_z} - \frac{1}{I_x}\right) - \frac{\Delta}{2}\sigma_x - \frac{\hbar^2 S}{I_z} J_z \sigma_z\,. \tag{3.36}$$

where we have used

$$\langle\psi_{\pm S}|S_z|\psi_{\pm S}\rangle = \pm S\,, \qquad \langle\psi_{\pm S}|S_{x,y}|\psi_{\pm S}\rangle = 0\,. \tag{3.37}$$

We construct eigenstates of this Hamiltonian according to

$$|\Psi_{JK}\rangle = \frac{1}{\sqrt{2}}(C_{\pm S}|\psi_S\rangle \pm C_{\mp S}|\psi_{-S}\rangle)|JK\rangle \tag{3.38}$$

where

$$\begin{aligned} &\mathbf{J}^2|JK\rangle = J(J+1)|JK\rangle,\ J = 0, 1, 2, \ldots \\ &J_z|JK\rangle = K|JK\rangle,\ K = -J, \ldots, J. \end{aligned} \tag{3.39}$$

Solution of $\hat{H}|\Psi_{JK}\rangle = E|\Psi_{JK}\rangle$ gives energy levels as

$$E_{JK}^{(\pm)} = E_{JK} \pm \sqrt{\left(\frac{\Delta}{2}\right)^2 + \left(\frac{\hbar^2 KS}{I_z}\right)^2}\,, \tag{3.40}$$

where E_{JK} is provided by Eq. (3.4) with L replaced by J. The upper (lower) sign in Eq. (3.40) corresponds to the lower (upper) sign in Eq. (3.38). For $K \neq 0$ each state is degenerate with respect to the sign of K. For $K = 0, 1, 2, \ldots$ the coefficients in Eq. (3.38) are given by

$$C_\pm = \sqrt{1 \pm \alpha K/\sqrt{S^2 + (\alpha K)^2}}\,, \tag{3.41}$$

where α is a dimensionless magneto-mechanical ratio,

$$\alpha = \frac{2(\hbar S)^2}{I_z \Delta}\,. \tag{3.42}$$

Energy levels in Eq. (3.40) can be given a simple semiclassical interpretation. Indeed, the last term in this equation is the tunnel splitting of the levels in the effective magnetic field that appears in the body reference frame due to rotation about the spin quantization axis at the angular velocity $\hbar K/I_z$. When $S = 0$ (which also means $\Delta = 0$) Eq. (3.40) with $J = L$ gives the energy of the quantum symmetric rigid rotor without a spin, Eq. (3.4). In the case of a heavy body (large moments of inertia) the ground state and the first excited state correspond to $J = K = 0$, and we recover

the tunnel-split spin states in a non-rotating macroscopic body, $E_{00\pm} = \pm\Delta/2$. In the general case, spin states of the rotator are entangled with mechanical rotations.

Equations (3.38)-(4.20) are our main analytical results for the low-energy states of a free magnetic particle. In general, numerical analysis is needed to find the ground state of the particle. Special cases of the aspect ratio that will be analyzed below include a needle of vanishing diameter (which is equivalent to the problem of the rotation about a fixed axis treated previously in the laboratory frame by two of the authors [21]), a finite-diameter needle, a sphere, and a disk.

3.4 Ground state

Minimization of the energy in Eq. (3.40) on J with the account of the fact that J cannot be smaller than K immediately yields $J = K$, that is, the ground state always corresponds to the maximal projection of the total angular momentum onto the spin quantization axis. In semiclassical terms this means that the minimal energy states in the presence of spin tunneling always correspond to mechanical rotations about the magnetic anisotropy axis. This is easy to understand by noticing that the sole reason for mechanical rotation is the necessity to conserve the total angular momentum while allowing spin tunneling to lower the energy. To accomplish this the particle needs to oscillate between clockwise and counterclockwise rotations about the spin quantization axis in unison with the tunneling spin. If such mechanical oscillation costs more energy than the energy gain from spin tunneling, then both spin tunneling and mechanical motion must be frozen in the ground state as, indeed, happens in very light particles (see below). Rotations about axes other than the spin quantization axis can only increase the energy and, thus, should be absent in the ground state.

For further analysis it is convenient to write Eq. (3.40) in the dimensionless form,

$$\frac{E_{JK}^{(\pm)}}{\Delta} = \frac{\alpha}{4}\left[\frac{J(J+1)-K^2}{S^2}\lambda + \frac{K^2}{S^2}\right] \pm \frac{1}{2}\sqrt{1+\frac{K^2}{S^2}\alpha^2}\,, \tag{3.43}$$

in terms of dimensionless parameters α and the aspect ratio for the moments of inertia

$$\lambda = I_z/I_x\,. \tag{3.44}$$

The range of λ for a symmetric rotator is $0 \le \lambda \le 2$. For, e.g., a symmetric ellipsoid with semiaxes

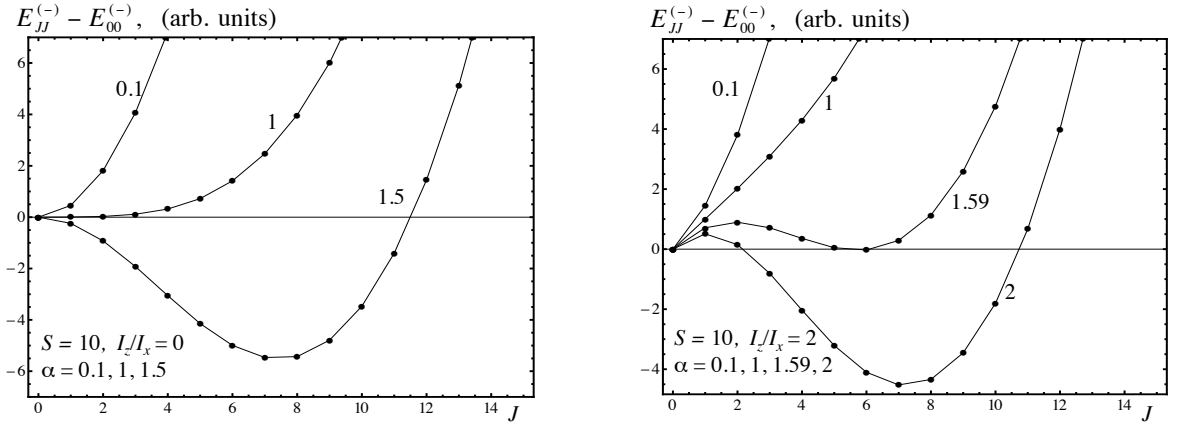

(a) (b)

Figure 3.2: (a) Dependence of energy on J at $K = J$ and $I_z/I_x = 0$ for different values of α. The plot shows second-order quantum phase transition on α. (b) Dependence of energy on J at $K = J$ and $I_z/I_x = 2$ for different values of α. The plot shows first-order quantum phase transition on α.

$a = b \neq c$, one has $\lambda = 2a^2/(a^2 + c^2)$.

The dependence of the energy levels (3.40) on J at $K = J$ is shown in Figure 3.2. It exhibits quantum phase transition on the parameter α between states with different values of J. Only for a needle of vanishing diameter, $I_z/I_x \to 0$, which corresponds to $a \to 0$ in the case of an ellipsoid, the transition is second order, see Fig. 3.2a. It occurs at $\alpha = \left[1 - 1/(2S)^2\right]^{-1}$. This case is equivalent to the rotation about a fixed axis studied in Ref. [21]. For any finite ratio I_z/I_x the transition is first order, see Fig. 3.2b. It occurs at the value of α that depends on I_z/I_x. The origin of the transfer from a second-order transition at $\lambda = 0$ to the first-order transition at $\lambda \neq 0$ can be traced to the term $[J(J+1) - K^2]S^{-2}\lambda$ in Eq. (3.43). We should notice that for a finite-size nanomagnet the analogy with first- and second-order phase transition is, of course, just an analogy. To talk about real phase transitions one has to take the limit of $S \to \infty, I_{x,z} \to \infty$ when the distances between quantum levels go to zero.

For a given λ, as α increases the ground state switches from $J = 0$ to higher J when

$$E_{00}^{(-)}(\alpha_J^0(\lambda)) = E_{JJ}^{(-)}(\alpha_J^0(\lambda))\,. \tag{3.45}$$

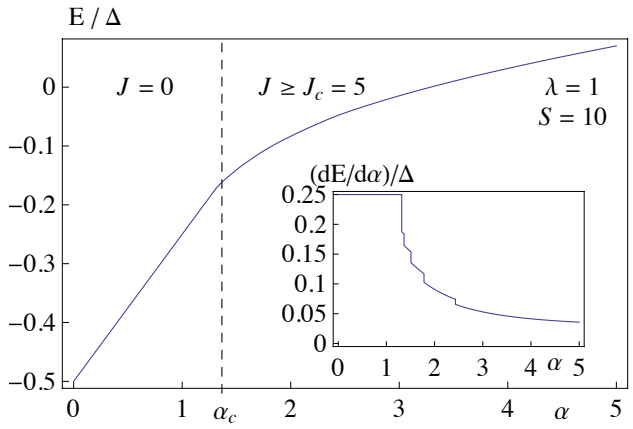

Figure 3.3: Dependence of the ground-state energy on α for a spherical particle. Inset shows the discontinuity of the derivative of the ground state energy on α.

Solution of this equation for $\alpha_J^0(\lambda)$ gives

$$\alpha_J^0 = \frac{(2S)^2(J+\lambda)}{J[(2S)^2-(J+\lambda)^2]}\,. \tag{3.46}$$

This first transition occurs for the smallest value of $\alpha_J^0(\lambda)$ and the transition is from $J=0$ to the corresponding critical value, J_c. For $\alpha < \alpha_{J_c}^0$ the ground state corresponds to $J=0$ and $C_{\pm S}=1$. After the first transition from $J=0$ to $J=J_c$, the ground state switches to sequentially higher J at values of α which satisfy

$$E^{(-)}_{J-1\;J-1}(\alpha_J(\lambda)) = E^{(-)}_{JJ}(\alpha_J(\lambda))\,. \tag{3.47}$$

Solution of this equation for $\alpha_J(\lambda)$ gives

$$\alpha_J = \frac{(2S)^2 T(J,\lambda)}{\sqrt{(2S)^2(2J-1)^2 - T(J,\lambda)^2}\sqrt{(2S)^2 - T(J,\lambda)^2}}\,, \tag{3.48}$$

with

$$T(J,\lambda) = 2J - 1 + \lambda\,. \tag{3.49}$$

The critical α_J has poles at $\lambda = 2(S-J)+1$. For $\lambda \geq 1$ there is no longer a ground state transition to $J=S$, even for very large values of α.

Needle of vanishing diameter: The case of a particle that can only rotate about its anisotropy

axis [21] is equivalent in our model to a needle of vanishing diameter ($a \to 0$ for an ellipsoid), having $\lambda = 0$. It is also equivalent to the problem of tunneling of the angular momentum of a superconducting current in a flux qubit coupled to a torsional resonator. In this limit we reproduce results of Ref. [21]. The quantum number K determines the ground state, as the energy, Eq. (3.43), no longer formally depends on J. However, the values of α_J at $\lambda = 0$, for which ground state transitions occur, are the same as those for which $E^{(-)}_{J\,K-1} = E^{(-)}_{JK}$, and we will use J to describe the ground state of the axial rotor as well. The first ground state transition occurs from $J = 0$ to $J = 1$ at $\alpha(\lambda) = \alpha_1(0) = \alpha^0_1(0)$, because $J_c = 1$ for $\lambda \lesssim 0.01$. At $\alpha = \alpha_2(0)$ the ground state switches from $J = 1$ to $J = 2$, and so on. The final transition is to a completely localized spin state $J = S$ in which spin tunneling is frozen for all $\alpha > \alpha_S(0)$. For example, when $S = 10$, $\alpha_1(0) = \alpha^0_1(0) = 1.0025$ and $\alpha_{10} = 3.2066$.

Needle of finite diameter: The ground state of a needle of finite diameter ($a \ll c$ for an ellipsoid) with $\lambda = 0.1$, that is free to rotate about any axis, shows qualitatively different behavior. As α increases, the ground state changes from $J = 0$ to $J_c = 3$ at $\alpha = \alpha^0_3(0.1)$, as the smallest value of $\alpha^0_J(0.1)$ for $1 \le J \le S$ occurs for $J_c = 3$. The $J = 1, 2$ states never become the ground state. After this, transitions occur to successively higher J, beginning with $J = 4$ at $\alpha = \alpha_4(0.1)$, and eventually localizing the spin with $J = S$ for $\alpha > \alpha_S(0.1)$. For $S = 10$, $\alpha^0_3(0.1) = 1.0588$ and $\alpha_{10}(0.1) = 3.3935$.

Sphere: As λ increases towards unity, the particle becomes more symmetric with the moment of inertia having (prolate) ellipsoidal symmetry, until it reaches spherical symmetry at $\lambda = 1$. The first ground state transition occurs from $J = 0$ to $J = J_c = 5$ at $\alpha = \alpha^0_5(1)$, and subsequent transitions occur at $\alpha = \alpha_J(1)$. However, the spin never localizes in the $J = S$ state even for very large α, as $\alpha_J(1)$ has a pole at $J = S$, so the last transition occurs to the $J = S - 1$ state at $\alpha = \alpha_{S-1}(1)$. For $S = 10$, $\alpha^0_5(1) = 1.3187$ and $\alpha_9(1) = 2.4325$.

Disk: With λ increasing from unity, the symmetry of the body becomes that of an oblate ellipsoid, and begins to flatten in the plane perpendicular to the anisotropy axis. It is easy to check from Eq. (3.43) that for $1 < \lambda \le 2$ the state with $J = S$ always has higher energy than the state with $J = S - 1$, even in the limit of $\alpha \to \infty$. This means that for an oblate particle some spin tunneling (accompanied by mechanical rotations) survives in the ground state no matter how light the particle is. This purely quantum-mechanical result has no semi-classical analogy. In the case

of a disk of vanishing thickness, $\lambda = 2$, the first ground state transition occurs from $J = 0$ to $J = J_c = 6$ at $\alpha = \alpha_6^0(2)$, and subsequent transitions occur at $\alpha = \alpha_J(2)$ up through $J = S - 1$. For $S = 10$, $\alpha_6^0(2) = 1.5873$ and $\alpha_9(2) = 3.5849$.

3.5 Ground-state magnetic moment

As has been already mentioned, the magnetic moment is due entirely to the spin of the particle, as L_z represents mechanical motion of the particle as a whole, and not electronic orbital angular momentum. Thus,

$$\mu = -g\mu_B \langle \Psi_{JK} | S_z | \Psi_{JK} \rangle = -g\mu_B S \frac{\alpha K}{\sqrt{S^2 + (\alpha K)^2}} \,. \tag{3.50}$$

Here g is the spin gyromagnetic factor, and the minus sign reflects the negative gyromagnetic ratio $\gamma = -g\mu_B/\hbar$. The ground state always corresponds to $J = K$, so these are used interchangeably in descriptions of the ground state. The dependence of the magnetic moment on α for different

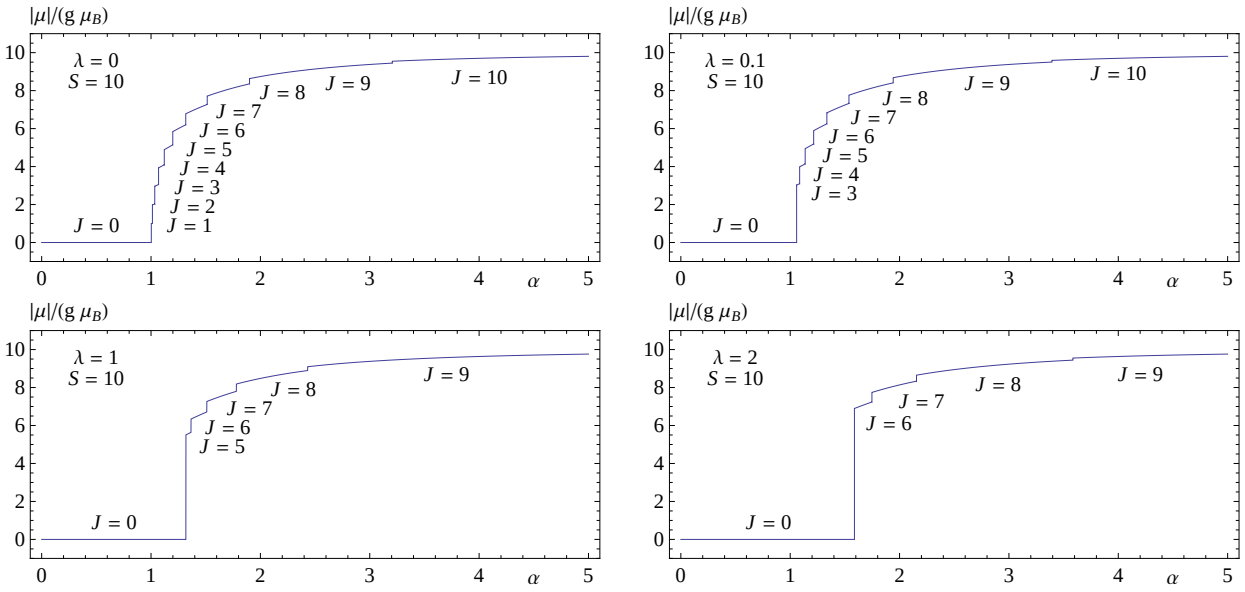

Figure 3.4: Ground state magnetic moment for a needle of vanishing diameter ($\lambda = 0$), finite-diameter needle ($\lambda = 0.1$), sphere ($\lambda = 1$), and a disk of vanishing thickness ($\lambda = 2$).

aspect ratios of the particle is shown in Fig. 3.4. For $\alpha < \alpha_{J_c}(\lambda)$ the ground state corresponds to $J = K = 0$, so the spin-up and spin-down states are in an equal superposition which produces zero magnetic moment. At greater values of α the spin states contribute in unequal amounts which

leads to a non-zero magnetic moment. As α becomes large, the magnetic moment approaches its maximal value $|\mu_{max}| = g\mu_B S$. Note that the magnetic moment approaches its maximum value even for values of λ that do not admit transitions to $J = S$ states.

Because the ground state is completely determined by the parameters α and λ, we can depict the ground state behavior in a quantum phase diagram shown in Fig. 3.5. The curves separate areas in the (α, λ) plane that correspond to different values of J and different values of the magnetic moment. Notice the fine structure of the diagram (lower picture in Fig. 3.5) near the first critical α. This very rich behavior of the ground state on parameters must have significant implications for magnetism of rigid atomic clusters.

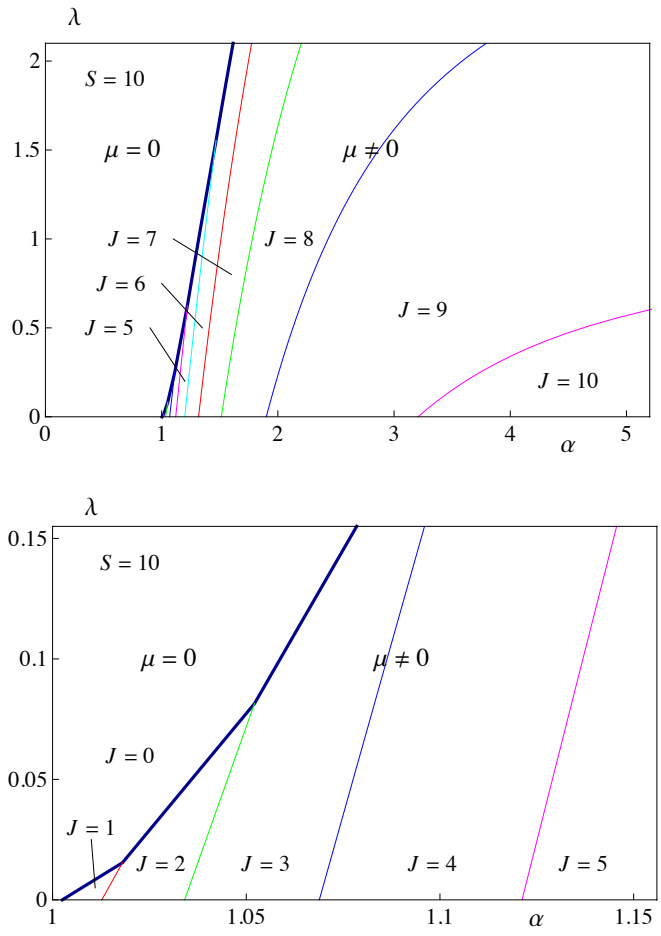

Figure 3.5: Quantum phase diagram for the ground-state magnetic moment and the total angular momentum.

3.6 Conclusions

We have studied the problem of a quantum rotator containing a tunneling spin. This problem is relevant to quantum mechanics of free magnetic nanoparticles. It also provides an interesting insight into quantum mechanics of molecules studied from the macroscopic end. The answer obtained for the energy levels of a symmetric rotator, Eq. (3.40), is non-perturbative and highly non-trivial. It is difficult to imagine how it could be obtained from first principles without the reduction to two spin states. Indeed, for spin S the tunnel splitting itself generally appears in the S-th order of perturbation theory, see Eq. (3.10), so the path from the full crystal-field Hamiltonian like, e.g., Eq. (3.9) to Eq. (3.40) must be very long. Equations (3.38) and (3.40) represent, therefore, a unique exact solution of the quantum-mechanical problem of a mechanical rotator with a spin. Striking feature of this solution is presence of first- and second-order quantum phase transitions between states with different values of the magnetic moment.

Our results provide the framework for comparison between theory and experiment on very small free magnetic clusters. Our main conclusion for experiment is that rotational states and magnetic moments of such clusters depend crucially and in a predictable way on size and aspect ratio. This dependence results in a complex phase diagram that separates regions in the parameter space, corresponding to different values of the magnetic moment. Broad distribution of the magnetic moments that does not simply scale with the volume, has, in fact, been reported in beams of free atomic clusters of ferromagnetic materials [66, 67, 68]. Our results may shed some additional light on these experiments. They may also apply to free magnetic molecules if one can justify the condition of rigidity. Direct comparison between theory and experiment may be possible for atomic clusters (molecules) in magnetic traps.

To see that the quantum problem studied in this paper may, indeed, be relevant to quantum states of free nanomagnets, consider, e.g., a spherical atomic cluster of radius R and average mass density ρ having spin $S = 10$ that, when embedded in a large body, can tunnel between up and down at a frequency of a few GHz, thus providing $\Delta \sim 0.1$ K. Significant changes in the magnetic moment of such a cluster would occur at $\alpha \sim 1$, which, according to Eq. (6.17), corresponds to $I = 8\pi\rho R^5/15 \sim 10^{-42}\mathrm{kg\,m^2}$ and $R \sim 1\mathrm{nm}$. For a magnetic molecule like, e.g., Mn_{12}, the moments of inertia would also be in the ballpark of $10^{-42}\mathrm{kg\,m^2}$. However, the natural spin tunnel splitting

in Mn_{12} is very small, thus, providing a very large α. The same is true for Fe_8 magnetic molecules. In this case the spin tunneling in a free molecule must be completely frozen. Even if the molecule cannot be considered as entirely rigid, such effect, if observed, would receive natural interpretation within the framework of our theory.

4

Conservation of Angular Momentum in a Flux Qubit

Oscillations of superconducting current between clockwise and counterclockwise directions in a flux qubit do not conserve the angular momentum of the qubit. To compensate for this effect the solid containing the qubit must oscillate to and in unison with the current. This requires entanglement of quantum states of the qubit with quantum states of a macroscopic body. The question then arises whether slow decoherence of quantum oscillations of the current is consistent with fast decoherence of quantum states of a macroscopic solid. This problem is analyzed within an exactly solvable quantum model of a qubit embedded in an absolutely rigid solid and for the elastic model that conserves the total angular momentum. We show that while the quantum state of a flux qubit is, in general, a mixture of a large number of rotational states, slow decoherence is permitted if the system is macroscopically large. Practical implications of entanglement of qubit states with mechanical rotations are discussed.

Flux qubits are formed by quantum superpositions of current states in a superconducting loop interrupted by one or more Josephson junctions [95, 96]. Oscillations of superconducting current between clockwise and counterclockwise directions in a flux qubit do not conserve the angular momentum of the qubit, and must transfer angular momentum to the surrounding solid. Consideration of the entire system (qubit + solid) which does conserve total angular momentum leads to entanglement between current and rotational states. Analyzing decoherence of the quantum state of a flux

qubit due to entanglement with rotations of the surrounding body shows that, contrary to what one might believe, macroscopicity of the body is necessary for slow decoherence.

Within an exactly solvable model of a flux qubit embedded in an absolutely rigid rotator we obtain entangled eigenstates of the system and their dependence on the total angular momentum J. When the system is prepared in the state with a certain direction of the superconducting current, this state is, in general, a quantum mixture of many rotational states of the body. However, only tunnel splittings Δ_J of the states belonging to the same J contribute to the oscillations of the superconducting current. We then study decoherence of a flux qubit due to torques generated by the oscillating current in the elastic solid and show how decoherence rates obtained within the two models match. Among other problems we discuss renormalization of the tunnel splitting by the elastic environment and superradiant relaxation in a system of closely packed qubits.

This chapter is structured as follows. Exactly solvable quantum model of a flux qubit interacting with rotations of a rigid body is studied in 4.1. Quantum states of the qubit entangled with rotations of the body are obtained in Section 4.1.1. Section 4.1.2 is devoted to decoherence due to rotational excitations of the body. Elastic environment is considered in Section 4.2. The model that conserves the total angular momentum is formulated in Section 4.2.1. Section 4.2.2 discusses decoherence of the flux qubit by internal torques. Renormalization of the tunnel splitting by the elastic environment is computed in Section 4.2.3. Section 4.3 contains numerical estimates, discussion of various effects originating from conservation of angular momentum, alternative interpretations of the results, and final conclusions.

4.1 Rigid Body

4.1.1 Rotational states of a flux qubit

First, we consider the tunnel-split states of a flux qubit and ignore conservation of the angular momentum. Let the lowest-energy doublet of a flux qubit be

$$\Psi_{\pm} = \frac{1}{\sqrt{2}} \left(|\uparrow\rangle \pm |\downarrow\rangle \right) , \tag{4.1}$$

where $|\uparrow\rangle$ and $|\downarrow\rangle$ are the eigenstates of the operator of the angular momentum of the electronic current inside superconducting loop $\hat{l}_z$,

$$\begin{aligned} \hat{l}_z|\uparrow\rangle &= l|\uparrow\rangle \\ \hat{l}_z|\downarrow\rangle &= -l|\downarrow\rangle \end{aligned} \tag{4.2}$$

Eigenfunctions $\Psi_\pm$ satisfy

$$\hat{H}\Psi_\pm = E_\pm \Psi_\pm \tag{4.3}$$

with $\hat{H}$ being the Hamiltonian of the qubit and

$$E_- - E_+ \equiv \Delta \tag{4.4}$$

being the tunnel splitting. It is convenient to describe such a two-state system by a pseudospin 1/2. Components of the corresponding Pauli operator $\boldsymbol{\sigma}$ are

$$\begin{aligned} \sigma_x &= |\downarrow\rangle\langle\uparrow| + |\uparrow\rangle\langle\downarrow| \\ \sigma_y &= i|\downarrow\rangle\langle\uparrow| - i|\uparrow\rangle\langle\downarrow| \\ \sigma_z &= |\uparrow\rangle\langle\uparrow| - |\downarrow\rangle\langle\downarrow| . \end{aligned} \tag{4.5}$$

The projection of $\hat{H}$ onto $|\uparrow\rangle$ and $|\downarrow\rangle$ states is

$$\hat{H}_\sigma = \sum_{m,n=\uparrow,\downarrow} \langle m|\hat{H}|n\rangle |m\rangle\langle n| . \tag{4.6}$$

According to Eq. (4.1),

$$\begin{aligned} |\uparrow\rangle &= \frac{1}{\sqrt{2}}(\Psi_+ + \Psi_-) \\ |\downarrow\rangle &= \frac{1}{\sqrt{2}}(\Psi_+ - \Psi_-) . \end{aligned} \tag{4.7}$$

It is now easy to see from Eq. (4.3) that

$$\begin{aligned}\langle\uparrow|\hat{H}|\uparrow\rangle &= \langle\downarrow|\hat{H}|\downarrow\rangle = 0\\ \langle\downarrow|\hat{H}|\uparrow\rangle &= \langle\uparrow|\hat{H}|\downarrow\rangle = -\Delta/2\,.\end{aligned} \tag{4.8}$$

With the help of these relations one obtains from equations (4.5) and (4.6)

$$\hat{H}_\sigma = -(\Delta/2)\sigma_x\,. \tag{4.9}$$

The general form of the wave function of our two-state system is

$$\Psi(t) = C_+\Psi_+ e^{i\Delta t/(2\hbar)} + C_-\Psi_- e^{-i\Delta t/(2\hbar)} \tag{4.10}$$

with $|C_-|^2 + |C_+|^2 = 1$. If one imposes the initial condition $\Psi(0) = |\uparrow\rangle$, then

$$\Psi(t) = \cos\left(\frac{\Delta t}{2\hbar}\right)|\uparrow\rangle + \sin\left(\frac{\Delta t}{2\hbar}\right)|\downarrow\rangle \tag{4.11}$$

and $\langle\hat{l}_z\rangle = l\langle\sigma_z\rangle$, with

$$\langle\sigma_z\rangle = \langle\Psi(t)|\sigma_z|\Psi(t)\rangle = \cos\left(\frac{\Delta t}{\hbar}\right)\,. \tag{4.12}$$

This equation describes harmonic oscillations of the superconducting current at the frequency $\Delta/\hbar$ between clockwise and counterclockwise directions. Another way to obtain this result is to use the equivalence [29] of the Schrödinger equation for spin one-half to the precession equation for the expectations value of $\boldsymbol{\sigma}$,

$$\hbar\frac{d}{dt}\left\langle\frac{\boldsymbol{\sigma}}{2}\right\rangle = -\left\langle\boldsymbol{\sigma}\times\frac{\delta\hat{H}_\sigma}{\delta\boldsymbol{\sigma}}\right\rangle = \frac{\Delta}{2}\langle\boldsymbol{\sigma}\rangle\times\mathbf{e}_x\,, \tag{4.13}$$

which gives

$$\begin{aligned}\frac{d}{dt}\langle\sigma_x\rangle &= 0\\ \frac{d}{dt}\langle\sigma_y\rangle &= \frac{\Delta}{\hbar}\langle\sigma_z\rangle\\ \frac{d}{dt}\langle\sigma_z\rangle &= -\frac{\Delta}{\hbar}\langle\sigma_y\rangle\,.\end{aligned} \tag{4.14}$$

The last two equations give Eq. (4.12).

We shall account now for mechanical rotations of the body containing the flux qubit. In this Section we shall deal with an absolutely rigid body that can only rotate as a whole. As we shall see, this problem contains all of the components needed to understand the effects of entanglement required by the conservation of the angular momentum. Rotation by the angle ϕ about the quantization axis Z transforms the Hamiltonian of the qubit into

$$\hat{H}' = e^{-i\hat{l}_z\phi}\hat{H}e^{i\hat{l}_z\phi}\,. \tag{4.15}$$

Noticing that the operator of the angular momentum of the superconducting current, $\hat{l}_z$ (that is chosen in units of $\hbar$), commutes with ϕ it is easy to project this Hamiltonian onto $|\uparrow\rangle$ and $|\downarrow\rangle$. Simple calculation yields the following generalization of Eq. (4.9):

$$\begin{aligned}\hat{H}'_\sigma &= \sum_{m,n=\uparrow,\downarrow}\langle m|\hat{H}'|n\rangle|m\rangle\langle n| \\ &= -\frac{\Delta}{2}\left[e^{-2il\phi}\sigma_+ + e^{2il\phi}\sigma_-\right] \\ &= -\frac{\Delta}{2}\left[\cos(2l\phi)\sigma_x + \sin(2l\phi)\sigma_y\right]\end{aligned} \tag{4.16}$$

where $\sigma_\pm = \frac{1}{2}(\sigma_x \pm i\sigma_y)$.

To develop a rigorous formulation of the problem let us first assume that the body with the qubit is an isolated system in a pure quantum state described by a single wave function. The full Hamiltonian of the system is

$$\hat{H} = \frac{(\hbar\hat{L}_z)^2}{2I} - \frac{\Delta}{2}\left[\sigma_x\cos(2l\phi) + \sigma_y\sin(2l\phi)\right]\,, \tag{4.17}$$

where $\hat{L}_z = -i(d/d\phi)$ and $I \equiv I_z$ is the moment of inertia of the body for rotation about the quantization axis. It is easy to check that this Hamiltonian commutes with the operator of the total angular momentum,

$$\hat{J}_z = \hat{L}_z + \hat{l}_z = -i\frac{d}{d\phi} + l\sigma_z\,. \tag{4.18}$$

Consequently, the eigenstates of (4.17) must be entangled states of $\hat{l}_z$ and $\hat{L}_z$ that are eigenstates

of the total angular momentum $\hat{J}_z$:

$$|\Psi_{J\pm}\rangle = \frac{C_{J\pm}}{\sqrt{2}}|\uparrow\rangle_l \otimes |J-l\rangle_L \pm \frac{C_{J\mp}}{\sqrt{2}}|\downarrow\rangle_l \otimes |J+l\rangle_L \,, \tag{4.19}$$

with $J \equiv J_z$. Simple calculation gives

$$C_{J\pm} = \sqrt{1 \pm \frac{1}{\sqrt{1+\frac{\Delta^2 I^2}{4(\hbar l)^2(\hbar J)^2}}}} \tag{4.20}$$

and

$$E_{J\pm} = \frac{(\hbar l)^2}{2I} + \frac{(\hbar J)^2}{2I} \pm \sqrt{\frac{\Delta^2}{4} + \frac{(\hbar l)^2(\hbar J)^2}{I^2}} \tag{4.21}$$

for the energy levels. Here $\pm$ corresponds to $\mp$ in Eq. (4.19) and $J = 0, \pm 1, \pm 2, ...$

Alternatively, the same results can be obtained in the coordinate frame attached to the current loop. In this case one starts with the Hamiltonian

$$\hat{H}_r = \frac{(\hbar \hat{L}_z)^2}{2I} - \frac{\Delta}{2}\sigma_x = \frac{(\hbar \hat{J}_z - \hbar \hat{l_z})^2}{2I} - \frac{\Delta}{2}\sigma_x \,. \tag{4.22}$$

Its eigenfunctions are

$$|\Psi_{J\pm}\rangle_r = \frac{1}{\sqrt{2}}\left(C_{J\pm}|\uparrow\rangle_l \pm C_{J\mp}|\downarrow\rangle_l\right) \otimes |J\rangle \,, \tag{4.23}$$

while eigenvalues are given by Eq. (4.21). The two coordinate frames are related by unitary transformation.

4.1.2 Decoherence from rotations

Any real macroscopic system should have some distribution over J. According to Eq. (4.21), at large I the energies of the states corresponding to different J can be very close. Consequently, a macroscopically large number of different J-states should contribute to the expectation value of any physical quantity. Since the phases of such states can differ significantly, the question then arises how the coherence of the flux qubit is influenced by this effect. Rigorous answer to this question is given below.

To study decoherence, one should prepare the system in a state with a certain direction of l_z,

e.g. $l_z = +l$, and study how $\langle \hat{l}_z \rangle$ would depend on time. Naturally, the initial state should be obtained by subjecting the system to a strong bias field in the direction of the magnetic moment of the current loop. Adding the term $-\frac{1}{2}W\sigma_z$ to the Hamiltonian, it is easy to work out the energy levels of the biased states:

$$E_{J\pm} = \frac{(\hbar l)^2}{2I} + \frac{(\hbar J)^2}{2I} \pm \sqrt{\frac{\Delta^2}{4} + \left[\frac{W}{2} + \frac{(\hbar l)(\hbar J)}{I}\right]^2} \,. \tag{4.24}$$

For a large positive bias the states corresponding to the plus sign in the above equation have too high energies and can be ignored. In this limit the relevant energies, up to a constant, are

$$E_{J-} \equiv E_J = \frac{\hbar^2 (J-l)^2}{2I} = \frac{(\hbar L_z)^2}{2I} \,, \tag{4.25}$$

in accordance with the expectation that they must be the energies of the rotational states of the body. To make sure that the system is magnetized in the direction of the field, that is $l_z = +l$, it must be put in contact with a thermal bath at temperature T. This provides thermal distribution over E_J with probabilities given by

$$P_J = \frac{1}{Z} \exp\left(-\frac{E_J}{k_B T}\right) \,, \qquad Z = \sum_J \exp\left(-\frac{E_J}{k_B T}\right) \,. \tag{4.26}$$

If at $t = 0$ the field is removed and the system is isolated from the bath, it will be a mixture of J-states,

$$|\Psi_{Jl}\rangle_0 = |l\rangle \otimes |J-l\rangle \,, \tag{4.27}$$

with the probability of each J determined by Eq. (4.26). Time evolution of each J-state is provided by

$$|\Psi_{Jl}\rangle = \frac{C_{J+}}{\sqrt{2}} |\Psi_{J+}\rangle e^{-iE_{J+}t/\hbar} + \frac{C_{J-}}{\sqrt{2}} |\Psi_{J-}\rangle e^{-iE_{J-}t/\hbar} \,. \tag{4.28}$$

Consequently, the time dependence of the expectation value of $\hat{l}_z = l\sigma_z$ is determined by

$$\langle \sigma_z \rangle = \sum_J P_J \langle \Psi_{Jl} | \sigma_z | \Psi_{Jl} \rangle \,. \tag{4.29}$$

Using the relations

$$\begin{aligned}
\langle \Psi_{J+}|\sigma_z|\Psi_{J+}\rangle &= \frac{1}{2}\left(C_{J+}^2 - C_{J-}^2\right) \\
\langle \Psi_{J-}|\sigma_z|\Psi_{J-}\rangle &= \frac{1}{2}\left(C_{J-}^2 - C_{J+}^2\right) \\
\langle \Psi_{J-}|\sigma_z|\Psi_{J+}\rangle &= \langle \Psi_{J+}|\sigma_z|\Psi_{J-}\rangle = C_{J+}C_{J-}
\end{aligned} \tag{4.30}$$

one obtains

$$\langle \sigma_z \rangle = \sum_J P_J \left[\frac{\beta_J^2}{1+\beta_J^2} + \frac{1}{1+\beta_J^2} \cos\left(\frac{\Delta_J}{\hbar} t\right) \right], \tag{4.31}$$

where

$$\Delta_J = E_{J+} - E_{J-} = \Delta\sqrt{1+\beta_J^2}, \qquad \beta_J = \frac{2(\hbar l)(\hbar J)}{I\Delta}. \tag{4.32}$$

Notice that only the energy splitting between states belonging to the same J, separated by Δ_J, contribute to $\langle \sigma_z \rangle$. For a given $J \neq 0$ oscillations of the superconducting current occur between $\langle l_z \rangle = l$ and $\langle l_z \rangle = l(\beta_J^2 - 1)/(\beta_J^2 + 1)$ as compared to the oscillations between $\pm l$ for $J = 0$ ($\beta_J = 0$).

Formally, at $T = 0$, only the non-rotating state with $J = l$ contributes to the sum in Eq. (4.31), providing

$$\langle \sigma_z \rangle = \frac{\beta_l^2}{1+\beta_l^2} + \frac{1}{1+\beta_l^2} \cos\left(\frac{\Delta_l}{\hbar} t\right), \tag{4.33}$$

where β_l equals β_J at $J = l$. For a macroscopic body with a large moment of inertia $\beta_l \ll 1$, so that the difference between Eq. (4.12) and Eq. (4.33) is very small. The absence of decoherence at $T = 0$ is related to the fact that the system is in a pure J-state.

At $T \neq 0$ rotations of a macroscopic body must be distributed over a macroscopically large number of $J \gg l$. Consequently, one can replace $J - l$ in Eq. (4.25) with J and replace summation in Eqs. (4.31), (4.26) by integration over J. This gives $Z = \sqrt{2\pi I k_B T}/\hbar$. Expectation value of σ_z depends on time through $(\Delta/\hbar)t$,

$$\begin{aligned}
\langle \sigma_z \rangle = \frac{1}{\sqrt{\pi}\beta_T} \int_{-\infty}^{+\infty} d\beta_J \exp\left(-\frac{\beta_J^2}{\beta_T^2}\right) \times \\
\left[\frac{\beta_J^2}{1+\beta_J^2} + \frac{1}{1+\beta_J^2} \cos\left(\sqrt{1+\beta_J^2}\frac{\Delta}{\hbar} t\right) \right],
\end{aligned} \tag{4.34}$$

and is determined by a single parameter,

$$\beta_T = 2\sqrt{\beta_l \frac{k_B T}{\Delta}} = 2^{3/2} \frac{\hbar l}{\Delta} \sqrt{\frac{k_B T}{I}} \,. \tag{4.35}$$

Note that $\beta_l = 2(\hbar l)^2/(I\Delta)$ contains a macroscopically large number I in the denominator. This provides

$$\beta_l \ll \beta_T \ll 1 \tag{4.36}$$

for any reasonable values of l, Δ, and T. Since the main contribution to the integral in Eq. (4.34) comes from $\beta_J \sim \beta_T \gg \beta_l$, the overwhelming majority of J contributing to the integral satisfy $J \gg l$ in accordance with our assumption.

From Eq. (4.34) the asymptotic value of $\langle \sigma_z \rangle$ is

$$\sigma_\infty \equiv \lim_{t\to\infty} \langle \sigma_z \rangle = \frac{1}{2}\beta_T^2 = 2\beta_l \frac{k_B T}{\Delta} \,. \tag{4.37}$$

For a macroscopic body it is small due to the smallness of β_l. In this limit the time dependence of the oscillating term in Eq. (4.34) can be computed exactly:

$$\langle \sigma_z \rangle_t = \mathrm{Re}\left[\frac{e^{i(\Delta/\hbar)t}}{\sqrt{1 - i\sigma_\infty (\Delta/\hbar) t}} \right] . \tag{4.38}$$

One can see that the amplitude of quantum oscillations is decreasing as $1/\sqrt{\sigma_\infty (\Delta/\hbar) t}$. Thus, the effective decoherence rate due to the entanglement of the flux qubit with rotations of the rigid body is

$$\Gamma_r = \sigma_\infty \frac{\Delta}{\hbar} = 2\beta_l \frac{k_B T}{\hbar} = \frac{4\hbar l^2}{I} \left(\frac{k_B T}{\Delta} \right) . \tag{4.39}$$

Notice that slow, $1/\sqrt{t}$, decay of coherent oscillations given by Eq. (4.38) is a consequence of the absolute rigidity of the body.

Proportionality of Γ_r to $1/I$ illustrates our point that, contrary to the naive picture that one might have [101], the entanglement of a flux qubit with rotations of a macroscopic body, dictated by the conservation of angular momentum, does not necessarily result in a strong decoherence. This comes as a consequence of the selection rule: According to Eq. (4.31) only tunnel splittings, $\Delta_J = E_{J+} - E_{J-}$, of the states (4.21) belonging to the same J contribute to $\langle \sigma_z \rangle$. For a macroscopic

body, all Δ_J are very close, thus providing low decoherence.

4.2 Elastic Body

4.2.1 Flux qubit in the elastic environment

Realistically, the body containing a flux qubit is not absolutely rigid. During half-period of oscillations of the superconducting current the elastic stress generated by the changing angular momentum of the current may only extend as far as half-wavelength, $\lambda/2 = \pi\hbar v_t/\Delta$, of the transverse sound of frequency $\Delta/\hbar$ and speed v_t. We shall assume that this distance is greater than the size of the current loop. For, e.g., a micron-size loop this condition would be typically fulfilled for $\Delta/\hbar < 10$GHz. It allows one to treat the flux qubit as a point source of the elastic stress, without considering interactions of segments of the current loop with the elastic environment.

Now the rotation angle ϕ that appears in the previous section is determined to the elastic twist, [142]

$$\phi = \frac{1}{2}[\boldsymbol{\nabla} \times \mathbf{u}]_z \,, \tag{4.40}$$

where $\mathbf{u}$ is the phonon displacement field at the location of the flux qubit $\mathbf{r} = 0$. Conventional quantization of phonons gives

$$\phi = \frac{1}{2}\sqrt{\frac{\hbar}{2\rho V}} \sum_{\mathbf{k}\lambda} \frac{[i\mathbf{k} \times \mathbf{e}_{\mathbf{k}\lambda}]_z}{\sqrt{\omega_{\mathbf{k}\lambda}}} \left(a_{\mathbf{k}\lambda} + a^\dagger_{-\mathbf{k}\lambda}\right) \,, \tag{4.41}$$

where $a^\dagger_{\mathbf{k}\lambda}, a_{\mathbf{k}\lambda}$ are operators of creation and annihilation of phonons of wave-vector $\mathbf{k}$ and polarization λ, $\mathbf{e}_{\mathbf{k}\lambda}$ are unit vectors of polarization, $\omega_{\mathbf{k}\lambda} = v_t k$ is the phonon frequency, ρ is the mass density of the solid and V is its volume. Since we limit our consideration to elastic twists, only the two transverse polarizations of sound contribute to Eq. (4.41).

Elastic Hamiltonian that replaces Hamiltonian (4.17) of the rigid-body approximation is

$$\begin{aligned}\hat{H} &= \sum_{\mathbf{k}\lambda} \hbar\omega_{\mathbf{k}\lambda} \left(a^\dagger_{\mathbf{k}\lambda} a_{\mathbf{k}\lambda} + \frac{1}{2} \right) - \\ &- \frac{\Delta}{2} \left\{ \sigma_+ \exp\left[l \sum_{\mathbf{k}\lambda} \xi_{\mathbf{k}\lambda} \left(a_{\mathbf{k}\lambda} - a^\dagger_{\mathbf{k}\lambda} \right) \right] \right. \\ &+ \left. \sigma_- \exp\left[-l \sum_{\mathbf{k}\lambda} \xi_{\mathbf{k}\lambda} \left(a_{\mathbf{k}\lambda} - a^\dagger_{\mathbf{k}\lambda} \right) \right] \right\} , \end{aligned} \tag{4.42}$$

where

$$\xi_{\mathbf{k}\lambda} \equiv \sqrt{\frac{\hbar}{2\rho V}} \frac{[\mathbf{k} \times \mathbf{e}_{\mathbf{k}\lambda}]_z}{\sqrt{\omega_{\mathbf{k}\lambda}}} . \tag{4.43}$$

Validity of this approximation relies on the fact that angular velocity of the local rotation, $\Omega = d\phi/dt$, is always small compared to the frequency of sound ω. Indeed, noticing that according to Eq. (4.40) $\Omega \sim \omega k u$ we see that $\Omega \ll \omega$ coincides with the condition of validity of the elastic theory: $ku \ll 1$.

Unitary transformation $\hat{H}_r = \hat{U}^{-1} \hat{H} \hat{U}$ with

$$\hat{U} = \exp\left[\frac{1}{2} l \sigma_z \sum_{\mathbf{k}\lambda} \xi_{\mathbf{k}\lambda} \left(a_{\mathbf{k}\lambda} - a^\dagger_{\mathbf{k}\lambda} \right) \right] \tag{4.44}$$

transforms Hamiltonian (4.42) into

$$\begin{aligned}\hat{H}_r &= \hat{U}^{-1} \left[\sum_{\mathbf{k}\lambda} \hbar\omega_{\mathbf{k}\lambda} \left(a^\dagger_{\mathbf{k}\lambda} a_{\mathbf{k}\lambda} + \frac{1}{2} \right) \right] \hat{U} - \frac{\Delta}{2} \sigma_x \\ &= \sum_{\mathbf{k}\lambda} \hbar\omega_{\mathbf{k}\lambda} \left[a^\dagger_{\mathbf{k}\lambda} a_{\mathbf{k}\lambda} - \frac{l\sigma_z}{2} \xi_{\mathbf{k}\lambda} \left(a_{\mathbf{k}\lambda} + a^\dagger_{\mathbf{k}\lambda} \right) \right] - \frac{\Delta}{2} \sigma_x , \end{aligned} \tag{4.45}$$

where an insignificant constant has been omitted. In the transition from the first to the second line of Eq. (4.45) we have used properties of the displacement operator,

$$\hat{D}^{-1}(\alpha) a \hat{D}(\alpha) = a + \alpha , \quad \hat{D}^{-1}(\alpha) a^\dagger \hat{D}(\alpha) = a^\dagger + \alpha^* , \tag{4.46}$$

with

$$\hat{D}(\alpha_{\mathbf{k}\lambda}) = e^{-\alpha^*_{\mathbf{k}\lambda} a_{\mathbf{k}\lambda} + \alpha_{\mathbf{k}\lambda} a^\dagger_{\mathbf{k}\lambda}}\,, \quad \alpha_{\mathbf{k}\lambda} = -\frac{1}{2}\, l\sigma_z \xi_{\mathbf{k}\lambda}\,. \tag{4.47}$$

Eq. (4.45) shows that from a mathematical point of view the problem formulated in this Section is a variance of spin-boson problem [103]. While some important theorems have been proved for this problem in recent years (see, e.g., Ref. [143] and references therein), its exact eigenstates are unknown. This prevents us from developing rigorous mathematical approach to decoherence along the lines of the previous Section. From a physical point of view, the attractiveness of our variance of the spin-boson model is in the absence of free parameters. The boson field in our case is the phonon displacement field. Its coupling to the flux qubit (described by spin $1/2$) is completely determined by the conservation of total angular momentum. In what follows, we will use an approximation based upon observation that local twists of the elastic solid due to oscillations of the superconducting current in a flux qubit must be very small. Within this approximation we will describe transverse phonons by a classical displacement field $\mathbf{u}(\mathbf{r}, t)$, satisfying $\boldsymbol{\nabla} \cdot \mathbf{u} = 0$.

Expanding Hamiltonian (4.42) to the lowest power on the elastic twist and replacing operators by their classical expectation values, one obtains

$$H = H_E - \frac{\Delta}{2}\sigma_x - \frac{\Delta}{2} l\sigma_y \int d^3 r \delta(\mathbf{r}) \left(\frac{\partial u_x}{\partial y} - \frac{\partial u_y}{\partial x} \right)\,, \tag{4.48}$$

where H_E is the Hamiltonian of free rotations,

$$H_E = \frac{1}{4} \int d^3 r \rho v_t^2 \left(\frac{\partial u_\alpha}{\partial r_\beta} + \frac{\partial u_\beta}{\partial r_\alpha} \right)^2\,. \tag{4.49}$$

The dynamical equation for the displacement field is

$$\rho \frac{\partial^2 u_\alpha}{\partial t^2} = \frac{\partial \sigma_{\alpha\beta}}{\partial r_\beta}\,, \tag{4.50}$$

where $\sigma_{\alpha\beta} = \delta H/\delta e_{\alpha\beta}$ is the stress tensor and $e_{\alpha\beta} = \partial u_\alpha/\partial r_\beta$ is the strain tensor. This gives

$$\rho\left(\frac{\partial^2 u_x}{\partial t^2} - v_t^2\nabla^2 u_x\right) = -\frac{\Delta}{2} l\sigma_y \frac{\partial}{\partial y}\delta(\mathbf{r}) \tag{4.51}$$

$$\rho\left(\frac{\partial^2 u_y}{\partial t^2} - v_t^2\nabla^2 u_y\right) = \frac{\Delta}{2} l\sigma_y \frac{\partial}{\partial x}\delta(\mathbf{r})\,. \tag{4.52}$$

The above equations should be solved together with the Landau-Lifshitz equation for $\boldsymbol{\sigma}$:

$$\frac{\hbar}{2}\frac{d\boldsymbol{\sigma}}{dt} = -\boldsymbol{\sigma}\times\frac{\delta H}{\delta\boldsymbol{\sigma}}\,, \tag{4.53}$$

which gives

$$\hbar\frac{d\sigma_x}{dt} = -\sigma_z\Delta l\int d^3r\delta(\mathbf{r})\left[\frac{\partial u_x}{\partial y} - \frac{\partial u_y}{\partial x}\right] \tag{4.54}$$

$$\hbar\frac{d\sigma_y}{dt} = \sigma_z\Delta \tag{4.55}$$

$$\hbar\frac{d\sigma_z}{dt} = -\sigma_y\Delta + \sigma_x\Delta l\int d^3r\delta(\mathbf{r})\left[\frac{\partial u_x}{\partial y} - \frac{\partial u_y}{\partial x}\right] \tag{4.56}$$

It is easy to see that Eqs. (4.54), (4.55) and (4.56) preserve the length of $\boldsymbol{\sigma}$: $\sigma_x^2 + \sigma_y^2 + \sigma_z^2 = 1$.

First, let us show that, in accordance with our general line of reasoning, the above equations conserve the Z-component of the total angular momentum,

$$J_z = \hbar l\sigma_z + L_z\,. \tag{4.57}$$

Here L_z is the Z-component of the mechanical angular momentum. Its time derivative equals the Z-component of the total mechanical torque, K_z, acting on the body. In the absence of the external torque applied to the surface of the body, K_z is given by [142]

$$K_z = \int d^3r\,(\sigma_{yx} - \sigma_{xy})\,. \tag{4.58}$$

Conventional elastic theory postulates no internal torques, in which case the stress tensor would be

symmetric and K_z would be zero. Situation changes when there are transitions between angular momentum states of a microscopic object inside the body, such as, e.g., a flux qubit. In this case the stress tensor is non-symmetric, yielding

$$\frac{dL_z}{dt} = \int d^3r \left(\sigma'_{yx} - \sigma'_{xy}\right), \tag{4.59}$$

where $\sigma'_{\alpha\beta} = \delta H_{\rm int}/\delta e_{\alpha\beta}$ is the part of the stress tensor related to the interaction of the flux qubit with the elastic environment, $H_{\rm int}$. The latter is given by the second term in Eq. (4.42). To prove conservation of the total angular momentum one needs to write this term with the accuracy to second-order terms on the elastic twists:

$$\begin{aligned} H_{\rm int} &= -\frac{l}{2}\Delta\sigma_y \int d^3r \delta(\mathbf{r}) \left(\frac{\partial u_x}{\partial y} - \frac{\partial u_y}{\partial x}\right) \\ &+ \frac{l^2}{4}\Delta\sigma_x \left[\int d^3r \delta(\mathbf{r}) \left(\frac{\partial u_x}{\partial y} - \frac{\partial u_y}{\partial x}\right)\right]^2 . \end{aligned} \tag{4.60}$$

This gives

$$\begin{aligned} \sigma'_{xy} &= -\frac{l}{2}\Delta\sigma_y \delta(\mathbf{r}) + \frac{l^2}{2}\Delta\sigma_x \delta(\mathbf{r}) \int d^3r \delta(\mathbf{r}) \left[\frac{\partial u_x}{\partial y} - \frac{\partial u_y}{\partial x}\right] \\ \sigma'_{yx} &= \frac{l}{2}\Delta\sigma_y \delta(\mathbf{r}) - \frac{l^2}{2}\Delta\sigma_x \delta(\mathbf{r}) \int d^3r \delta(\mathbf{r}) \left[\frac{\partial u_x}{\partial y} - \frac{\partial u_y}{\partial x}\right] \end{aligned} \tag{4.61}$$

so that

$$\begin{aligned} \frac{dJ_z}{dt} &= \hbar l \frac{d\sigma_z}{dt} + \frac{dL_z}{dt} = \hbar l \frac{d\sigma_z}{dt} + l\Delta\sigma_y \\ &- l^2\Delta\sigma_x \int d^3r \delta(\mathbf{r}) \left(\frac{\partial u_x}{\partial y} - \frac{\partial u_y}{\partial x}\right) . \end{aligned} \tag{4.62}$$

It is now easy to see that condition $dJ_z/dt = 0$ coincides with one of the equations of motion, Eq. (4.56).

4.2.2 Decoherence from internal torques

At $\mathbf{u} = 0$ equations (4.55) and (4.56) would describe coherent precession of $\boldsymbol{\sigma}$ about the X-axis, with $\sigma_x = const$, $\sigma_z \propto \cos(t\Delta/\hbar)$, and $\sigma_y \propto \sin(t\Delta/\hbar)$. Conservation of angular momentum makes the flux qubit wiggle mechanically when the current oscillates between clockwise and counterclockwise. Consequently, it becomes a source of sound, as can be seen from Eqs. (4.51) and (4.52). Let us linearize all equations of motion around $\sigma_x = 1$, $\mathbf{u} = 0$, with small $\sigma_{y,z}(t) \propto e^{-i\omega t}$ and

$$u_{x,y}(\mathbf{r}, t) \propto e^{-i\omega t} \int \frac{d^3k}{(2\pi)^3} e^{i\mathbf{k}\cdot\mathbf{r}} u_{x,y}(\mathbf{k})\,. \tag{4.63}$$

Writing $\delta(\mathbf{r})$ as $\int \frac{d^3k}{(2\pi)^3} e^{i\mathbf{k}\cdot\mathbf{r}}$ one obtains from Eqs. (4.51) and (4.52)

$$u_x(\mathbf{k}) = -\frac{l\Delta}{2\rho}\,\frac{ik_y\sigma_y}{k^2v_t^2 - \omega^2}\,, \quad u_y(\mathbf{k}) = \frac{l\Delta}{2\rho}\,\frac{ik_x\sigma_y}{k^2v_t^2 - \omega^2}\,, \tag{4.64}$$

where $k^2 = k_x^2 + k_y^2 + k_z^2$. Substitution into Eqs. (4.55) and (4.56) results in

$$\hbar^2\omega^2 = \Delta^2\left(1 - \frac{l^2\Delta}{2\rho}\int \frac{d^3k}{(2\pi)^3}\,\frac{k_x^2 + k_y^2}{k^2v_t^2 - \omega^2}\right) \tag{4.65}$$

The integral in this equation should be computed in the complex plane with account of a small imaginary part of ω,

$$\int \frac{d^3k}{(2\pi)^3}\,\frac{k_x^2 + k_y^2}{k^2v_t^2 - \omega^2} = \frac{1}{3\pi^2}\int \frac{k^4dk}{k^2v_t^2 - \omega^2} = \frac{i\omega^3}{3\pi v_t^5}\,. \tag{4.66}$$

This gives

$$\hbar^2\omega^2 = \Delta^2\left(1 - i\frac{l^2\omega^3\Delta}{6\pi\rho v_t^5}\right)\,, \tag{4.67}$$

that is,

$$\omega = \frac{\Delta}{\hbar} - i\Gamma_0\,, \tag{4.68}$$

where

$$\Gamma_0 = \frac{l^2\Delta^5}{12\pi\hbar^4\rho v_t^5} \tag{4.69}$$

is the $T = 0$ rate of the decay of the coherent precession of $\boldsymbol{\sigma}$. This result is in full agreement with the decoherence rate computed with the help of the Fermi golden rule by considering spontaneous quantum transition from the excited state ($|l\rangle - |-l\rangle$) to the ground state ($|l\rangle + |-l\rangle$) with the radiation of a phonon of energy Δ [20]. Its generalization to finite temperature is $\Gamma_e = \Gamma_0 \coth[\Delta/(2k_BT)]$. At $k_BT \gg \Delta$ it gives $\Gamma_e \propto T$ as in Eq. (4.39) obtained for the rigid body. Comparison of the decoherence provided by the two models will be done in Section 4.3.

As is clear from the derivation, the above result corresponds to the decoherence of a weakly excited state of the flux qubit. Our method, however, permits study of decoherence of the state prepared with $\mathbf{u} = 0$ and arbitrary σ_z (including $\sigma_z = 1$) at $t = 0$. Dynamics of the vector $\boldsymbol{\sigma}$ consists of fast precession about the X-axis and slow relaxation towards the energy minimum that according to Eq. (4.48) corresponds to $\sigma_x = 1$, $\sigma_{y,z} = 0$. It is accompanied by radiation of sound due to the torque acting on the flux qubit from the oscillating current. Noticing that the space-time Fourier transform of the displacement generated by the torque, $\mathbf{u}(\mathbf{k}, \omega)$, and the time Fourier transform, $\boldsymbol{\sigma}(\omega)$, of $\boldsymbol{\sigma}(t)$ are always related by Eqs. (4.64) due to the linearity of Eqs. (4.51) and (4.52), one can transform the integral in Eqs. (4.54) and (4.56) as

$$\int d^3r \delta(\mathbf{r}) \left(\frac{\partial u_x}{\partial y} - \frac{\partial u_y}{\partial x} \right) = \frac{l\Delta}{6\pi v_t^5} \int \frac{d\omega}{2\pi} i\omega^3 \sigma_y(\omega) e^{-i\omega t} \,. \tag{4.70}$$

To the first approximation, fast-precessing and slowly-relaxing solution of Eqs. (4.55) and (4.56) that satisfies $\sigma_x^2 + \sigma_y^2 + \sigma_z^2 = 1$ is

$$\begin{aligned} \sigma_y(t) &= \sqrt{1 - \langle \sigma_x \rangle^2} \sin\left(\frac{\Delta}{\hbar} t \right) \\ \sigma_z(t) &= \sqrt{1 - \langle \sigma_x \rangle^2} \cos\left(\frac{\Delta}{\hbar} t \right) , \end{aligned} \tag{4.71}$$

where $\langle \sigma_x \rangle$ is a slow function of time. Within this approximation the Fourier transform of σ_y in Eq. (4.70) is dominated by the Fourier transform of $\sin(t\Delta/\hbar)$ that equals

$$i\pi[\delta(\omega + \Delta/\hbar) - \delta(\omega - \Delta/\hbar)] \,, \tag{4.72}$$

so that the integral (4.70) becomes

$$-2\frac{\hbar\Gamma_0}{\Delta}\sqrt{1-\langle\sigma_x\rangle^2}\cos\left(\frac{\Delta}{\hbar}t\right) \tag{4.73}$$

where Γ_0 is given by Eq. (4.69). Substituting this result into Eq. (4.54), taking into account the first of Eqs. (4.71), and averaging the resulting equation over fast oscillations, $\langle\cos^2(t\Delta/\hbar)\rangle = 1/2$, one obtains

$$\frac{\partial\langle\sigma_x\rangle}{\partial t} = \Gamma_0\left(1-\langle\sigma_x\rangle^2\right). \tag{4.74}$$

This leads to the following relaxation law at $t > 0$ after the system was prepared in the state with arbitrary $\sigma_x = \tanh(\Gamma_0 t_0) \leq 1$ at the moment of time $t = 0$:

$$\langle\sigma_x\rangle = \tanh[\Gamma_0(t+t_0)] \tag{4.75}$$

$$\sigma_y = \frac{\sin\left(\frac{\Delta}{\hbar}t\right)}{\cosh[\Gamma_0(t+t_0)]} \tag{4.76}$$

$$\sigma_z = \frac{\cos\left(\frac{\Delta}{\hbar}t\right)}{\cosh[\Gamma_0(t+t_0)]}. \tag{4.77}$$

Our previous consideration of small oscillations of $\sigma_{y,z}$ (that is, precession around $\sigma_x \to 1$) corresponds to the choice of $\Gamma_0 t_0 \gg 1$, in which case the decay of the oscillations is always exponential with the rate Γ_0, as has been previously found. If the system is prepared in the state with $\sigma_z = 1$ (that corresponds to the choice of $t_0 = 0$ in the above equations), it exhibits exponential relaxation,

$$\sigma_z = 2e^{-\Gamma_0 t}\cos(t\Delta/\hbar), \tag{4.78}$$

only at $\Gamma_0 t \gg 1$. The initial relaxation at $\Gamma_0 t \ll 1$ is slower:

$$\sigma_z = \frac{\cos(t\Delta/\hbar)}{1+\frac{1}{2}(\Gamma_0 t)^2}. \tag{4.79}$$

This later result for a two-state system should be taken with a grain of salt, though, as it is likely to be the consequence of the approximation in which the expectation value of the second term in Eq. (4.48) is replaced by the product of expectation values of σ_y and phonon field. Such approximation neglects quantum correlations between spin 1/2 and the boson field. In this connection, it is

interesting to notice that our model can be easily extended to a system of more than one flux qubit if all the qubits have the same resonance frequency, $\omega = \Delta/\hbar$, and are located within a distance from each other that is small compared to the wavelength of sound of frequency ω. Indeed, for such a system $\boldsymbol{\sigma}/2$ in Eq. (4.42) gets replaced with the total effective spin $\mathbf{S} = \boldsymbol{\sigma}_1/2 + \boldsymbol{\sigma}_2/2 + \boldsymbol{\sigma}_3/2 + ...$ Since the resulting Hamiltonian is linear on $\mathbf{S}$, it commutes with $\mathbf{S}^2$. Consequently, when the number of qubits, N, is large, $\mathbf{S}$ must behave as a classical large spin of constant length. In this case, the approximation that neglects quantum correlations must be good. It leads to the same equations (4.51) - (4.56) in which $\boldsymbol{\sigma}$ is replaced with $N\boldsymbol{\sigma}$. This amplifies the amplitude of sound by a factor N. Consequently, Γ_0 is amplified by a factor N^2. One immediately recognizes Dicke superradiance [144] in this effect. We, therefore, expect Eqs. (4.75) - (4.77) with $\Gamma_0 \to N^2\Gamma_0$ to correctly describe decoherence in a system of $N \gg 1$ closely packed flux qubits.

4.2.3 Renormalization of the tunnel splitting by the elastic environment

The above consideration shows that decoherence of the flux qubit in the elastic environment is dominated by phonons of energy Δ. Meantime, even at $T = 0$ there are zero-point oscillations of the solid that produce elastic twists. Such twists interact with the flux qubit and, as we shall see below, renormalize the tunnel splitting. This problem cannot be treated semiclassically as it requires consideration of the entanglement of the qubit with the excitation modes of the solid. It is based upon computation of the quantum average of the Hamiltonian (4.42), $\langle 0|\hat{H}|0\rangle$ over the ground state of the solid, $|0\rangle$, that has no real phonons.

Noticing that

$$\begin{aligned}\langle 0|e^{l\xi_{\mathbf{k}\lambda}\left(a_{\mathbf{k}\lambda}-a^\dagger_{\mathbf{k}\lambda}\right)}|0\rangle &= \langle 0|e^{-l\xi_{\mathbf{k}\lambda}\left(a_{\mathbf{k}\lambda}-a^\dagger_{\mathbf{k}\lambda}\right)}|0\rangle \\ &= 1 - \frac{1}{2}|l\xi_{\mathbf{k}\lambda}|^2 + ... = e^{-|l\xi_{\mathbf{k}\lambda}|^2/2}\,,\end{aligned} \tag{4.80}$$

one obtains

$$\hat{H}_\sigma \equiv \langle 0|\hat{H}|0\rangle = -\frac{\Delta}{2}\exp\left(-\frac{l^2}{2}\sum_{\mathbf{k}\lambda}|\xi_{\mathbf{k}\lambda}|^2\right)(\sigma_+ + \sigma_-)\,, \tag{4.81}$$

that is,

$$\hat{H}_\sigma = -\frac{\Delta_{\rm eff}}{2}\sigma_x\,, \tag{4.82}$$

where

$$\Delta_{\text{eff}} = \Delta \exp\left(-\frac{l^2}{2}\sum_{\mathbf{k}\lambda}|\xi_{\mathbf{k}\lambda}|^2\right) \tag{4.83}$$

is the tunnel splitting renormalized by zero-point quantum elastic twists. Here $\xi_{\mathbf{k}\lambda}$ is given by Eq. (4.43).

The sum over $\mathbf{k}$ in Eq. (4.83) can be computed by replacing it with the integral $V\int d^3k/(2\pi)^3$. For the two transverse phonon modes $\mathbf{k}\times\mathbf{e}_{\mathbf{k}t_1} = \pm k\mathbf{e}_{\mathbf{k}t_2}$. Averaging over the angles then gives $\langle[\mathbf{e}_{\mathbf{k}t}]_z^2\rangle = 1/3$. Integrating over k from zero to $k_{\max}$ determined by the size of the flux qubit, one obtains

$$\Delta_{\text{eff}} = \Delta \exp\left(-\frac{\hbar l^2 k_{\max}^4}{48\pi^2\rho v_t}\right) \tag{4.84}$$

A quick estimate (see Section 4.3) shows that the exponent in Eq. (4.84) is always small, thus providing negligible renormalization of the tunnel splitting in a flux qubit. However, the above result illustrates an important point. If, for some reason, the shear modulus of the solid, $G = \rho v_t^2$, disappeared, this, according to Eq. (4.84), would lead to the disappearance of the tunnel splitting as well. The latter is a consequence of the conservation of angular momentum: The current cannot reverse direction if it cannot transfer momentum to the body. As is discussed in the next Section this effect may, in principle, be observed in some two-state systems.

4.3 Discussion and Conclusions

We have studied two models that take into account mechanical effects associated with quantum oscillations of a superconducting current in a flux qubit. These effects have simple physical origin. To change direction, the current must transfer momentum to the underlying crystal lattice. For the current oscillating in a SQUID loop, it is a microscopic analogue of the Einstein - de Haas effect: The change in the angular momentum of the current associated with its magnetic moment must be compensated by the change in the angular momentum of the body containing the current. This inevitably entangles quantum states of a flux qubit with quantum states of a macroscopic body containing the qubit. One can naively imagine that almost instantaneous decoherence of quantum states of the macroscopic body would have a detrimental effect on the decoherence of the flux qubit. We show that this is not the case due to the selection rule originating from conservation of angular

momentum. While quantum state of a macroscopic system is, in general, an admixture of a large number of rotational states corresponding to different total angular momenta, only tunnel splittings of the states belonging to the same J contribute to quantum oscillations of the superconducting current. Broadening of the tunnel splitting by the rotational states of a qubit is small as long as the body is sufficiently large.

In the first part of the chapter we have studied an exactly solvable model of a flux qubit entangled with a rigid mechanical rotator. We show that decoherence in such a system is weak due to inverse proportionality of the decoherence rate, $\Gamma_r = (4\hbar l^2/I)(k_BT/\Delta)$, to the moment of inertia of the rotator, I. To put things in perspective, consider, e.g., a micron-size flux qubit embedded in a body of a comparable small size that is free to rotate. Sound of frequency $\omega = \Delta/\hbar \sim 10^{10}\mathrm{s}^{-1}$ would have a wavelength comparable to the size of the body. Consequently, in reaction to the oscillations of the superconducting current, such a system would rotate as a whole, making the rigid-body approximation developed in Section 4.1 a reasonably good one. Typical value of the moment of inertia of a micron-size body is in the ballpark of $10^{-19}\mathrm{g}\cdot\mathrm{cm}^2$. Taking $l \sim 10^5$ for a micron-size current loop, one obtains the following values of the parameters in equations (4.35) - (4.39): $\beta_l \approx 2\times 10^{-8}$, $\beta_T \approx 3\times 10^{-4}(k_BT/\Delta)^{1/2}$, $\sigma_\infty \sim 4\times 10^{-8}(k_BT/\Delta)$. Decoherence is dominated by $J \sim 10^9(k_BT/\Delta)^{1/2}$, which corresponds to frequencies of the rotational Brownian motion $\omega = \hbar J/I \sim 10(k_BT/\Delta)^{1/2}\mathrm{s}^{-1}$. This provides $\Gamma \sim 500\mathrm{s}^{-1}$ that corresponds to a rather high quality factor of quantum oscillations, $Q = \Delta/(\hbar\Gamma) \sim 2\times 10^7[\Delta/(k_BT)]$, even in the extreme case of a micron size system.

In the second part of the chapter we have studied interaction of the flux qubit with the twists of the elastic body, dictated by the conservation of angular momentum. Such model has no free parameters. While its exact quantum states are not known, one can develop a reasonably good approximation in which the internal torque produced inside the body by the oscillating current is treated as a source of elastic shear waves. If the elastic environment is considered to be infinite in space, this is an open system as compared to the closed system that consists of a finite-size rotator with a flux qubit. In the infinite elastic system the shear waves generated by the point source of torque escape to infinity, thus allowing finite decoherence at $T = 0$ as compared to the closed system. The corresponding decoherence rate is given by $\Gamma_e = l^2\Delta^5/(12\pi\hbar^4\rho v_t^5)\coth[\Delta/(2k_BT)]$. At $l \sim 10^5$, $\omega = \Delta/\hbar \sim 10^{10}\mathrm{s}^{-1}$ it is of the order of $10^6\mathrm{s}^{-1}$, which provides $Q = \Delta/(\hbar\Gamma) \sim 10^4$.

This shows that the effect studied here, while allowing weak decoherence, can hardly be ignored in designing flux qubits.

A good check of the validity of the above results can be obtained by comparing decoherence rates obtained within the rigid-rotator model and within the elastic model. At $k_BT \geq \Delta$ the ratio of the two rates is $\Gamma_e/\Gamma_r = (4\pi^4/3)(I/\rho\lambda^5)$ where $\lambda = 2\pi\hbar v_t/\Delta$ is the wavelength of shear waves of frequency $\omega = \Delta/\hbar$. Noticing that the moment of inertia of a rigid body of radius R is of order ρR^5, we see that $\Gamma_e/\Gamma_r \sim 1$ at $\lambda \sim 2R$. This agreement between the two models that consider the same effect from two very different angles is quite remarkable.

In our consideration of the conservation of angular momentum, certain effects that may exist in real systems have been left out. Among them are interactions of the flux qubit with magnetic atoms and nuclear spins that can, in principle, absorb some part of the angular momentum of the SQUID. For $l \gg 1$ such processes must be suppressed, however, as they require coherent participation of many magnetic atoms and many nuclear spins. Interaction of the flux qubit with the shear waves of the body must be the primary mechanism of the conservation of angular momentum. Being unavoidable, it imposes a universal upper bound on the quality factor of the qubit.

The effect of rotations on decoherence can also be understood from another angle. At $\phi = \omega t$ that corresponds to the uniform rotation of the flux qubit about the Z-axis the Hamiltonian (4.16) is equivalent to the Hamiltonian of spin 1/2 in the effective magnetic field of amplitude $\Delta/(2\mu_B)$ (μ_B being the Bohr magneton) rotating in the XY plane at an angular velocity $\Omega = 2l\omega$. Switching to the coordinate frame rotating with the field, gives an effective constant field applied along the X-axis plus the effective bias field in the Z-direction, $\hat{H}''_\sigma = -l\hbar\omega\sigma_z - \frac{\Delta}{2}\sigma_x$. The first term is simply $-\boldsymbol{\omega}\cdot\hbar\mathbf{l}$, that appears in the frame rotating at the mechanical angular velocity $\boldsymbol{\omega}$, projected into the $|\uparrow\rangle$ and $|\downarrow\rangle$ states. Real bias magnetic field B adds the term $-\mathbf{B}\cdot(\mu_B\mathbf{l})$ to the Hamiltonian. When the field is applied along the Z-axis the full two-state Hamiltonian in the rotating (SQUID) frame of reference becomes $\hat{H}''_\sigma = -l(\hbar\omega + \mu_B B)\sigma_z - \frac{\Delta}{2}\sigma_x$. This proves that the rotation of a truncated two-state SQUID system satisfies Larmor theorem. It is equivalent to the magnetic field $B/\omega = \hbar/\mu_B \sim 10^{-7}$Oe/Hz. Effective fields generated by slow rotations of the equipment must have negligible effect on the flux qubit. However, the effect of local dynamic shear deformations on a microscopic SQUID must be noticeable because the corresponding angular velocities $(ku)(\Delta/\hbar)$ can easily reach 10^7Hz, providing effective fields in the range of $1G$.

Experiments with flux qubits have shown that significant decoherence comes from $1/f$ noise, the origin of which has been debated [145, 146]. Notice in this connection that relaxation of microscopic shear strains in a solid must be a source of dynamical local twists that, according to the above discussion, generate local effective magnetic fields. It is, therefore, plausible that relaxation of shear strains at the location of the qubit is, in fact, responsible for the observed $1/f$ noise affecting quantum dynamics of the qubit.

Another observation worth mentioning is amplification of decoherence in a system of flux qubits positioned in close proximity to each other. This effect may be important in designing architectures of flux qubits if they are to be used for quantum computing. It will reveal itself when N microscopic qubits with identical tunnel splitting Δ are positioned within the wavelength of sound of frequency $\Delta/\hbar$. As has been demonstrated in Section 4.2.2, radiation of sound by such a system and, thus, decoherence will be amplified by a factor N^2. This is an acoustic analogue of Dicke superradiance that may impose an upper limit on the density of flux qubits. One way to avoid this effect in a dense assembly of qubits would be to use qubits of significantly different Δ.

In Section 4.2.3 we studied renormalization of the tunnel splitting of a flux qubit arising from its interaction with zero-point shear deformations. The magnetic moment of the current of strength J in a loop of area a is $\mu = Ja/c$, which gives $l = Ja/(c\mu_B)$. With $a = \pi r^2$ and $k_{\max} = 2\pi/r$, the exponent in Eq. (4.84) becomes $\pi^4\hbar J/(3c^2\mu_B^2\rho v_t)$. At $J \sim 1\mu$A it is hopelessly small, thus, making this kind of renormalization irrelevant for a flux qubit.

Notice in this connection that a similar effect, described by Eq. (4.84), may exist for the tunnel splitting of the atomic magnetic cluster. In this case l would be significantly smaller but $k_{\max}$ would be much greater than for a flux qubit. An estimate for, e.g., a magnetic molecule frozen in solid He-4 shows that the exponent in Eq. (4.84) can easily be of order unity. As the He-solid approaches melting transition on decreasing pressure, its shear modulus would go to zero, resulting in the freezing of tunneling.

Finally, we would like to notice that the treatment developed here should apply to nanomechanical devices incorporating SQUIDs. Such devices have been recently made and measured [98, 99]. They open the whole new field of the entanglement of qubit states with mechanical oscillations. Possible manipulation of superconducting qubits by mechanical rotations is another interesting aspect of the research on nanomechanical superconducting qubits. Our model of a rigid rotator with

a flux qubit may provide a framework for theoretical studies of these effects.

5

Spin-Boson Model

5.1 Background

The single mode spin-boson model describes a two-level system interacting with a single quantized harmonic oscillator. The spin-boson Hamiltonian is ($\hbar = 1$)

$$\hat{H}_{SB} = \omega a^\dagger a + \frac{\Delta}{2}\sigma_x + \sigma_z(g^* a + g a^\dagger) \tag{5.1}$$

where ω is the frequency of the bosonic mode, Δ is the level splitting of the two-level system, and g is the coupling between the two systems. $a^\dagger$ and a are creation and annihilation operators of the bosonic mode, respectively, and $\sigma_{x,z}$ are Pauli matrices of the two-level system. It is also known as the quantum Rabi model, usually written with $x \leftrightharpoons z$.

A related model which we have studied,

$$\hat{H} = \omega a^\dagger a + \frac{\Delta}{2}\left(\sigma_+ e^{-i\lambda(a+a^\dagger)} + \sigma_- e^{i\lambda(a+a^\dagger)}\right) \tag{5.2}$$

describes the lowest tunneling doublet of a spin coupled to a torsional resonator (see Section 6.1.2 for details). Transforming this Hamiltonian to the rotating frame shows its relation to the spin-boson model,

$$\hat{U}\hat{H}\hat{U}^\dagger \longrightarrow \hat{H}_{SB}, \qquad \hat{U} = e^{i\lambda\sigma_z(a+a^\dagger)/2} \tag{5.3}$$

(up to an unessential constant) with $g = -i\omega\lambda/2$. The multimode generalization of the spin-

resonator Hamiltonian describes a nanomagnet or flux qubit embedded in an elastic environment, discussed in Chapter 4.

The Jaynes-Cummings model [106] describes the near-resonant, weak coupling limit of the spin-boson Hamiltonian, obtained by making the rotating wave approximation. Splitting $\hat{H}_{SB}$ into noninteracting $\hat{H}_0 = \omega a^\dagger a + \frac{\Delta}{2}\sigma_x$ and interacting $\hat{H}_1 = g\sigma_z(a + a^\dagger)$ terms (we have taken $g = g^*$), we switch to the interaction picture and expand in terms of raising and lowering operators $\sigma_\pm = (\sigma_z \mp i\sigma_y)$ in the σ_x basis,

$$\hat{H}^I_{int} = e^{i\hat{H}_0 t}\hat{H}_1 e^{-i\hat{H}_0 t} = g(\sigma_+ a\, e^{-i(\omega-\Delta)} + \sigma_- a^\dagger\, e^{i(\omega-\Delta)} + \sigma_+ a^\dagger\, e^{i(\omega+\Delta)} + \sigma_- a\, e^{-i(\omega+\Delta)}). \quad (5.4)$$

In the limit of near-resonance $\omega \approx \Delta$ the first two terms oscillate slowly while the final two terms oscillate rapidly. For weak coupling $g \ll \omega$, the rotating wave approximation is made by neglecting these so-called counter-rotating terms and switching back to the Schrödinger picture. The Jaynes-Cummings Hamiltonian is

$$\hat{H}_{JC} = \omega a^\dagger a + \frac{\Delta}{2}\sigma_x + g(\sigma_+ a + \sigma_- a^\dagger). \quad (5.5)$$

Another way to understand the rotating wave approximation is that the first two terms in $\hat{H}_1$ describe transitions between states that are nearly equal in energy in the absence of interactions, i.e. excitation (deexcitation) of the two-level system coincides with annihilation (creation) of an oscillator quantum, while the last two terms describe simultaneous excitation or deexcitation of the two-level system and oscillator. The Jaynes-Cummings model commutes with the excitation number,

$$\hat{N} = a^\dagger a + \frac{1}{2}(\sigma_x + 1), \qquad [\hat{N}, \hat{H}_{JC}] = 0. \quad (5.6)$$

which makes it block-diagonalizable into an infinite number of 2×2 non-interacting subsystems. Projecting $\hat{H}_{JC}$ onto the basis $|n, +x\rangle, |n+1, -x\rangle$, where $\sigma_x|n, \pm x\rangle = \pm|n, \pm x\rangle$, and diagonalizing gives

$$E_{n\pm} = n\omega \pm \frac{1}{2}\sqrt{(\omega - \Delta)^2 + \Omega_n^2}, \qquad \Omega_n = 2g\sqrt{n+1}, \quad (5.7)$$

where Ω_n is the quantum electrodynamic Rabi frequency which depends on the occupation number

of the oscillator [107].

5.2 Parity Chains and Diagonalization

In the Jaynes-Cummings model, the conserved quantity $\hat{N}$ generates a continuous $U(1)$ symmetry. When the counter-rotating terms are included to return to the spin-boson model, the $U(1)$ symmetry is reduced to $\mathbb{Z}_2$ parity symmetry. The corresponding constant of motion which generates this symmetry is the overall parity operator,

$$\hat{\Pi} = \sigma_x P_\pi, \qquad [\hat{\Pi}, \hat{H}_{SB}] = 0, \tag{5.8}$$

where $P_\pi = e^{i\pi a^\dagger a}$ is the bosonic parity operator. This can be used to take $\hat{H}_{SB}$ to the diagonal form $\hat{H}_{SB}^D = \hat{T}^{-1}\hat{H}_{SB}\hat{T}$ within the two-level space by means of a Fulton-Gouterman transformation [147],

$$\hat{H}_{SB}^D = \begin{bmatrix} H_+ + \frac{\Delta}{2}P_\pi & 0 \\ 0 & H_- - \frac{\Delta}{2}P_\pi \end{bmatrix}, \qquad H_\pm = \omega a^\dagger a \pm (g^* a + g a^\dagger), \tag{5.9}$$

where

$$\hat{T} = \frac{1}{\sqrt{2}}\begin{bmatrix} 1 & -P_\pi \\ P_\pi & 1 \end{bmatrix}, \qquad \hat{T}^{-1} = \frac{1}{\sqrt{2}}\begin{bmatrix} 1 & P_{-\pi} \\ -P_\pi & 1 \end{bmatrix}. \tag{5.10}$$

Gardas finds $\hat{T}$ by solving the Riccati operator equation [143]. One of Gardas's major results is the form of the time evolution operator, which is then given by

$$\hat{U} = \hat{T}(e^{-i\hat{H}_{SB}^D t})\hat{T}^{-1}, \tag{5.11}$$

or explicitly in matrix form,

$$\hat{U} = \frac{1}{2}\begin{bmatrix} e^{-i(H_+ + \frac{\Delta}{2}P_\pi)t} + e^{-i(H_+ - \frac{\Delta}{2}P_\pi)t} & \left(e^{-i(H_+ + \frac{\Delta}{2}P_\pi)t} - e^{-i(H_+ - \frac{\Delta}{2}P_\pi)t}\right)P_\pi \\ \left(e^{-i(H_- + \frac{\Delta}{2}P_\pi)t} - e^{-i(H_- - \frac{\Delta}{2}P_\pi)t}\right)P_\pi & e^{-i(H_- + \frac{\Delta}{2}P_\pi)t} + e^{-i(H_- - \frac{\Delta}{2}P_\pi)t} \end{bmatrix}. \tag{5.12}$$

The missing step is finding an exact expression for the dynamics is solving the eigenvalue equation for each parity chain,

$$(H_{\pm} \pm \frac{\Delta}{2} P_{\pi})\psi = E_{\pm}\psi. \tag{5.13}$$

Braak has recently shown the $\mathbb{Z}_2$ symmetry is adequate to solve each parity chain in the quantum Rabi model [115]. We summarize some of Braak's major results here. Using the Bargmann representation for the creation and annihilation operators [148] in the complex variable z,

$$a \longrightarrow \frac{\partial}{\partial z}, \qquad a^{\dagger} \longrightarrow z \tag{5.14}$$

the parity chain Hamiltonians take the form

$$H_{z\pm} = \omega z \frac{\partial}{\partial z} \pm g\left(z + \frac{\partial}{\partial z}\right) \pm \frac{\Delta}{2} P_z \tag{5.15}$$

where P_z is the parity operator in the Bargmann space of functions $f(z)$, such that $P_z f(z) = f(-z)$. The time-independent Schrödinger equation $H_z\psi(z) = E\psi(z)$ can be solved by taking $\psi(z) = \phi_1(z)$, $\psi(-z) = \phi_2(z)$. These two representations must coincide, i.e. $\phi_1(z) = \phi_2(-z)$, which gives $G_{\pm}(x) = 0$, where

$$G_{\pm}(x) = \sum_{n=0}^{\infty} K_n(x) \left[1 \mp \frac{\Delta/2}{x - n\omega}\right] \left(\frac{g}{\omega}\right)^n \tag{5.16}$$

where

$$nK_n = f_{n-1}(x)K_{n-1} - K_{n-2} \tag{5.17}$$

with initial conditions $K_0 = 1$, $K_1 = f_0$, and

$$f_n(x) = \frac{2g}{\omega} + \frac{1}{2g}\left(n\omega - x + \frac{(\Delta/2)^2}{x - n\omega}\right). \tag{5.18}$$

There are two types of eigenvalues, regular and exceptional. Regular eigenvalues $E_{n\pm} = x_{n\pm} - g^2/\omega$ correspond to zeros of $G_{\pm}(x)$. Exceptional eigenvalues occur when $K_n(n\omega)$ lifts a pole of $G_{\pm}(x)$ at $x_n = n\omega$, and have no definite parity. This corresponds to crossing of eigenvalues from different parity spaces.

While this analytic solution is a major breakthrough [149], the dynamics of this system based on

this solution still require numerical evaluation [116] and the crossover from the Jaynes-Cummings to quantum Rabi model is not as simple as expected [118]. The open question remains whether one can construct closed-form expressions for the energies, eigenstates, and dynamics of the spin-boson model, both in its single and multi-mode versions. These may provide further physical insight into the nature of Braak's solution. We describe a preliminary approach and some possible avenues for further research.

5.3 Displaced Oscillator Basis

As a first step, we use the displaced oscillator basis to find an approximate expression for the energy eigenvalues of the parity chains. The positive parity chain Hamiltonian is (in units of ω)

$$H = D(-f)a^\dagger a D(f) - |f|^2 + \frac{\Delta}{2}P_\pi, \tag{5.19}$$

where $f = g/\omega$ is the dimensionless coupling and $D(\beta)$ is the displacement operator,

$$D(\beta) = e^{\beta a^\dagger - \beta^* a}, \qquad D^\dagger(\beta) a D(\beta) = a + \beta, \qquad D^\dagger(\beta) = D(-\beta) \tag{5.20}$$

Expanding the wavefunction in terms of displaced oscillator states,

$$\psi = \sum_n a_n |-f, n\rangle, \qquad |-f, n\rangle = D(-f)|n\rangle \tag{5.21}$$

the time-independent Schrödinger equation $H\psi = \lambda\psi$ gives

$$\sum_n a_n \left[(n - \lambda)|-f, n\rangle + (-1)^n \frac{\Delta}{2}|f, n\rangle \right] = 0 \tag{5.22}$$

where we have used $P_\pi|-f, n\rangle = (-1)^n|f, n\rangle$ and included the constant term $|f|^2$ in λ. Taking the inner product with $\langle -f, m|$ gives

$$a_m \left[\lambda - m - (-1)^m \frac{\Delta}{2} V_{mm}(-2f) \right] = \sum_{n \neq m} a_n \left[(-1)^n \frac{\Delta}{2} V_{mn}(-2f) \right] \tag{5.23}$$

where

$$V_{m,n}(\beta) = \langle m|D(\beta)|n\rangle = \begin{cases} \sqrt{\dfrac{n!}{m!}}\,\beta^{m-n}e^{-|\beta^2|/2}L_n^{m-n}(|\beta|^2), & m > n \\ e^{-|\beta^2|/2}L_n(|\beta|^2), & m = n \\ \sqrt{\dfrac{m!}{n!}}\,(-\beta)^{n-m}e^{-|\beta^2|/2}L_m^{n-m}(|\beta|^2), & m < n \end{cases} \tag{5.24}$$

The first approximation of the eigenvalues comes from setting the left hand side of Eq. (5.23) to zero, giving

$$\lambda \approx m + (-1)^m \frac{\Delta}{2} V_{mm}(-2f). \tag{5.25}$$

Even this first correction displays good agreement with numerical diagonalization, shown in Fig. 5.1. To find the next order correction, we proceed along the lines of Ref. [150]. Solving Eq. (5.23) for a_m and substituting this for a_n on the right hand side gives

$$a_m \left[\lambda - m - (-1)^m \frac{\Delta}{2} V_{mm}\right] = \left(\frac{\Delta}{2}\right)^2 \sum_{n\neq m} \sum_{l\neq n} a_l \frac{(-1)^{n+l} V_{mn} V_{nl}}{\lambda - n - (-1)^n \frac{\Delta}{2} V_{nn}}. \tag{5.26}$$

Pulling out the $l = m$ terms on the right hand side and neglecting all other terms gives

$$a_m \left[\lambda - m - (-1)^m \frac{\Delta}{2} V_{mm} - \left(\frac{\Delta}{2}\right)^2 \sum_{n\neq m} \frac{(-1)^{n+m} V_{mn} V_{nm}}{\lambda - n - (-1)^n \frac{\Delta}{2} V_{nn}}\right] = 0. \tag{5.27}$$

Making use of the first approximation of the eigenvalues Eq. (5.25) in the denominator of the sum, we obtain

$$\begin{aligned} \lambda_{m+} \approx\ & m\omega + (-1)^m \frac{\Delta}{2} V_{mm}(-2f) \\ & + \left(\frac{\Delta}{2}\right)^2 \sum_{n\neq m} \frac{(-1)^{n+m} V_{mn}(-2f) V_{nm}(-2f)}{(m-n)\omega + \left[(-1)^m V_{mm}(-2f) - (-1)^n V_{nn}(-2f)\right] \dfrac{\Delta}{2}}. \end{aligned} \tag{5.28}$$

Taking $f \to -f$ and $\Delta \to -\Delta$ gives the negative parity solutions λ_{m-}. These eigenvalues are shown in Fig. 5.1, and show remarkable agreement with numerical diagonalization, with excellent agreement for stronger coupling $f \sim 1$.

The eigenvalue expression we have obtained in Eq. (5.28) resembles second order nondegenerate perturbation theory. However, it is not *a priori* obvious what the perturbation parameter is. We will continue to study this model with the goal of obtaining closed-form solutions for the eigenvalues,

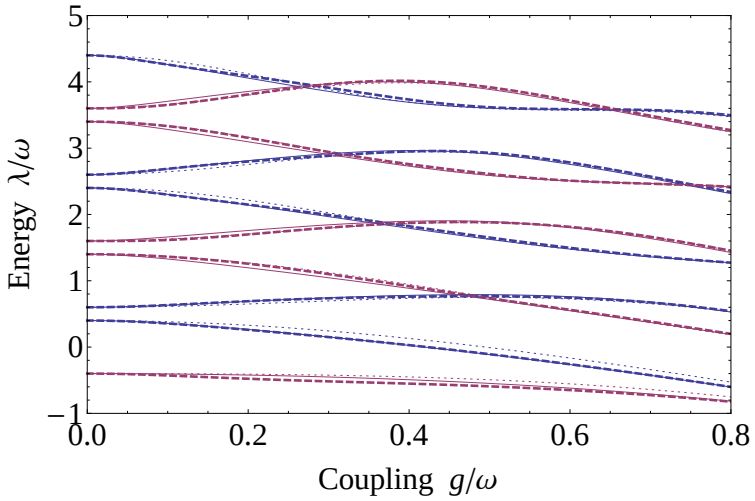

Figure 5.1: Energy spectrum as a function of coupling (both in units of ω) for $\Delta = 0.8\omega$. Comparison of first order approximation (Eq. (5.25), dotted line), second order correction (Eq. (5.28), thick dashed line) and numerical diagonalization (solid line).

eigenstates, and dynamics of the spin-boson model.

6

Landau-Zener dynamics of a nanoresonator containing a tunneling spin

We study the Landau-Zener dynamics of a tunneling spin coupled to a torsional resonator. For strong spin-phonon coupling, when the oscillator frequency is large compared to the tunnel splitting, the system exhibits multiple Landau-Zener transitions. Entanglement of spin and mechanical angular momentum results in abrupt changes of oscillator dynamics which coincide in time with spin transitions. We show that a large number of spins on a single oscillator coupled only through the in-phase phonon field behave as a single large spin, greatly enhancing the spin-phonon coupling. We compare purely quantum and semiclassical dynamics of the system and discuss their experimental realizations. An experiment is proposed in which the field sweep is used to read out the exact quantum state of the mechanical resonator.

Realizing a quantum magneto-mechanical system with strong spin-phonon coupling has been an experimental challenge. A recent experiment [28] has shown the first evidence of strong spin-phonon coupling in a single molecule magnet grafted onto a carbon nanotube. Spin reversal of the single molecule magnet during a Landau-Zener sweep coincides with an abrupt increase in the differential conductance through the carbon nanotube. This has been interpreted as the spin transition exciting a longitudinal stretching mode of the carbon nanotube, which enhances electron tunneling from the

lead onto the nanotube through electron-phonon coupling.

We propose multiple schemes to realize strongly coupled dynamics of a tunneling macrospin with torsional oscillations of a nanoresonator in a Landau-Zener experiment. We investigate the Landau-Zener dynamics of a tunneling spin coupled to a torsional oscillator, using a fully quantum mechanical model. The oscillator could be a torsional paddle resonator, a microcantilever, a carbon nanotube, or a single magnetic molecule between two point contacts. The tunneling spin could be a single molecule magnet, an ensemble of single molecule magnets, or a single-domain ferromagnetic particle with strong uniaxial anisotropy. For a collection of single molecule magnets placed on a torsional resonator or cantilever far apart from each other that they are not directly coupled through dipole interactions, we develop a semiclassical model of magnetization dynamics. We predict superradiant enhancement [125] of the spin-phonon coupling for this ensemble system. Comparison of these two models shows their correspondence.

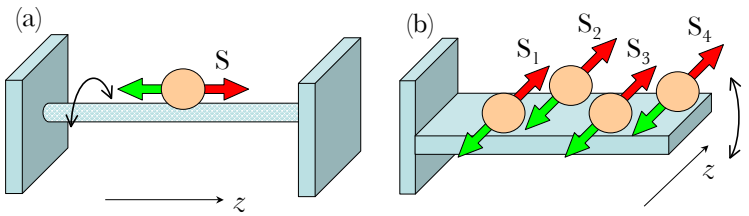

Figure 6.1: Possible experimental geometries described by the models studied here. In both cases the easy axis of the macrospin coincides with the rotation axis of the oscillator. (a) Single molecule magnet grafted on a carbon nanotube. (b) Ensemble of single molecule magnets on a nanocantilever.

This chapter is organized as follows. In Sec. 6.1 we briefly review the Landau-Zener model, and construct the quantum mechanical model of a spin coupled to a torsional resonator with an external magnetic field that varies linearly in time. Sec. 6.2 contains numerical and analytical results of the fully quantum spin dynamics for a variety of parameter ranges. Oscillator dynamics are presented in Sec. 6.3. A semiclassical model of superradiant dynamics in an ensemble of spins on a single resonator is developed in Sec. 6.4. Finally, we discuss the interpretation of our results for various experimental realizations in Sec. 6.5.

6.1 Model

6.1.1 Landau-Zener Transitions in a Two-State System

We review relevant features of the Landau-Zener model, which describes a two-level system driven by a classical field that varies linearly in time. The LZ Hamiltonian is

$$\hat{H}_{LZ} = -\frac{vt}{2}\sigma_z - \frac{\Delta}{2}\sigma_x, \tag{6.1}$$

in terms of Pauli matrices σ_z and $\sigma_x = \sigma_+ + \sigma_-$, where v is the sweep rate and Δ is the tunnel splitting. Diabatic states $|\uparrow\rangle$ and $|\downarrow\rangle$ are eigenstates of σ_z with diabatic energies $E_{\uparrow\downarrow}(t) = \pm vt/2$, which are the linear functions in Fig. 6.2a. We take the sweep rate v positive, so the positive (negative) sign corresponds to spin down (up). For nonzero Δ, the diabatic states are not eigenstates of the Hamiltonian. Diagonalizing $\hat{H}_{LZ}$ gives adiabatic energies

$$E_\pm(t) = \pm\frac{1}{2}\sqrt{(vt)^2 + \Delta^2} \tag{6.2}$$

which are the upper and lower curves in Fig. 6.2a with splitting Δ at $t = 0$. The corresponding adiabatic eigenstates $|+\rangle$ and $|-\rangle$ are

$$|\pm\rangle = \frac{1}{\sqrt{2}}(C_\mp|\uparrow\rangle \mp C_\pm|\downarrow\rangle), \tag{6.3}$$

where $C_\pm$ depend explicitly on time,

$$C_\pm = \sqrt{1 \pm \frac{vt}{\sqrt{(vt)^2 + \Delta^2}}}. \tag{6.4}$$

For times $|t| \gg \Delta/v$ the adiabatic states asymptotically coincide with the diabatic states.

The state of the system

$$\Psi(t) = c_\uparrow(t)|\uparrow\rangle + c_\downarrow(t)|\downarrow\rangle \tag{6.5}$$

evolves according to the time-dependent Schrödinger equation

$$i\hbar\frac{\partial\Psi}{\partial t} = \hat{H}\Psi \tag{6.6}$$

with initial conditions $c_\uparrow(-\infty) = 0$, $|c_\downarrow(-\infty)| = 1$. After eliminating $c_\downarrow$, we obtain the second order differential equation

$$\ddot{c}_\uparrow(t) + \left[\left(\frac{\Delta}{2\hbar}\right)^2 - \frac{iv}{2\hbar} + \left(\frac{vt}{2\hbar}\right)\right] c_\uparrow(t) = 0 \tag{6.7}$$

which can be put into the standard form of the Weber equation. The exact solution [120] gives

$$c_\uparrow(t) = \sqrt{\gamma}e^{-\pi\gamma/4}D_{-\nu-1}(-iz) \tag{6.8}$$

where

$$\gamma = \frac{\Delta^2}{4\hbar v}, \qquad \nu = i\gamma, \qquad z = \sqrt{\frac{v}{\hbar}}e^{-i\pi/4}t, \tag{6.9}$$

and $D_{-\nu-1}(-iz)$ are parabolic cylinder functions. The staying probability for the spin-down state as function of time is $P(t) = |c_\downarrow(t)|^2$. The exact asymptotic limit for $t = \infty$, known as the Landau-Zener probability, is

$$P_{LZ} = e^{-\epsilon}, \qquad \epsilon = \frac{\pi\Delta^2}{2\hbar v}. \tag{6.10}$$

$P(t)$ and P_{LZ} are shown in Fig. 6.2b. The same $P(t)$ and P_{LZ} can be obtained from the Heisenberg equations of motion for $\langle\sigma_z(t)\rangle$. An intuitive understanding of the Landau-Zener transition comes

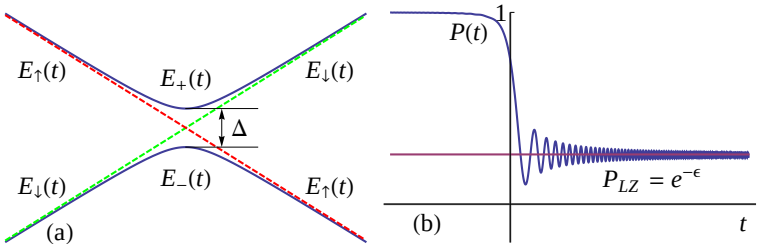

Figure 6.2: (a) Adiabatic $E_\pm(t)$ and diabatic $E_{\uparrow\downarrow}(t)$ energy levels of the LZ Hamiltonian as a function of time. (b) Probability $P(t)$ of staying in the initial $|\downarrow\rangle$ state as a function of time, and asymptotic staying probability P_{LZ}.

from considering the time spent in the tunneling region between adiabatic states and the tunneling time between these states. Let $\tau_{LZ} \sim \max(\sqrt{\hbar/v}, \Delta/v)$ be the time spent in the tunneling region

and $\tau_\Delta \sim \hbar/\Delta$ be the tunneling time at the crossing. The Landau-Zener exponent is proportional to the ratio of these times $\epsilon \sim \tau_{LZ}/\tau_\Delta$. For a slow sweep the system will evolve adiabatically, spending long enough in the tunneling region that it will continually relax to the ground state, making $\epsilon \gg 1$ and $P_{LZ} \to 0$. In the opposite limit, a fast sweep through the tunneling region makes $\epsilon \ll 1$ and the staying probability saturates at $P_{LZ} \to 1$.

6.1.2 Landau-Zener Transitions in a Spin-Oscillator System

Consider a tunneling spin which is projected onto the lowest tunneling doublet. This spin is coupled to a torsional nanoresonator with rigidity k that can rotate about the z-axis, which coincides with the easy axis of the spin. The Hamiltonian is [24, 23],

$$\hat{H} = \frac{\hbar^2 L_z^2}{2I} + \frac{I_z \omega_r^2 \phi^2}{2} - \frac{W(t)}{2}\sigma_z - \frac{\Delta}{2}\left(e^{-i2S\phi}\sigma_+ + e^{i2S\phi}\sigma_-\right). \tag{6.11}$$

The fundamental frequency of torsional oscillations is $\omega_r = \sqrt{k/I_z}$, where I_z is the moment of inertia of the resonator about its rotation axis. An external longitudinal magnetic field $B_z(t)$ applied along this axis creates a time-dependent energy bias $W(t) = 2Sg\mu_B B_z(t)$. The Landau-Zener problem describes a linear field sweep, $W(t) = vt$. The operator of mechanical angular momentum, $L_z = -i\partial_\phi$, and the angular displacement ϕ of the oscillator obey the usual commutation relation $[\phi, L_z] = i$.

The last term in the Hamiltonian describes the entanglement between spin transitions and mechanical rotations. A typical single molecule magnet has a large spin and strong uniaxial anisotropy, producing a zero-field splitting between degenerate ground states $|\psi_{\pm S}\rangle$ pointing in either direction along the easy axis. Any symmetry breaking interactions, such as transverse anisotropy or an external field, break this degeneracy producing tunnel split states $\Psi \sim |\psi_S\rangle \pm |\psi_{-S}\rangle$ which are represented by the pseudospin $\boldsymbol{\sigma}$. The tunnel splitting Δ is generally many orders of magnitude less than the energy to the next spin level. In the case of the spin-10 single molecule magnet Fe_8, the crystal field Hamiltonian describing the magnetic anisotropy is $\hat{H}_S = -D\hat{S}_z^2 + d\hat{S}_y^2$, with $d \ll D$. Full perturbation theory [140] gives

$$\Delta = \frac{8S^{3/2}}{\pi^{1/2}}\left(\frac{d}{4D}\right)^S D, \tag{6.12}$$

where we can see that $\Delta \ll 2SD$, which is the distance to the next spin level. The crystal field Hamiltonian $\hat{H}_S$ is defined with respect to coordinate axes that are rigidly coupled to the molecule or crystal. Because the particle is free to rotate, the crystal field Hamiltonian must be transformed to the fixed frame of the laboratory. Projecting the crystal field Hamiltonian onto the lowest tunneling doublet, rotating to the lab frame using $\hat{U}(\hat{S}_z) = e^{i\hat{S}_z\phi}$, where $\hat{S}_z|\psi_{\pm S}\rangle \simeq \pm S|\psi_{\pm S}\rangle$, $\hat{H}'_S = \hat{U}\hat{H}_S\hat{U}^{-1}$ gives the final term of the Hamiltonian.

We now consider the spin-oscillator Hamiltonian with a linear field sweep $W(t) = vt$. Introducing the usual annihilation and creation operators, a and $a^\dagger$,

$$\phi = \sqrt{\frac{\hbar}{2I_z\omega_r}}(a^\dagger + a), \qquad L_z = i\sqrt{\frac{I_z\omega_r}{2\hbar}}(a^\dagger - a) \tag{6.13}$$

into Eq. (6.11) gives

$$\hat{H} = \hbar\omega_r a^\dagger a - \frac{vt}{2}\sigma_z - \frac{\Delta}{2}(e^{-i\lambda(a^\dagger+a)}\sigma_+ + e^{i\lambda(a^\dagger+a)}\sigma_-), \tag{6.14}$$

where we have dropped unessential constant terms. We will find it useful to adopt dimensionless units $\hat{H}' = \hat{H}/\Delta$ and $t' = \Delta t/\hbar$,

$$\hat{H}' = ra^\dagger a - \frac{v't'}{2}\sigma_z - \frac{1}{2}(e^{-i\lambda(a^\dagger+a)}\sigma_+ + e^{i\lambda(a^\dagger+a)}\sigma_-), \tag{6.15}$$

which shows that the system depends on three parameters. The parameters

$$\lambda = \sqrt{\frac{2\hbar S^2}{I_z\omega_r}}, \qquad r = \frac{\hbar\omega_r}{\Delta} \tag{6.16}$$

describe the spin-oscillator relationship. λ is the coupling strength between the spin and oscillator and r is the ratio of mechanical oscillation to tunnel splitting frequency. The relationship between λ and r can be understood by the so-called magneto-mechanical ratio,

$$\alpha = \lambda^2 r = \frac{2\hbar^2 S^2}{I_z\Delta}, \tag{6.17}$$

which is the ratio of the change in rotational kinetic energy associated with a spin transition $\mathbf{S} \to -\mathbf{S}$

to the tunnel splitting energy. The third parameter is the effective sweep rate v', or equivalently the Landau-Zener exponent ϵ defined in Eq. (6.10),

$$v' = \frac{\pi}{2\epsilon} = \frac{\hbar v}{\Delta^2}. \tag{6.18}$$

We choose the spin up/down basis for the two-level system and a Fock state basis for the harmonic oscillator. A direct product of these two bases will form the basis of the spin-oscillator system. Matrix elements of the Hamiltonian Eq. (6.14) are

$$\begin{aligned} H_{m\sigma,n\sigma'} = &\left(\hbar\omega_r m - \frac{vt}{2}\sigma\right)\delta_{mn}\delta_{\sigma\sigma'} \\ &- \left[\frac{\Delta_{mn}}{2}\delta_{\sigma,-1}\delta_{\sigma',1} + \frac{\Delta^*_{mn}}{2}\delta_{\sigma,1}\delta_{\sigma',-1}\right], \end{aligned} \tag{6.19}$$

where $\sigma = -1, 1$ corresponds to spin down and up states, respectively. The full Fock space has an infinite number of states, although we will use a truncated basis for numerical computations. Tunneling matrix elements

$$\Delta_{mn} = \Delta\,\kappa_{mn}(\lambda), \tag{6.20}$$

depend on the coupling λ through matrix elements of the displacement operator $\hat{D}(\xi) = \exp(\xi a^\dagger - \xi^* a)$, $\xi = -i\lambda$,

$$\kappa_{mn}(\lambda) = e^{-\lambda^2/2}(-i\lambda)^{m-n}\sqrt{\frac{n!}{m!}}L_n^{(m-n)}(\lambda^2) \tag{6.21}$$

for $m \geq n$, and $m \leftrightharpoons n$ for $m < n$. $L_n^{(m-n)}(x)$ are generalized Laguerre polynomials, and the real parameter λ is defined in Eq. (6.16). The first few κ_{mn} are

$$\begin{aligned} &\kappa_{00} = e^{-\lambda^2/2}, \qquad \kappa_{01} = \kappa_{10} = -i\lambda e^{-\lambda^2/2}, \\ &\kappa_{11} = (1-\lambda^2)e^{-\lambda^2/2}. \end{aligned} \tag{6.22}$$

6.2 Landau-Zener Spin-Oscillator Dynamics

6.2.1 Adiabatic energy levels

Numerically solving $\det(\hat{H} - EI) = 0$ gives the adiabatic energy levels $E_{n\pm}$, shown in Fig. 6.3. Diabatic energy levels $E_{n\downarrow\uparrow}$, dotted lines in the insets of Fig. 6.3, are eigenvalues of the noninteracting part of the Hamiltonian (the first two terms in Eq. (6.14)), given by

$$\frac{E_{n\downarrow\uparrow}}{\Delta} = nr \pm \frac{v't'}{2}. \tag{6.23}$$

The spin down (up) states have positive (negative) slopes with y-intercepts $n\omega$. Diabatic energies $E_{n\downarrow}$ and $E_{m\uparrow}$ cross at times

$$t'_k = k\frac{r}{v'}, \qquad k = m - n \in \mathbb{Z}. \tag{6.24}$$

When the oscillator frequency is much larger than the sweep rate, $r \gg v'$, the transitions are

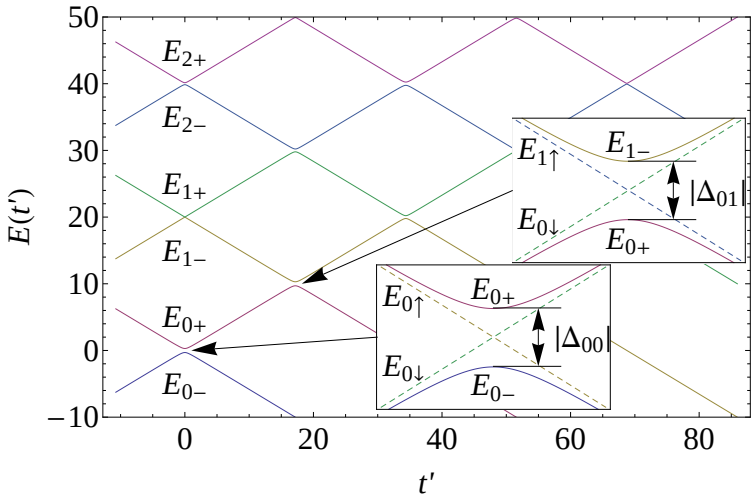

Figure 6.3: Energy (in units of Δ) as a function of time for $r = 20$, $\lambda = 1$, $\epsilon = 1.35$. Solid lines are adiabatic energy levels $E_{n\pm}$, and diabatic energies $E_{n\downarrow\uparrow}$ are dashed lines in the insets. Crossings occur at t_k.

independent. Note that the indices on the adiabatic and diabatic energies only coincide near $t = 0$, but will in general be different after successive crossings. The tunnel splittings $|\Delta_{mn}|$ between adiabatic states occur at the crossing of diabatic energies $E_{m\downarrow}$ and $E_{n\uparrow}$, and depend on the coupling strength through Eqs. (6.20) and (6.21). When $r \gtrsim v'$, successive transitions occur within short

times of each other. Once $r \lesssim v'$ there are many closely spaced levels near $t = 0$.

Consider a single spin initially spin-down with the oscillator in the zero phonon state, i.e. $\Psi(t = -\infty) = |0\rangle|\downarrow\rangle$. The system is initially in the adiabatic energy state E_{0-} which corresponds to the diabatic state $E_{0\downarrow}$. At $t_0 = 0$, diabatic states $E_{0\downarrow}$ and $E_{0\uparrow}$ cross, and adiabatic states E_{0-} and E_{0+} approach each other with minimum separation $|\Delta_{00}| = \Delta e^{-\lambda^2/2}$. If the spin remains in the initial adiabatic state E_{0-} after the avoided crossing, it flips and will see no more possible transitions, as E_{0-} coincides with $E_{0\uparrow}$ long after the avoided crossing at t_0. If the spin does not flip, it will follow the adiabatic state E_{0+} which coincides with $E_{0\downarrow}$ long after t_0. The next crossing between diabatic states $E_{0\downarrow}$ and $E_{1\uparrow}$ occurs at t_1, with tunnel splitting $|\Delta_{01}| = \Delta e^{-\lambda^2/2}\lambda$ between diabatic states E_{0+} and E_{1-}. Remaining in the adiabatic state E_{0+} will coincide with $E_{1\uparrow}$ for times long after t_1. If the spin does not flip at t_1, the system will remain in the E_{1-} adiabatic state, coinciding with $E_{0\downarrow}$ long after t_1. In general the crossing between state $|0\rangle|\downarrow\rangle$ and $|k\rangle|\uparrow\rangle$ occurs at t_k with splitting $|\Delta_{0k}| = \Delta e^{-\lambda^2/2}|\kappa_{0k}(\lambda)|$. Notice that the avoided crossing between E_{1-} and E_{1+} at $t_0 = 0$, given by $|\Delta_{11}| = \Delta e^{-\lambda^2/2}|1 - \lambda^2|$ does exactly go to zero when $\lambda = 1$.

6.2.2 Strong coupling

We study the dynamics of the spin-oscillator system for various parameter ranges. Expanding the wave function of the system in this basis

$$|\Psi(t)\rangle = \sum_{m=0}^{\infty} \sum_{\sigma=\pm 1} C_{m\sigma}(t)|m\rangle|\sigma\rangle, \tag{6.25}$$

the time-dependent Schrödinger equation yields the system of coupled differential equations,

$$\begin{aligned} i\frac{dC_{m,\sigma}}{dt'} &= (rm - \frac{v't'}{2}\sigma)C_{m,\sigma} \\ &\quad - \sum_{n,\sigma'} \left[\frac{\kappa_{mn}}{2}\delta_{\sigma,-1}\delta_{\sigma',1} + \frac{\kappa^*_{mn}}{2}\delta_{\sigma,1}\delta_{\sigma',-1} \right] C_{n,\sigma'}. \end{aligned} \tag{6.26}$$

We solve this system of equations numerically with a truncated oscillator basis. First we consider the initial state of the spin system to be spin-down with the oscillator in its quantum ground state $|\Psi(-\infty)\rangle = |0\rangle|\downarrow\rangle$, which gives $C_{0,-1}(-\infty) = 1$ with all other $C_{m,\sigma}(-\infty) = 0$.

Strong coupling ($\lambda \sim 1$) of spin dynamics to torsional oscillations results in rich dynamics of

both the spin and the oscillator. Calculating the expectation value of σ_z,

$$\langle \sigma_z \rangle = \sum_{m,\sigma} \sigma |C_{m,\sigma}|^2 \tag{6.27}$$

we define the probability of staying in the initial spin-down state as

$$P(t) = \frac{1}{2}(1 - \langle \sigma_z \rangle). \tag{6.28}$$

A comparison of staying probabilities for different parameters is shown in Fig. 6.4. For $r \gg 1$, the spin transitions are clearly independent, as shown in Figs. 6.4a and 6.4b. The tunnel splitting at each crossing is strongly renormalized, according to Eq. (6.20), which leads to strong dependence of the transition probability on the coupling. Consider the crossing of diabatic energies $E_{m\downarrow}$ and $E_{n\uparrow}$. For the system initially in the $|m\rangle|\downarrow\rangle$ state, which corresponds to the lower of the two adiabatic states long before the avoided crossing, the probability that the system will stay in the initial state is

$$P_{mn} = e^{-\epsilon_{mn}}, \qquad \epsilon_{mn} = \frac{\pi \Delta^2 |\kappa_{mn}|^2}{2\hbar v}. \tag{6.29}$$

When the system is initially in the $|0\rangle|\downarrow\rangle$ state, all diabatic crossings will occur between energies $E_{0\downarrow}$ and $E_{n\uparrow}$. The transition probability $P_{0n} = e^{-\epsilon_{0n}}$ at each crossing depends on $|\kappa_{0n}|^2$. Using $L_0^n(x) = 1$ we obtain

$$\epsilon_{0n} = \frac{\pi \Delta^2 e^{-\lambda^2}}{2\hbar v} \frac{\lambda^{2n}}{n!}. \tag{6.30}$$

After the first avoided crossing at $t_0 = 0$, the asymptotic staying probability in the initial state is $P_{00} = e^{-\epsilon_{00}}$. The next avoided crossing occurs at t_1, and the probability of staying in the spin down state after t_1 is $P_{01} = e^{-\epsilon_{01}}$. Thus the total staying probability after two avoided crossings is $P_{00}P_{01}$. We define P_N as the probability of remaining in the initial state after N avoided crossings,

$$P_N = \exp\left(-\sum_{n=0}^{N} \epsilon_{0n} \right). \tag{6.31}$$

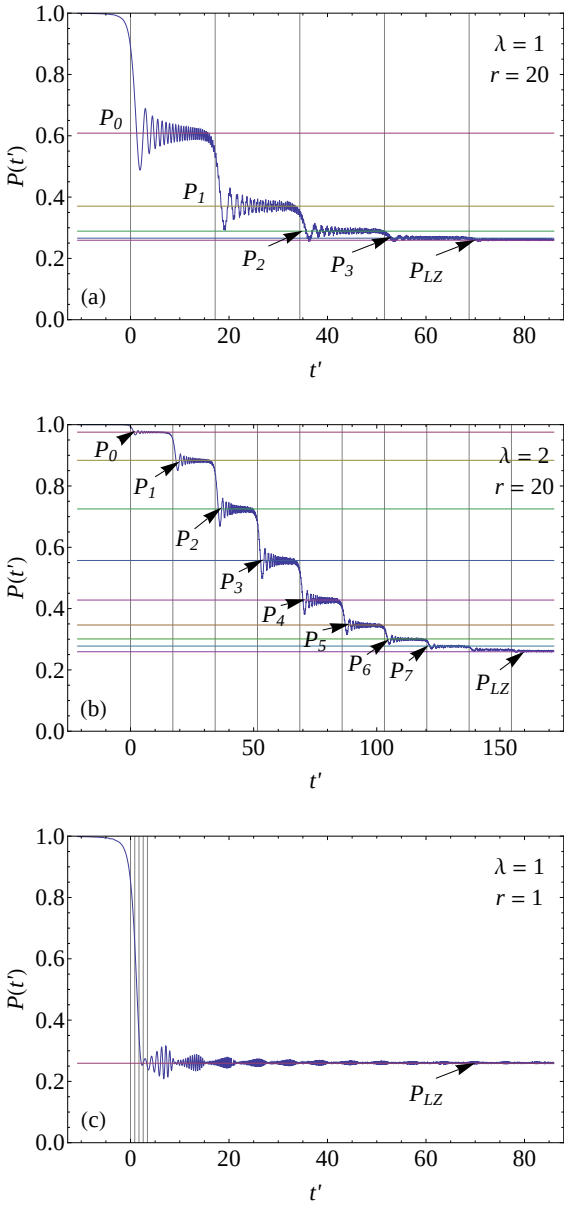

Figure 6.4: Time dependence of the probability that the spin stays in the initial spin-down state for initial state $\Psi(-\infty) = |0\rangle|\downarrow\rangle$ with $\epsilon = 1.35$. Vertical lines at t_k denote avoided crossing of adiabatic energy levels. Horizontal lines are exact results P_N for independent transitions.

In the limit $N \to \infty$, we recover the exact Landau Zener probability P_{LZ},

$$\lim_{N\to\infty} P_N = \exp\left(-\frac{\pi\Delta^2 e^{-\lambda^2}}{2\hbar v}\sum_{n=0}^{\infty}\frac{\lambda^{2n}}{n!}\right) = \exp\left(-\frac{\pi\Delta^2}{2\hbar v}\right). \tag{6.32}$$

Fig. 6.4b shows staying probability for larger coupling, $\lambda = 2$. We see that as the tunnel splitting at each avoided crossing is more strongly renormalized, it takes more crossings to reach the final

Landau-Zener probability.

As the oscillator frequency decreases compared to the sweep rate, $r \gtrsim 1$, the transitions are no longer completely independent, although small oscillations about individual plateaus can still be seen in $P(t)$. This is because the transitions happen within a small multiple of the Landau-Zener tunneling time τ_{LZ}. When the oscillator frequency and tunnel splitting are close to resonance $r \sim 1$, the transition probability initially approaches P_{LZ} and then shows collapse and revival behavior around this limit, as shown in Fig. 6.4c. For $r \ll 1$ the revivals become much weaker and the probability resembles the traditional LZ probability.

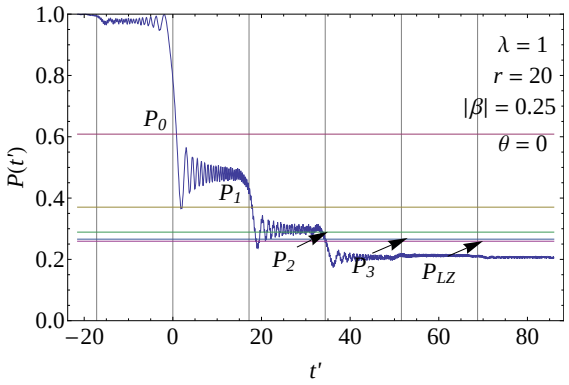

Figure 6.5: Time dependence of the probability that the spin stays in the initial spin-down state for an initial coherent oscillator state $\Psi(-\infty) = |\beta\rangle|\downarrow\rangle$ with $\epsilon = 1.35$. Vertical lines at t_k denote avoided crossing of adiabatic energy levels. Horizontal lines are exact results P_N for independent transitions when starting in the $|0\rangle|\downarrow\rangle$ state.

When the oscillator is initially in a coherent state $|\beta\rangle$,

$$\Psi(-\infty) = |\beta\rangle|\downarrow\rangle = e^{-|\beta|^2/2} \sum_{n=0}^{\infty} \frac{\beta^n}{\sqrt{n!}} |n\rangle|\downarrow\rangle \tag{6.33}$$

where the complex number $\beta = |\beta| e^{i\theta}$ is proportional to the amplitude of initial oscillations. When $\beta \ll 1$ the spin transitions follow approximately the same asymptotic values P_N as the quantum ground state case. For $\beta \lesssim 1$ the staying probabilities, an example of which is shown in Fig. 6.5, depend on the magnitude and phase of the initial coherent state. The maximum angular displacement and velocity of a coherent state are related to β through

$$\varphi_{\max} = 2\lambda|\beta|, \qquad \left(\frac{d\varphi}{dt'}\right)_{\max} = 2r\lambda|\beta|, \tag{6.34}$$

where $\varphi = 2S\langle\phi\rangle$.

6.2.3 Weak coupling

When the spin dynamics of the nanomagnet are weakly coupled to its rotational dynamics $\lambda \ll 1$, there is little observable effect of rotations on spin flip probability. The first crossing that occurs at $t_0 = 0$ has tunnel splitting $\Delta_{00} = \Delta e^{-\lambda^2/2}$, which tends to unity for small λ. When $r \gg 1$ the first transition at $t_0 = 0$ approaches $P_{00} = e^{-\epsilon_{00}}$. The second independent transition occurs at t_1 approaches P_{LZ}, although the difference between P_{00} and P_{LZ} is very small. When $r \sim 1$ the adiabatic transitions are no longer independent, and occur close to the Landau-Zener tunneling time interval.

6.3 Oscillator dynamics

We compute the expectation value of the torsional rotation angle as a function of time

$$\varphi = \lambda \sum_{m,\sigma} \left(C^*_{m+1,\sigma} C_{m,\sigma} \sqrt{m+1} + C^*_{m-1,\sigma} C_{m,\sigma} \sqrt{m} \right). \tag{6.35}$$

For strong coupling $\lambda \sim 1$, the dynamics of the resonator shows a delay before the onset of large oscillations for $r \gg 1$, which occurs at t_1, shown in Fig. 6.6a. When the coupling is stronger, Fig. 6.6b shows many more changes in the oscillatory motion, consistent with more avoided crossings. The oscillation amplitude changes slightly at subsequent t_k. As r decreases towards 1, the interval of large oscillations becomes shorter. When $r \lesssim 1$, there is a single transition region which gives way to harmonic oscillations, shown in Fig. 6.6c. Near $r = 1$, the amplitude of oscillations tends to increase as r decreases for fixed λ.

The angular displacement of the torsional resonator also shows interesting effects even for small coupling. When $r \gg 1$, large torsional oscillations do not begin at the first crossing. This can be understood as follows. The $t = 0$ crossing occurs between spin up and down states, both of which correspond to the ground state of the resonator. Although there is a small increase in displacement angle at this crossing, the largest increase occurs at the second crossing between $|0\rangle|\downarrow\rangle$ and $|1\rangle|\uparrow\rangle$ at t_1. This delay agrees exactly with the semiclassical treatment by Jaafar et al. [22]. Following

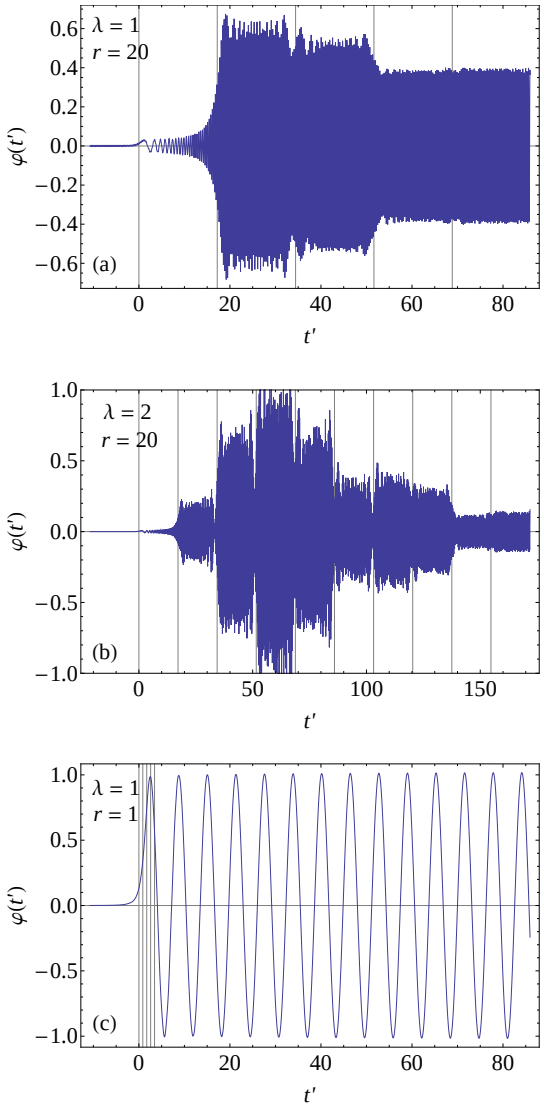

Figure 6.6: Time dependence of the rotation angle expectation value for initial state $\Psi(-\infty) = |0\rangle|\downarrow\rangle$ with $\epsilon = 1.35$. Vertical lines at t_k denote avoided crossing of adiabatic energy levels.

this time the oscillator is in a superposition of ground and excited states. When $r \lesssim 1$ successive transitions occur in a short duration compared to τ_{LZ}, and there is no observable delay in the onset of oscillations. The oscillation amplitude depends on the sweep rate. Numerical results suggest that the largest amplitude oscillation reaches a maximum near $\epsilon \simeq 2$ for $\lambda = 1$ and $r = 20$.

When the oscillator is initially in a coherent state $|\beta\rangle$, normal oscillations with maximum amplitude $\varphi_{\max} = 2\lambda|\beta|$ occur up to t_{-1}, as shown in Fig. 6.7. At t_{-1} the amplitude decreases slightly and decreases again at t_0. A large increase occurs at t_1, similar to the case where the oscillator is initially in its quantum ground state. The amplitude of oscillations after t_1 tends to be larger when

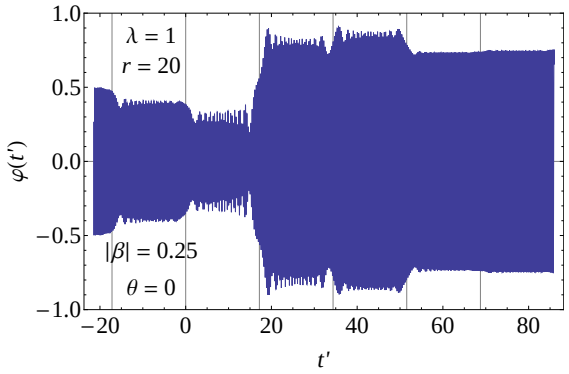

Figure 6.7: Time dependence of the rotation angle expectation value for initial coherent state $\Psi(-\infty) = |\beta\rangle| \downarrow\rangle$ with $\epsilon = 1.35$. Vertical lines at t_k denote avoided crossing of adiabatic energy levels.

the oscillator is initially in a coherent state, but not by a large amount. We observe a subsequent change in oscillation amplitude at t_2 and t_3. The oscillator dynamics are not as sensitive to the initial phase of the coherent state as the spin dynamics, although there is some variation in maximum amplitude.

6.4 Collective dynamics of spins coupled to a mechanical resonator

Consider, instead of a single nanomagnet, an array of single molecule magnets with their easy axes mutually aligned with the axis of rotation of the resonator. If they are far enough apart that dipolar coupling is negligible, they will only be coupled through the effective field due to torsional oscillations. Because the angular displacement is the same for each molecule, this results in collective coherent dynamics, described by a variant of the Dicke Hamiltonian. For N single molecule magnets, we define the operator of total low-energy dynamics as

$$\hat{H}_R = -\frac{\Delta}{2} R_x, \qquad \mathbf{R} = \sum_{i=1}^{N} \boldsymbol{\sigma}^i \tag{6.36}$$

where the index i labels each magnetic particle. Again transforming to the lab frame by performing a rotation by angle ϕ to the lab frame, but now using the total spin, we obtain

$$\begin{aligned}\hat{H}'_R &= -\frac{\Delta}{2}\left(e^{-2iS\phi}R_+ + e^{2iS\phi}R_-\right) \\ &= -\frac{\Delta}{2}\left(\cos\left(2S\phi\right)R_x + \sin\left(2S\phi\right)R_y\right).\end{aligned} \tag{6.37}$$

The full Hamiltonian for the array of single molecule magnets is

$$\begin{aligned}\hat{H}_{SR} = \frac{\hbar^2 L_z^2}{2I_z} + \frac{I_z\omega_r^2\phi^2}{2} - \frac{W(t)}{2}R_z \\ - \frac{\Delta}{2}\left(\cos\left(2S\phi\right)R_x + \sin\left(2S\phi\right)R_y\right),\end{aligned} \tag{6.38}$$

where $W(t) = vt$. The Hamiltonian can be written as

$$\hat{H}_{SR} = \hat{H}_{\text{osc}} - \frac{1}{2}\mathbf{H}_{\text{eff}}\cdot\mathbf{R}, \tag{6.39}$$

where $\hat{H}_{\text{osc}}$ is the uncoupled oscillator Hamiltonian and

$$\mathbf{H}_{\text{eff}} = -\frac{\delta\hat{H}}{\delta\mathbf{R}} = \Delta\cos\left(2S\phi\right)\mathbf{e}_x + \Delta\sin\left(2S\phi\right)\mathbf{e}_y + W\mathbf{e}_z \tag{6.40}$$

is the effective magnetic field. Noticing that $\hat{H}_{SR}$ is linear in R_x, R_y, R_z, we can see that $[\mathbf{R}^2, \hat{H}_{SR}] = 0$, so $\mathbf{R}^2 = R(R+1)$ is a conserved quantum number and $\mathbf{R}$ behaves as a single large isospin. We are interested in the maximum value of R, $R_{\max} = N/2$, which can be experimentally realized by preparing the system with a strong longitudinal magnetic field such that all spins are pointing down.

The Heisenberg equations of motion $i\hbar\, d\hat{A}/dt = [\hat{A}, \hat{H}]$ are

$$\hbar\dot{L}_z = -I_z\omega^2\phi - \Delta S\left(\sin\left(2S\phi\right)R_x - \cos\left(2S\phi\right)R_y\right) \tag{6.41}$$

$$\dot{\phi} = \frac{\hbar L_z}{I_z} \tag{6.42}$$

$$\hbar\dot{R}_x = WR_y - \Delta\sin\left(2S\phi\right)R_z \tag{6.43}$$

$$\hbar\dot{R}_y = -WR_x + \Delta\cos\left(2S\phi\right)R_z \tag{6.44}$$

$$\hbar\dot{R}_z = -\Delta\cos\left(2S\phi\right)R_y + \Delta\sin\left(2S\phi\right)R_x. \tag{6.45}$$

The equations of motion show a few important properties. First, the time derivative of the z-component of the total angular momentum equals the elastic torque

$$\frac{d}{dt}(\hbar L_z + \hbar S R_z) = -I_z \omega^2 \phi. \tag{6.46}$$

If the spin-rotor system were completely uncoupled from its environment the total angular momentum, spin plus rotational, would be conserved. In the limit $\phi \to 0$, we would obtain Heisenberg equations of motion for $R_{x,y,z}$. Solving this system of equations gives the same Landau-Zener probability of spin flip as the Schrödinger picture, discussed in Sec. 6.1.1. Second, these equations are not independent, but

$$\frac{d}{dt}\mathbf{R}^2 = 0 \tag{6.47}$$

which is equivalent to $\mathbf{R}^2 = \text{constant}$, which we had found as a constant of motion of the Hamiltonian. Because the length of $\mathbf{R}$ is fixed and large in magnitude, we see that the equations of motion for $\mathbf{R}$ are equivalent to the Landau-Lifshitz equations for a classical spin of fixed length precessing in a magnetic field. Dividing Eqs.(6.41)-(6.45) by R shows that the direction of the total spin follows the Landau-Lifshitz equation, which is mathematically equivalent to the Schrödinger equation of a spin-half particle precessing in a magnetic field,

$$\hbar \frac{d\boldsymbol{\sigma}}{dt} = \boldsymbol{\sigma} \times \mathbf{H}_{\text{eff}}, \quad \boldsymbol{\sigma} = \frac{\mathbf{R}}{R}. \tag{6.48}$$

The equations of motion for $R_{x,y,z}$ can be divided through by R to giving identical equations of motion for a pseudospin $\boldsymbol{\sigma} = \mathbf{R}/R$ of unit length. Substituting this into the equation of motion for ϕ and eliminating L_z gives a second order equation of motion for for the dynamics of the resonator,

$$\frac{d^2\varphi}{dt'^2} + r^2 \varphi = -\alpha R \left(\sin(\varphi)\sigma_x - \cos(\varphi)\sigma_y\right), \tag{6.49}$$

where $\varphi = 2S\phi$, the prime denotes derivative with respect to dimensionless time $t' = \Delta t/\hbar$, r and α are defined in Eqs. (6.16) and (6.17), respectively.

The right hand side of Eq. (6.49) shows that the spins exert a collective torque on the resonator. This is a simple yet meaningful result. The equation of motion is similar to the semiclassical

treatment of a single spin [91], but with the torque on the resonator increased by a factor of R. Because the amplitude of oscillation is proportional to the number of magnetic molecules N, this can be interpreted as a signature of Dicke phonon superradiance [125]. For a simple harmonic torsional oscillator, the phonon field is the angle of displacement from equilibrium ϕ, and the driving torque is proportional to $R = N/2$.

Returning to the quantum model we see that for the case of superradiance, $\alpha \to \alpha R$, and $\lambda = \sqrt{\alpha/r}$ becomes

$$\lambda_{SR} = \sqrt{\frac{\alpha R}{r}} = \sqrt{R}\,\lambda \propto \sqrt{N}\,\lambda. \tag{6.50}$$

This provides a viable method of increasing the coupling in a realistic experiment, by increasing the number of individual nanomagnets on the resonator. The usual difficulty of realizing strong coupling is that reducing the moment of inertia by even two orders of magnitude has a small effect on the coupling due to the inverse quartic root dependence of the coupling on the moment of inertia.

The Heisenberg equations of motion, Eqs. (6.41)-(6.45) are operator equations which should be averaged over the quantum state of the system. Since the spin $\mathbf{R}$ is classical the averages decouple, such as $\langle \sin(\varphi)\sigma_x \rangle \to \langle \sin(\varphi) \rangle \langle \sigma_x \rangle$ in Eq. (6.49), which yields classical-like equations of motion. We solve these equations of motion numerically.

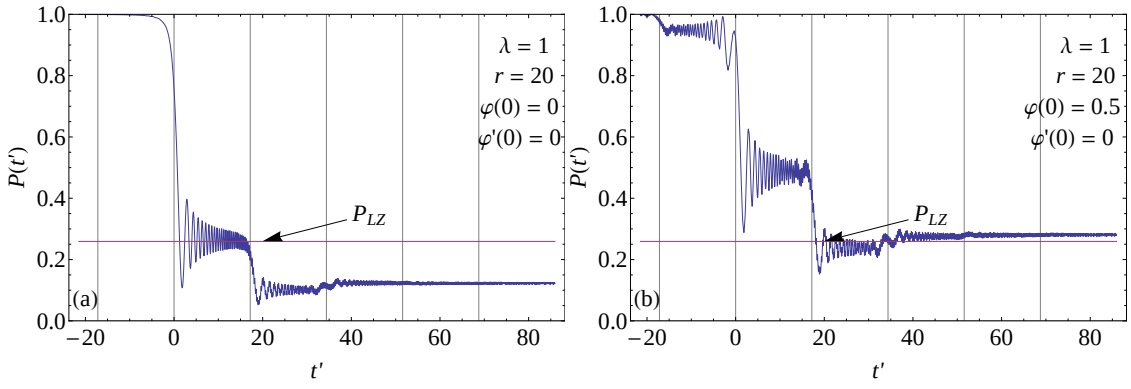

Figure 6.8: Time dependence of the effective probability $P(t) = (1 - \langle \sigma_z \rangle)/2$ for the z-component of a large spin in the semiclassical model, with various initial conditions and $\epsilon = 1.35$.

We emphasize that a large spin will display the classical dynamics of a magnetic moment precessing in a time-dependent magnetic field. Plots of the probability as a function of time for the semiclassical equations of motion of a superradiant ensemble of spins are shown in Fig. 6.8. We

see multi-stage transitions similar to the quantum case. A semiclassical explanation is as follows. Transitions occur when the energy separation between spin states equals a multiple of the oscillator frequency. These occur at the same times $t_k = r/v'$ given by Eq. (6.24) for the quantum case when avoided crossings between adiabatic energies occur.

When the oscillator is initially at rest at its equilibrium position $\varphi = 0$, the initial transition occurs at t_0 as shown in Fig. 6.8a. $P(t)$ oscillates about the regular Landau-Zener probability $P_{LZ} = e^{-\epsilon}$. Subsequent transitions occur at t_1 and t_2, with the long-time probability much different from P_{LZ}. The spin dynamics depend strongly on the initial state of the oscillator. Fig. 6.8b shows the transition probability for different initial conditions of the oscillator with the same amplitude of oscillation as the coherent state studied in the fully quantum-mechanical model.

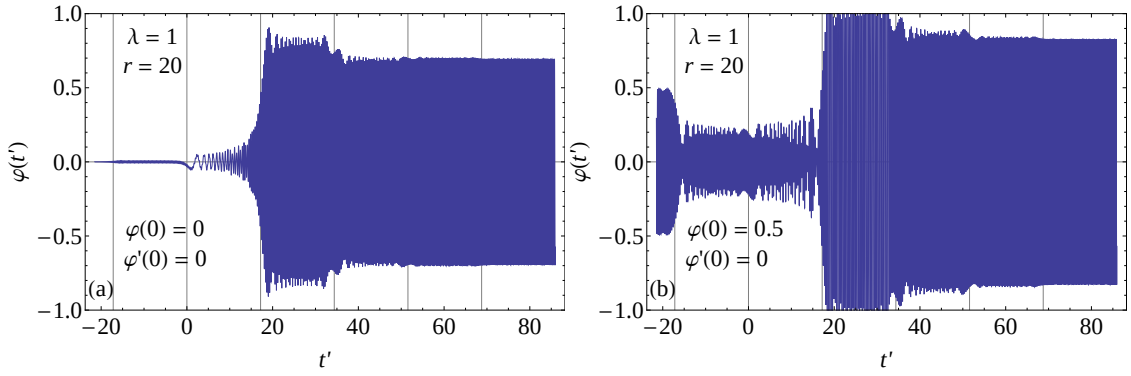

Figure 6.9: Time dependence of the rotation angle in the semiclassical model, with various initial conditions and $\epsilon = 1.35$.

The oscillator dynamics show a similar delay in the onset of strong oscillations as in the quantum model, shown in Fig. 6.9. We notice a large increase in the amplitude of oscillations at t_1 for the cantilever initially at rest at equilibrium. For the cantilever initially oscillating with amplitude φ_0, the behavior is very similar to the quantum model with the oscillator initially in a coherent state. We observe normal oscillations up to t_{-1} at which the amplitude decreases, then a large increase at t_1, with subsequent changes at t_2, t_3. While there is not a strong dependence on the initial conditions with the same initial energy, there is some variation in maximum amplitude.

6.5 Discussion and conclusions

We have studied the Landau-Zener dynamics of a tunneling spin rigidly coupled to a torsional oscillator. Starting with a quantum model describing the low energy dynamics of a tunneling macrospin, we numerically solve the time-dependent Schrödinger equation to obtain the dynamics of the expectation values of the spin and oscillator. We find that when the oscillator is initially in its quantum ground state, there are a series of plateaus in the staying probability as a function of time. We analytically obtain exact probabilities in terms of tunnel splittings of the spin which are dressed by the quantum states of the torsional oscillator. These results perfectly fit the plateaus obtained from numerical simulations. The oscillator dynamics show abrupt changes in amplitude which occur at the same times as the steps between steps of the staying probability. For an oscillator initially in a coherent state we also find a stepwise staying probability curve, but these deviate from the analytical results found for the initial ground state because there are multiple occupied states of the resonator. The oscillator dynamics continue to show changes in amplitude which coincide with the steps. We also consider a large number of spins, N, on a single oscillator, and find a superradiant enhancement of the spin-oscillator coupling which scales as $\sqrt{N}$. As in the Dicke model, the ensemble of spins acts as a single large spin. This justifies decoupling quantum averages of separate observables in the Heisenberg equations of motion, giving semiclassical equations of motion for a large spin in a time-dependent effective field which depends on the motion of the cantilever. The cantilever experiences a harmonic restoring torque but also a driving torque due to the dynamics of the large spin. We numerically solve the set of coupled equations and compare the results to the Schrödinger picture. The spin dynamics show sensitivity to the initial state of the resonator, although the oscillator dynamics are fairly insensitive to this.

It is important to distinguish the interpretation of these results in the context of the system being measured. Consider the single molecule magnet grafted to a carbon nanotube, depicted in Fig. 6.1a. With the system prepared in the spin down state by a strong magnetic field along the negative z-axis, the magnetic field is swept. If the oscillator is initially in the zero phonon state, the first crossing of an occupied energy level with an unoccupied level occurs at $t_0 = 0$ between $E_{0\downarrow}$ and $E_{0\uparrow}$. $P_0 = P_{00} = e^{-\epsilon_{00}}$ is the probability that the spin will remain in the down state. If the spin remains in the down state after the first crossing, it will encounter a second crossing between $E_{0\downarrow}$

and $E_{1\uparrow}$ at t_1, at which it will remain spin-down with probability $P_{01} = e^{-\epsilon_{01}}$. The total probability of the spin remaining spin-down after t_1 is $P_1 = P_{00}P_{01} = e^{-(\epsilon_{00}+\epsilon_{01})}$. If the spin reverses at any t_k it will see no more crossings. When the spin does reverse it will exert a torque on the carbon nanotube, exciting a phonon mode. The onset of oscillations shows that the spin has tunnelled. This provides a method of detecting the mechanical quantum state of the nanotube.

This situation is similar to the recent demonstration of electronic readout of nuclear spin states of a terbium-based single magnetic molecule [27]. Terbium nuclear spin 3/2 has four possible projections onto the quantization axis, each projection providing a different hyperfine shift of the resonance of the Landau-Zener transition of the spin of the molecule. Time-resolved measurements show an increase in the differential conductance at the time the spin makes a transition. This occurs at a different value of the external field for each sweep, that depends on the quantum state of the nuclear spin. In our model the role of nuclear spin states is played by the resonator states given by Eq. (6.23). We, therefore, propose a similar experiment in which the field sweep is used to read out the quantum state of the mechanical resonator.

When there is a large number of magnetic molecules on a cantilever, as in Fig. 6.1b, they will act as a single large classical spin $\mathbf{R}(t)$. This spin not only responds to the external field but also to the motion of the cantilever. The latter has been treated in Sec. V as a classical oscillator described by the angle $\phi(t)$. Such treatment is the classical limit of the quantum-mechanical consideration in which the cantilever is described by the coherent state, Eq. (6.33). Mechanical rotation at an angular frequency $\dot{\phi}$ is equivalent to a magnetic field $B_{\text{eff}} = \dot{\phi}/\gamma$, where γ is the gyromagnetic ratio. In turn, the spin dynamics act as a driving torque on the cantilever, resulting in coupled dynamics which change at the same moments of time, t_k, as in the quantum case. The non-linear coupled equations of motion lead to the excitations of harmonics of the cantilever that correspond to its quantum modes in the dynamics described by the Schrödinger equation. Higher harmonics are excited with smaller amplitude.

To put some of these statements into perspective, consider a spin-10 single molecule magnet grafted to a carbon nanotube [28]. The moment of inertia of the magnetic molecule is of the order $I_z \sim 10^{-42}$ kg·m^2. With a carbon nanotube torsional stiffness of $k \sim 10^{-18}$ N·m the simple harmonic model gives $\omega_r \sim 1000$ GHz, which means coupling on the order of $\lambda \sim 10^{-1}$. Typical phonon frequencies of carbon nanotubes in the 10-100 GHz range would increase the coupling by

an order of magnitude. Recent observation [28] of strong spin-phonon coupling in such a system estimates $\lambda \simeq 0.5$. While this is certainly large enough to observe the influence of the oscillator on spin dynamics, there is no way to directly observe oscillations in a carbon nanotube.

If the same spin-10 magnetic molecule were mounted on a paddle-shaped torsional resonator of size $20 \times 20 \times 10$ nm^3 supported by a single carbon nanotube with torsional rigidity $k = 10^{-18}$ N·m. The moment of inertia is dominated by the paddle, $I_z \sim 10^{-36}$ kg·m^2, which gives $\omega_r = \sqrt{k/I_z} \sim 10^9$ s^{-1}. The coupling parameter λ is then on the order of 10^{-2}, which would be too small to observe an effect on the spin dynamics. With $\Delta/\hbar \ll 10^9$ s^{-1} there should be a detectable delay between the $t = 0$ crossing and the onset of maximal oscillation amplitude. With $\Delta/\hbar > 10^9$ s^{-1}, the delay will be undetectable. The tunnel splitting can be tuned by orders of magnitude by applying a transverse magnetic field.

A macroscopic resonator in which even small amplitude oscillations could be observed comes at the expense of weak coupling with no observable effect on the spin dynamics. In terms of the moment of inertia and torsional stiffness, the coupling goes as $\lambda \propto 1/\sqrt[4]{kI_z}$, so a very small torsional stiffness of $k \sim 10^{-22}$ N·m would be needed. One way to overcome this limitation is to put a large number of spins on a torsional resonator or microcantilever. For a cantilever with dimensions $1000 \times 200 \times 100$ nm^3 we would expect $\omega \sim 1$ GHz with $Q \sim 500$. Single molecule magnets have a diameter on the order of 1 nm. It would be possible to place hundreds of single molecule magnets on the tip of a nanocantilever separated by over 10 nm from their nearest neighbors to weaken dipolar interactions. They would act as a single large spin due to the collective quantum effect of superradiance. This would increase the coupling by at least an order of magnitude, as $\lambda_{SR} \propto \sqrt{N}$. Therefore it would be possible to directly observe the coupled dynamics of the magnetization and oscillatory motion in a Landau-Zener experiment.

7

Conclusion

We have investigated the effects of full or partial mechanical freedom on quantum tunneling of the magnetic moment in nanomagnets, as well as on tunneling of the magnetic flux in superconductors. We have shown that mechanical freedom can significantly alter tunneling and decoherence rates. While most of the research on spin tunneling in molecules has focused on crystals of molecular magnets, future experiments may involve molecules loosely attached to a substrate, as well as free magnetic molecules. Such experiments are driven in part by the widely spread belief that decoupling from the environment may decrease decoherence and, thus, can offer viable qubit designs. Our results show that loose coupling with the environment that provides partial mechanical freedom is, in fact, a double-edged sword. In a small system, the necessity to conserve the total angular momentum may significantly affect the tunneling rate. In, e.g., free Mn-12 or Fe-8 molecules the spin tunneling would be completely frozen.

The instanton method previously developed for spin tunneling in a stationary nanomagnet has been generalized for the case of a nanomagnet that is free to rotate about the easy magnetization axis. The problem of a free rotator with a tunneling spin involves anomalous commutation relations for spin and rotational angular momentum in the rotating frame of reference. We have solved this mathematically challenging problem in the case of a symmetric rotator. The dependence of the magnetic moment of the rotator on its moments of inertia has been obtained. For a nanomagnet, or a micro-SQUID, embedded in a solid, some mechanical freedom arises from the finite rigidity of the solid. This problem has been analyzed within the spin-boson model. Solutions have been obtained for the tunnel splitting and the decoherence rate. Large effects have been found for magnetic

molecules embedded in a helium crystal.

The Landau-Zener problem for a macrospin coupled to a mechanical resonator has been studied within a rigorous quantum-mechanical approach. The time-dependent Schrödinger equation has been solved numerically to obtain the dynamics of the expectation values of physical quantities for the spin and oscillator. Exact probabilities in terms of tunnel splittings of the spin which are dressed by the quantum states of the torsional oscillator have been obtained analytically. Perfect agreement has been found between analytical and numerical results. These studies offer suggestions for recent experiments with a single magnetic molecule bridged between conducting leads and a magnetic molecule attached to a carbon nanotube. We discuss how measurements of such systems can provide read-out of exact quantum states of the nano-mechanical oscillator.

Bibliography

[1] Jonathan R. Friedman and Myriam P. Sarachik. Single-molecule nanomagnets. *Annual Review of Condensed Matter Physics*, 1(1):109–128, 2010.

[2] M. Razavy. *Quantum Theory of Tunneling*. World Scientific, 2003.

[3] F. Hund. Zur deutung der molekelspektren. i. *Zeitschrift für Physik*, 40:742–764, 1927.

[4] F. Hund. Zur deutung der molekelspektren. iii. *Zeitschrift für Physik*, 43:805–826, 1927.

[5] J. R. Oppenheimer. Three notes on the quantum theory of aperiodic effects. *Phys. Rev.*, 31:66–81, Jan 1928.

[6] G. Gamow. Zur quantentheorie des atomkernes. *Zeitschrift für Physik*, 51:204–212, 1928.

[7] G. Gamow. The Quantum Theory of Nuclear Disintegration. *Nature*, 122:805–806, November 1928.

[8] R. W. Gurney and E. U. Condon. Wave Mechanics and Radioactive Disintegration. *Nature*, 122:439, September 1928.

[9] R. W. Gurney and E. U. Condon. Quantum mechanics and radioactive disintegration. *Phys. Rev.*, 33:127–140, Feb 1929.

[10] Max Born. Zur theorie des kernzerfalls. *Zeitschrift für Physik*, 58:306–321, 1929.

[11] R.P. Feynman, R.B. Leighton, M.L. Sands, and M.A. Gottlieb. *The Feynman lectures on physics*. The Feynman Lectures on Physics. Pearson/Addison-Wesley, 1963.

[12] A. J. Leggett. Macroscopic quantum systems and the quantum theory of measurement. *Progress of Theoretical Physics Supplement*, 69:80–100, 1980.

[13] E.M. Chudnovsky and J. Tejada. *Macroscopic Quantum Tunneling of the Magnetic Moment*. Number 4 in Cambridge Studies in Magnetism. Cambridge University Press, Cambridge, England, 1998.

[14] Jonathan R. Friedman, Vijay Patel, W. Chen, S. K. Tolpygo, and J. E. Lukens. Quantum superposition of distinct macroscopic states. *Nature*, 406(6791):43–46, 07 2000.

[15] Rudolf L. Mössbauer. Kernresonanzfluoreszenz von gammastrahlung in Ir191. *Zeitschrift für Physik*, 151(2):124–143, 1958.

[16] Richard P. Feynman. *Statistical mechanics: a set of lectures by R. P. Feynman*. Frontiers in physics. Benjamin, 1972.

[17] Eugene M. Chudnovsky. Conservation of angular momentum in the problem of tunneling of the magnetic moment. *Phys. Rev. Lett.*, 72:3433–3436, May 1994.

[18] E. M. Chudnovsky and X. Martinez-Hidalgo. Tunneling with dissipation and decoherence for a large spin. *Phys. Rev. B*, 66:054412, Aug 2002.

[19] Eugene M. Chudnovsky. Universal decoherence in solids. *Phys. Rev. Lett.*, 92:120405, Mar 2004.

[20] E. M. Chudnovsky, D. A. Garanin, and R. Schilling. Universal mechanism of spin relaxation in solids. *Phys. Rev. B*, 72(9):094426, Sep 2005.

[21] E. M. Chudnovsky and D. A. Garanin. Rotational states of a nanomagnet. *Phys. Rev. B*, 81(21):214423, Jun 2010.

[22] R. Jaafar, E. M. Chudnovsky, and D. A. Garanin. Single magnetic molecule between conducting leads: Effect of mechanical rotations. *EPL (Europhysics Letters)*, 89(2):27001, 2010.

[23] D. A. Garanin and E. M. Chudnovsky. Quantum entanglement of a tunneling spin with mechanical modes of a torsional resonator. *Phys. Rev. X*, 1:011005, Aug 2011.

[24] Alexey A. Kovalev, Lorien X. Hayden, Gerrit E. W. Bauer, and Yaroslav Tserkovnyak. Macrospin tunneling and magnetopolaritons with nanomechanical interference. *Phys. Rev. Lett.*, 106:147203, Apr 2011.

[25] T. M. Wallis, J. Moreland, and P. Kabos. Einstein–de haas effect in a nife film deposited on a microcantilever. *Applied Physics Letters*, 89(12):122502, 2006.

[26] J P Davis, D Vick, J A J Burgess, D C Fortin, P Li, V Sauer, W K Hiebert, and M R Freeman. Observation of magnetic supercooling of the transition to the vortex state. *New Journal of Physics*, 12(9):093033, 2010.

[27] Romain Vincent, Svetlana Klyatskaya, Mario Ruben, Wolfgang Wernsdorfer, and Franck Balestro. Electronic read-out of a single nuclear spin using a molecular spin transistor. *Nature*, 488(7411):357–360, 08 2012.

[28] Marc Ganzhorn, Svetlana Klyatskaya, Mario Ruben, and Wolfgang Wernsdorfer. Strong spin-phonon coupling between a single-molecule magnet and a carbon nanotube nanoelectromechanical system. *Nat. Nano.*, 8(3):165–169, 03 2013.

[29] E.M. Chudnovsky and J. Tejada. *Lectures on Magnetism.* Rinton Press, Princeton, New Jersey, 2006.

[30] C. P. Bean, R. W. DeBlois, and L. B. Nesbitt. Eddy-current method for measuring the resistivity of metals. *Journal of Applied Physics*, 30(12):1976–1980, 1959.

[31] L. Weil. Texture des catalyseurs et propriétés ferromagnetiques a trés basse temperature. *J. Chim. Phys*, 51:715, 1954.

[32] D. Stauffer. Quantum tunneling nucleation for superparamagnetic spin cluster reversals. *Solid State Communications*, 18(4):533 – 535, 1976.

[33] M. Uehara, B. Barbara, B. Dieny, and P.C.E. Stamp. Staircase behaviour in the magnetization reversal of a chemically disordered magnet at low temperature. *Physics Letters A*, 114(1):23 – 26, 1986.

[34] E. M. Chudnovsky. Quantum effects in small ferromagnetic particles. *Zh. Eksp. Teor. Fiz.*, 77(5):2157–2161, 1979.

[35] E. M. Chudnovsky and L. Gunther. Quantum tunneling of magnetization in small ferromagnetic particles. *Phys. Rev. Lett.*, 60(8):661–664, Feb 1988.

[36] M Enz and R Schilling. Magnetic field dependence of the tunnelling splitting of quantum spins. *Journal of Physics C: Solid State Physics*, 19(30):L711, 1986.

[37] J. L. van Hemmen and A. Sütö. Tunnelling of quantum spins. *EPL (Europhysics Letters)*, 1(10):481, 1986.

[38] L.D. Landau and E.M. Lifshitz. On the theory of the dispersion of magnetic permeability in ferromagnetic bodies. *Phys. Z. Sowjetunion*, 8(153):101–114, 1935.

[39] D. D. Awschalom, M. A. McCord, and G. Grinstein. Observation of macroscopic spin phenomena in nanometer-scale magnets. *Phys. Rev. Lett.*, 65:783–786, Aug 1990.

[40] C. Paulsen, L.C. Sampiao, B. Barbara, D. Fruchard, A. Marchand, J.L. Tholence, and M. Uehara. Mesoscopic quantum tunneling in small ferromagnetic particles. *Physics Letters A*, 161(3):319 – 322, 1991.

[41] C. Paulsen, L.C. Sampaio, R. Tucoulou Tachoueres, B. Barbara, D. Fruchart, A. Marchand, J.L. Tholence, and M. Uehara. Mesoscopic quantum tunneling in small ferromagnetic particles. *Journal of Magnetism and Magnetic Materials*, 116:67 – 69, 1992.

[42] J. Tejada, Ll. Balcells, S. Linderoth, R. Perzynski, B. Rigau, B. Barbara, and J. C. Bacri. Quantum tunneling of magnetization in single domain particles. *Journal of Applied Physics*, 73(10):6952–6954, 1993.

[43] Andrea Caneschi, Dante Gatteschi, Roberta Sessoli, Anne Laure Barra, Louis Claude Brunel, and Maurice Guillot. Alternating current susceptibility, high field magnetization, and millimeter band epr evidence for a ground s = 10 state in [Mn12O12(Ch3COO)16(H2O)4].2CH3COOH.4H2O. *Journal of the American Chemical Society*, 113(15):5873–5874, 1991.

[44] R. Sessoli, D. Gatteschi, A. Caneschi, and M. A. Novak. Magnetic bistability in a metal-ion cluster. *Nature*, 365(6442):141–143, 09 1993.

[45] T. Lis. Preparation, structure, and magnetic properties of a dodecanuclear mixed-valence manganese carboxylate. *Acta Crystallographica Section B*, 36(9):2042–2046, Sep 1980.

[46] B. Barbara, W. Wernsdorfer, L.C. Sampaio, J.G. Park, C. Paulsen, M.A. Novak, R. Ferré, D. Mailly, R. Sessoli, A. Caneschi, K. Hasselbach, A. Benoit, and L. Thomas. Mesoscopic quantum tunneling of the magnetization. *Journal of Magnetism and Magnetic Materials*, 140-144, Part 3(0):1825 – 1828, 1995. International Conference on Magnetism.

[47] Jonathan R. Friedman, M. P. Sarachik, J. Tejada, and R. Ziolo. Macroscopic measurement of resonant magnetization tunneling in high-spin molecules. *Phys. Rev. Lett.*, 76:3830–3833, May 1996.

[48] J. M. Hernández, X. X. Zhang, F. Luis, J. Bartolomé, J. Tejada, and R. Ziolo. Field tuning of thermally activated magnetic quantum tunnelling in Mn12-Ac molecules. *EPL (Europhysics Letters)*, 35(4):301, 1996.

[49] L. Thomas, F. Lionti, R. Ballou, D. Gatteschi, R. Sessoli, and B. Barbara. Macroscopic quantum tunnelling of magnetization in a single crystal of nanomagnets. *Nature*, 383(6596):145–147, 09 1996.

[50] K. Ziemelis. The difficult middle ground. *Nat. Phys.*, 4:S19, February 2008.

[51] Louisa Bokacheva, Andrew D. Kent, and Marc A. Walters. Crossover between thermally assisted and pure quantum tunneling in molecular magnet mn_{12}-acetate. *Phys. Rev. Lett.*, 85:4803–4806, Nov 2000.

[52] E. del Barco, A. D. Kent, N. E. Chakov, L. N. Zakharov, A. L. Rheingold, D. N. Hendrickson, and G. Christou. Distribution of internal transverse magnetic fields in a mn_{12}-based single molecule magnet. *Phys. Rev. B*, 69:020411, Jan 2004.

[53] M. V. Berry. Quantal phase factors accompanying adiabatic changes. *Proceedings of the Royal Society of London. A. Mathematical and Physical Sciences*, 392(1802):45–57, 1984.

[54] Jan von Delft and Christopher L. Henley. Destructive quantum interference in spin tunneling problems. *Phys. Rev. Lett.*, 69:3236–3239, Nov 1992.

[55] Daniel Loss, David P. DiVincenzo, and G. Grinstein. Suppression of tunneling by interference in half-integer-spin particles. *Phys. Rev. Lett.*, 69:3232–3235, Nov 1992.

[56] Anupam Garg. Topologically quenched tunnel splitting in spin systems without kramers' degeneracy. *EPL (Europhysics Letters)*, 22(3):205, 1993.

[57] W. Wernsdorfer and R. Sessoli. Quantum phase interference and parity effects in magnetic molecular clusters. *Science*, 284(5411):133–135, 1999.

[58] E. del Barco, A. D. Kent, E. M. Rumberger, D. N. Hendrickson, and G. Christou. Symmetry of magnetic quantum tunneling in single molecule magnet mn_{12}-acetate. *Phys. Rev. Lett.*, 91:047203, Jul 2003.

[59] A. J. Millis, A. D. Kent, M. P. Sarachik, and Y. Yeshurun. Pure and random-field quantum criticality in the dipolar ising model: Theory of mn_{12} acetates. *Phys. Rev. B*, 81:024423, Jan 2010.

[60] Bo Wen, P. Subedi, Lin Bo, Y. Yeshurun, M. P. Sarachik, A. D. Kent, A. J. Millis, C. Lampropoulos, and G. Christou. Realization of random-field ising ferromagnetism in a molecular magnet. *Phys. Rev. B*, 82:014406, Jul 2010.

[61] D. M. Cox, D. J. Trevor, R. L. Whetten, E. A. Rohlfing, and A. Kaldor. Magnetic behavior of free-iron and iron oxide clusters. *Phys. Rev. B*, 32:7290–7298, Dec 1985.

[62] Walt A. de Heer, Paolo Milani, and A. Chtelain. Spin relaxation in small free iron clusters. *Phys. Rev. Lett.*, 65:488–491, Jul 1990.

[63] J. P. Bucher, D. C. Douglass, and L. A. Bloomfield. Magnetic properties of free cobalt clusters. *Phys. Rev. Lett.*, 66:3052–3055, Jun 1991.

[64] D. C. Douglass, A. J. Cox, J. P. Bucher, and L. A. Bloomfield. Magnetic properties of free cobalt and gadolinium clusters. *Phys. Rev. B*, 47:12874–12889, May 1993.

[65] Isabelle M. L. Billas, J. A. Becker, A. Châtelain, and Walt A. de Heer. Magnetic moments of iron clusters with 25 to 700 atoms and their dependence on temperature. *Phys. Rev. Lett.*, 71:4067–4070, Dec 1993.

[66] Isabelle M.L. Billas, A. Châtelain, and Walt A. de Heer. Magnetism from the atom to the bulk in iron, cobalt, and nickel clusters. *Science*, 265(5179):1682–1684, 1994.

[67] Xiaoshan Xu, Shuangye Yin, Ramiro Moro, and Walt A. de Heer. Magnetic moments and adiabatic magnetization of free cobalt clusters. *Phys. Rev. Lett.*, 95:237209, Dec 2005.

[68] F. W. Payne, Wei Jiang, J. W. Emmert, Jun Deng, and L. A. Bloomfield. Magnetic structure of free cobalt clusters studied with stern-gerlach deflection experiments. *Phys. Rev. B*, 75:094431, Mar 2007.

[69] S. Peredkov, M. Neeb, W. Eberhardt, J. Meyer, M. Tombers, H. Kampschulte, and G. Niedner-Schatteburg. Spin and orbital magnetic moments of free nanoparticles. *Phys. Rev. Lett.*, 107:233401, Nov 2011.

[70] J. Tejada, R. D. Zysler, E. Molins, and E. M. Chudnovsky. Evidence for quantization of mechanical rotation of magnetic nanoparticles. *Phys. Rev. Lett.*, 104(2):027202, Jan 2010.

[71] Laura Zobbi, Matteo Mannini, Mirko Pacchioni, Guillaume Chastanet, Daniele Bonacchi, Chiara Zanardi, Roberto Biagi, Umberto Del Pennino, Dante Gatteschi, Andrea Cornia, and Roberta Sessoli. Isolated single-molecule magnets on native gold. *Chem. Commun.*, 0:1640–1642, 2005.

[72] R.V. Martínez, F. García, R. García, E. Coronado, A. Forment-Aliaga, F.M. Romero, and S. Tatay. Nanoscale deposition of single-molecule magnets onto sio2 patterns. *Advanced Materials*, 19(2):291–295, 2007.

[73] Salvador Barraza-Lopez, Michael C. Avery, and Kyungwha Park. First-principles study of a single-molecule magnet mn_{12} monolayer on the au(111) surface. *Phys. Rev. B*, 76:224413, Dec 2007.

[74] U. del Pennino, V. Corradini, R. Biagi, V. De Renzi, F. Moro, D. W. Boukhvalov, G. Panaccione, M. Hochstrasser, C. Carbone, C. J. Milios, and E. K. Brechin. Electronic structure of a mn_6 ($S = 4$) single molecule magnet grafted on au(111). *Phys. Rev. B*, 77:085419, Feb 2008.

[75] J.-P. Cleuziou, W. Wernsdorfer, V. Bouchiat, T. Ondarcuhu, and M. Monthioux. Carbon nanotube superconducting quantum interference device. *Nat. Nano.*, 1(1):53–59, 10 2006.

[76] J.-P. Cleuziou, W. Wernsdorfer, S. Andergassen, S. Florens, V. Bouchiat, Th. Ondarçuhu, and M. Monthioux. Gate-tuned high frequency response of carbon nanotube josephson junctions. *Phys. Rev. Lett.*, 99:117001, Sep 2007.

[77] Lapo Bogani, Romain Maurand, Laetitia Marty, Claudio Sangregorio, Claudia Altavilla, and Wolfgang Wernsdorfer. Effect of sequential grafting of magnetic nanoparticles onto metallic and semiconducting carbon-nanotube devices: towards self-assembled multi-dots. *J. Mater. Chem.*, 20:2099–2107, 2010.

[78] H. B. Heersche, Z. de Groot, J. A. Folk, H. S. J. van der Zant, C. Romeike, M. R. Wegewijs, L. Zobbi, D. Barreca, E. Tondello, and A. Cornia. Electron transport through single mn_{12} molecular magnets. *Phys. Rev. Lett.*, 96:206801, May 2006.

[79] Moon-Ho Jo, Jacob E. Grose, Kanhayalal Baheti, Mandar M. Deshmukh, Jennifer J. Sokol, Evan M. Rumberger, David N. Hendrickson, Jeffrey R. Long, Hongkun Park, and D. C. Ralph. Signatures of molecular magnetism in single-molecule transport spectroscopy. *Nano Letters*, 6(9):2014–2020, 2006.

[80] J. J. Henderson, C. M. Ramsey, E. Del Barco, A. Mishra, and G. Christou. Fabrication of nanogapped single-electron transistors for transport studies of individual single-molecule magnets. *Journal of Applied Physics*, 101(9):09E102–09E102–3, May 2007.

[81] S. Voss, O. Zander, M. Fonin, U. Rüdiger, M. Burgert, and U. Groth. Electronic transport properties and orientation of individual mn_{12} single-molecule magnets. *Phys. Rev. B*, 78:155403, Oct 2008.

[82] Salvador Barraza-Lopez, Kyungwha Park, Victor García-Suárez, and Jaime Ferrer. First-principles study of electron transport through the single-molecule magnet mn_{12}. *Phys. Rev. Lett.*, 102:246801, Jun 2009.

[83] A. Einstein and W. J. de Haas. Experimenteller nachweis der amperеschen molekularstörme. *Deutsche Physikalische Gesellschaft, Verhandlungen*, 17:152–170, 1915.

[84] A. Einstein and W. J. de Haas. Einfaches experiment zum nachweis der ampèreschen molekularströme. *Deutsche Physikalische Gesellschaft, Verhandlungen*, 18:173–177, 1916.

[85] S. J. Barnett. Magnetization by rotation. *Phys. Rev.*, 6:239–270, Oct 1915.

[86] Guiti Zolfagharkhani, Alexei Gaidarzhy, Pascal Degiovanni, Stefan Kettemann, Peter Fulde, and Pritiraj Mohanty. Nanomechanical detection of itinerant electron spin flip. *Nat. Nano.*, 3(12):720–723, 12 2008.

[87] Alexey A. Kovalev, Gerrit E. W. Bauer, and Arne Brataas. Magnetovibrational coupling in small cantilevers. *Applied Physics Letters*, 83(8):1584–1586, 2003.

[88] Alexey A. Kovalev, Gerrit E. W. Bauer, and Arne Brataas. Nanomechanical magnetization reversal. *Phys. Rev. Lett.*, 94:167201, Apr 2005.

[89] Alexey A. Kovalev, Gerrit E. W. Bauer, and Arne Brataas. Current-driven ferromagnetic resonance, mechanical torques, and rotary motion in magnetic nanostructures. *Phys. Rev. B*, 75:014430, Jan 2007.

[90] Reem Jaafar and E. M. Chudnovsky. Magnetic molecule on a microcantilever: Quantum magnetomechanical oscillations. *Phys. Rev. Lett.*, 102:227202, Jun 2009.

[91] Reem Jaafar. Effect of the ac field on a single-molecule magnet bridged between conducting leads. *Journal of Magnetism and Magnetic Materials*, 323(23):3151 – 3155, 2011.

[92] M. F. O'Keeffe, E. M. Chudnovsky, and D. A. Garanin. Landau-Zener dynamics of a nanoresonator containing a tunneling spin. *ArXiv e-prints*, February 2013.

[93] M.F. O'Keeffe, E.M. Chudnovsky, and D.A. Garanin. Quantum tunneling of the magnetic moment in a free nanoparticle. *Journal of Magnetism and Magnetic Materials*, 324(18):2871 – 2878, 2012.

[94] Michael F. O'Keeffe and Eugene M. Chudnovsky. Renormalization of the tunnel splitting in a rotating nanomagnet. *Phys. Rev. B*, 83:092402, Mar 2011.

[95] A. J. Leggett. Superconducting qubits–a major roadblock dissolved? *Science*, 296(5569):861–862, 2002.

[96] John Clarke and Frank K. Wilhelm. Superconducting quantum bits. *Nature*, 453(7198):1031–1042, 06 2008.

[97] Caspar H. van der Wal, A. C. J. ter Haar, F. K. Wilhelm, R. N. Schouten, C. J. P. M. Harmans, T. P. Orlando, Seth Lloyd, and J. E. Mooij. Quantum superposition of macroscopic persistent-current states. *Science*, 290(5492):773–777, 2000.

[98] MD LaHaye, J. Suh, PM Echternach, KC Schwab, and ML Roukes. Nanomechanical measurements of a superconducting qubit. *Nature*, 459(7249):960–964, June 2009.

[99] A. D. O'Connell, M. Hofheinz, M. Ansmann, Radoslaw C. Bialczak, M. Lenander, Erik Lucero, M. Neeley, D. Sank, H. Wang, M. Weides, J. Wenner, John M. Martinis, and A. N. Cleland. Quantum ground state and single-phonon control of a mechanical resonator. *Nature*, 464(7289):697–703, 04 2010.

[100] I. Chiorescu, Y. Nakamura, C. J. P. M. Harmans, and J. E. Mooij. Coherent quantum dynamics of a superconducting flux qubit. *Science*, 299(5614):1869–1871, 2003.

[101] A. V. Nikulov. Flux-qubit and the law of angular momentum conservation. *ArXiv e-prints*, May 2010.

[102] E. Chudnovsky, D. Garanin, and M. O'Keeffe. Conservation of angular momentum in a flux qubit. *Journal of Superconductivity and Novel Magnetism*, 25:1007–1016, 2012. 10.1007/s10948-012-1410-y.

[103] A. J. Leggett, S. Chakravarty, A. T. Dorsey, Matthew P. A. Fisher, Anupam Garg, and W. Zwerger. Dynamics of the dissipative two-state system. *Rev. Mod. Phys.*, 59:1–85, Jan 1987.

[104] I. I. Rabi. On the process of space quantization. *Phys. Rev.*, 49:324–328, Feb 1936.

[105] I. I. Rabi. Space quantization in a gyrating magnetic field. *Phys. Rev.*, 51:652–654, Apr 1937.

[106] E.T. Jaynes and F.W. Cummings. Comparison of quantum and semiclassical radiation theories with application to the beam maser. *Proceedings of the IEEE*, 51(1):89 – 109, jan. 1963.

[107] C. Gerry and P. Knight. *Introductory Quantum Optics*. Cambridge University Press, 2005.

[108] S. Schweber. On the application of bargmann hilbert spaces to dynamical problems. *Annals of Physics*, 41(2):205 – 229, 1967.

[109] S Swain. A continued fraction solution to the problem of a single atom interacting with a single radiation mode in the electric dipole approximation. *Journal of Physics A: Mathematical, Nuclear and General*, 6(2):192, 1973.

[110] T. Niemczyk, F. Deppe, H. Huebl, E. P. Menzel, F. Hocke, M. J. Schwarz, J. J. Garcia-Ripoll, D. Zueco, T. Hummer, E. Solano, A. Marx, and R. Gross. Circuit quantum electrodynamics in the ultrastrong-coupling regime. *Nat. Phys.*, 6(10):772–776, 10 2010.

[111] P. Forn-Diaz, J. Lisenfeld, D. Marcos, J. J. García-Ripoll, E. Solano, C. J. P. M. Harmans, and J. E. Mooij. Observation of the bloch-siegert shift in a qubit-oscillator system in the ultrastrong coupling regime. *Phys. Rev. Lett.*, 105:237001, Nov 2010.

[112] E. K. Irish. Generalized rotating-wave approximation for arbitrarily large coupling. *Phys. Rev. Lett.*, 99:173601, Oct 2007.

[113] J. Casanova, G. Romero, I. Lizuain, J. J. García-Ripoll, and E. Solano. Deep strong coupling regime of the jaynes-cummings model. *Phys. Rev. Lett.*, 105:263603, Dec 2010.

[114] Victor V. Albert, Gregory D. Scholes, and Paul Brumer. Symmetric rotating-wave approximation for the generalized single-mode spin-boson system. *Phys. Rev. A*, 84:042110, Oct 2011.

[115] D. Braak. Integrability of the rabi model. *Phys. Rev. Lett.*, 107:100401, Aug 2011.

[116] F. Alexander Wolf, Marcus Kollar, and Daniel Braak. Exact real-time dynamics of the quantum rabi model. *Phys. Rev. A*, 85:053817, May 2012.

[117] K Ziegler. Short note on the rabi model. *Journal of Physics A: Mathematical and Theoretical*, 45(45):452001, 2012.

[118] F. A. Wolf, F. Vallone, G. Romero, M. Kollar, E. Solano, and D. Braak. Dynamical correlation functions and the quantum rabi model. *Phys. Rev. A*, 87:023835, Feb 2013.

[119] L.D. Landau. Zur theorie der energieubertragung. ii. *Physikalische Zeitschrift der Sowjet Union*, 2:46–51, 1932.

[120] C. Zener. Non-adiabatic crossing of energy levels. *Proceedings of the Royal Society of London*, A137:7, 1932.

[121] E.C.G. Stueckelberg. Theorie der unelastischen stösse zwischen atomen. *Helvetica Physica Acta*, 5:369, 1932.

[122] Ettore Majorana. Atomi orientati in campo magnetico variabile. *Il Nuovo Cimento (1924-1942)*, 9:43–50, 1932. 10.1007/BF02960953.

[123] D. A. Garanin and R. Schilling. Many-body landau-zener effect at fast sweep. *Phys. Rev. B*, 71:184414, May 2005.

[124] E. M. Chudnovsky and D. A. Garanin. Superradiance from crystals of molecular nanomagnets. *Phys. Rev. Lett.*, 89:157201, Sep 2002.

[125] E. M. Chudnovsky and D. A. Garanin. Phonon superradiance and phonon laser effect in nanomagnets. *Phys. Rev. Lett.*, 93:257205, Dec 2004.

[126] S Brundobler and Veit Elser. S-matrix for generalized landau-zener problem. *Journal of Physics A: Mathematical and General*, 26(5):1211, 1993.

[127] N A Sinitsyn. Counterintuitive transitions in the multistate landau–zener problem with linear level crossings. *Journal of Physics A: Mathematical and General*, 37(44):10691, 2004.

[128] N. A. Sinitsyn. Landau-zener transitions in chains. *ArXiv e-prints*, December 2012.

[129] Wojciech H. Zurek, Uwe Dorner, and Peter Zoller. Dynamics of a quantum phase transition. *Phys. Rev. Lett.*, 95:105701, Sep 2005.

[130] Bogdan Damski. The simplest quantum model supporting the kibble-zurek mechanism of topological defect production: Landau-zener transitions from a new perspective. *Phys. Rev. Lett.*, 95:035701, Jul 2005.

[131] J. Keeling and V. Gurarie. Collapse and revivals of the photon field in a landau-zener process. *Phys. Rev. Lett.*, 101:033001, Jul 2008.

[132] Zhe Sun, Jian Ma, Xiaoguang Wang, and Franco Nori. Photon-assisted landau-zener transition: Role of coherent superposition states. *Phys. Rev. A*, 86:012107, Jul 2012.

[133] Martijn Wubs, Keiji Saito, Sigmund Kohler, Peter Hänggi, and Yosuke Kayanuma. Gauging a quantum heat bath with dissipative landau-zener transitions. *Phys. Rev. Lett.*, 97:200404, Nov 2006.

[134] Keiji Saito, Martijn Wubs, Sigmund Kohler, Yosuke Kayanuma, and Peter Hänggi. Dissipative landau-zener transitions of a qubit: Bath-specific and universal behavior. *Phys. Rev. B*, 75:214308, Jun 2007.

[135] Robert S. Whitney, Maxime Clusel, and Timothy Ziman. Temperature can enhance coherent oscillations at a landau-zener transition. *Phys. Rev. Lett.*, 107:210402, Nov 2011.

[136] S.N. Shevchenko, S. Ashhab, and Franco Nori. Landau–zener–stückelberg interferometry. *Physics Reports*, 492(1):1 – 30, 2010.

[137] A. R. Edmonds. *Angular Momentum in Quantum Mechanics*. Princeton University Press, 2nd edition, 1960.

[138] J. H. Van Vleck. The coupling of angular momentum vectors in molecules. *Rev. Mod. Phys.*, 23:213–227, Jul 1951.

[139] O. Klein. Zur frage der quantelung des asymmetrischen kreisels. *Zeitschrift für Physik A Hadrons and Nuclei*, 58:730–734, 1929. 10.1007/BF01339735.

[140] D A Garanin. Spin tunnelling: a perturbative approach. *Journal of Physics A: Mathematical and General*, 24(2):L61, 1991.

[141] H. Goldstein, C.P. Poole, and J.L. Safko. *Classical mechanics*. Addison Wesley, 3rd edition, 2002.

[142] Lev Davidovich Landau and Evgenii Mikhailovich Lifshitz. *Theory of Elasticity*. Pergamon, 1959.

[143] Bartłomiej Gardas. Exact solution of the schrödinger equation with the spin-boson hamiltonian. *Journal of Physics A: Mathematical and Theoretical*, 44(19):195301, 2011.

[144] R. H. Dicke. Coherence in spontaneous radiation processes. *Phys. Rev.*, 93:99–110, Jan 1954.

[145] F. Yoshihara, K. Harrabi, A. O. Niskanen, Y. Nakamura, and J. S. Tsai. Decoherence of flux qubits due to $1/f$ flux noise. *Phys. Rev. Lett.*, 97:167001, Oct 2006.

[146] Roger H. Koch, David P. DiVincenzo, and John Clarke. Model for $1/f$ flux noise in squids and qubits. *Phys. Rev. Lett.*, 98:267003, Jun 2007.

[147] R. L. Fulton and M. Gouterman. Vibronic coupling. i. mathematical treatment for two electronic states. *J. Chem. Phys.*, 35:1059, 1961.

[148] V. Bargmann. On a hilbert space of analytic functions and an associated integral transform part i. *Communications on Pure and Applied Mathematics*, 14(3):187–214, 1961.

[149] Enrique Solano. The dialogue between quantum light and matter. *Physics*, 4:68, Aug 2011.

[150] Michael D. Crisp. Application of the displaced oscillator basis in quantum optics. *Phys. Rev. A*, 46:4138–4149, Oct 1992.

Publications

[1] Michael F. O'Keeffe and Eugene M. Chudnovsky. Renormalization of the tunnel splitting in a rotating nanomagnet. *Phys. Rev. B*, 83:092402, Mar 2011.

[2] M.F. O'Keeffe, E.M. Chudnovsky, and D.A. Garanin. Quantum tunneling of the magnetic moment in a free nanoparticle. *Journal of Magnetism and Magnetic Materials*, 324(18):2871 – 2878, 2012.

[3] E. Chudnovsky, D. Garanin, and M. O'Keeffe. Conservation of angular momentum in a flux qubit. *Journal of Superconductivity and Novel Magnetism*, 25:1007–1016, 2012. 10.1007/s10948-012-1410-y.

[4] M. F. O'Keeffe, E. M. Chudnovsky, and D. A. Garanin. Landau-Zener dynamics of a nanoresonator containing a tunneling spin. *ArXiv e-prints*, February 2013.